U.S. Army Corps of Engineers, Hydrologic Engineering Center

GeoTrans, Inc.

Tooele Army Depot Groundwater Flow and Contaminant Transport Model (2004)

April 2004

Prepared for:
US Army Corps of Engineers, Sacramento District, Environmental Engineering Branch
1325 J. St., Sacramento, CA 95814

PR-57

Tooele Army Depot Groundwater Flow and Contaminant Transport Model (2004)

April 2004

U.S. Army Corps of Engineers, Hydrologic Engineering Center
609 Second St, Davis CA 95616 (530) 756-1104

GeoTrans, Inc.
A TETRA TECH COMPANY
1080 Holcomb Bridge Road, Building 100, Suite 190, Roswell, GA 30076 • (770) 642-1000

Prepared for:

Prepared for:
U.S. Army Corps of Engineers, Sacramento District, Environmental Engineering Branch
1325 J. St., Sacramento, CA 95814

ACKNOWLEGEMENTS

The authors of this document are Jon Fenske of the U.S. Army Corps of Engineers, Hydrologic Engineering Center (HEC) and Lisa Grogin and Peter Andersen of GeoTrans, Inc. Construction and calibration of the Tooele groundwater flow model were performed by Jon Fenske of HEC. Lisa Grogin and Yan Zhang of GeoTrans, Inc performed construction and calibration of the contaminant transport model. The Tooele Army Depot Project Manager is Maryellen Mackenzie of the U.S. Army Corps of Engineers, Sacramento District. The Technical Team Leader for the groundwater-modeling project is Carl Cole of the U.S. Army Corps of Engineers, Sacramento District. Carl Cole and Gary Benvenuto of the U.S. Army Corps of Engineers, Sacramento, provided assistance with site conceptualization.

TABLE OF CONTENTS

LIST OF FIGURES

LIST OF TABLES

LIST OF ACRONYMNS AND ABBREVIATIONS

$\partial c/\partial x_i$	concentration gradient
∂h/∂l	Hydraulic gradient
α_H	horizontal-transverse dispersivity
α_L	longitudinal dispersivity
α_V	vertical-transverse dispersivity
λ	decay rate
µg	Microgram
ρ_b	porous medium bulk density
θ	effective porosity
A	flow area
ac	Acre
Bldg	Building
BRAC	Base Realignment and Closure
c	Concentration
°C	degrees Celsius
cDCE	cis-1,2-dichloroethylene
c_s	source/sink concentration
d	day
D_{ij}	dispersion coefficient tensor
DOD	(United States) Department of Defense
DRMO	Defense Reutilization and Marketing Office
EPA	(United States) Environmental Protection Agency
°F	degrees Fahrenheit
ft	foot
gpm	gallons per minute
h	hydraulic head
HCM	hydrogeologic conceptual model
HEC	Hydrologic Engineering Center
in	inch
IWL	Industrial Waste Lagoon
JMM	James. M. Montgomery Consulting Engineers, Inc.
K	Hydraulic conductivity
K_d	sorption coefficient
kg	kilogram
K_x	horizontal (x-direction) hydraulic conductivity
K_y	horizontal (y-direction) hydraulic conductivity
K_z	vertical hydraulic conductivity
L	liter
lb	pound
MAR	Mean Absolute Residual
mg	milligram
NAD83	North American Datum of 1983

NGVD	National Geodetic Vertical Datum
OIWL	Old Industrial Waste Lagoon
PCG2	preconditioned conjugate gradient (version 2) solver
Q	volumetric flow
q_s	source/sink groundwater flow per unit volume
RCRA	Resource Conservation and Recovery Act
TCE	trichloroethylene
tDCE	trans-1,2-dichloroethylene
TEAD	Tooele Army Depot
TVD	total-variation-diminishing solver
USACE	United States Army Corps of Engineers
USGS	United States Geological Survey
v_i	velocity vector
yr	year

1. INTRODUCTION

This report documents a numerical model of groundwater flow and trichloroethylene (TCE) transport at the Tooele Army Depot (TEAD). The model is based on the known physical characteristics of the site, is calibrated to observed site conditions, and is used to predict future migration of the TCE plume. This model can be used to better understand the site, manage groundwater contamination, and test hypothetical remediation scenarios.

1.1 Overview

TEAD covers 25,172 acres approximately 35 miles southwest of Salt Lake City (Figure 1) in the Tooele Valley. The principal population centers in the area are the cities of Tooele and Grantsville. TEAD served as a site for the servicing, rebuilding, and storage of military vehicles and equipment. From 1942 to 1988, various hazardous wastes produced by TEAD activities in the industrial area of the site (Figures 2 and 3) were disposed in wastewater, which flowed through unlined ditches to spreading areas and unlined lagoons. These disposal practices led to groundwater contamination, which began to be investigated in 1979. The ditches and the Industrial Waste Lagoon (IWL) were closed in 1988. A Resource Conservation and Recovery Act (RCRA) post-closure permit was subsequently issued for this site on January 7, 1991.

Several phases of environmental assessment and remedial field investigations identified TCE contamination in groundwater. The monitoring wells used to characterize the TCE plume are identified in Figures 2 and 3. A pump-and-treat system to isolate and remediate TCE contamination in the groundwater was designed, and construction of initial injection and extraction wells was completed in 1993. The system became operational in the fall of 1993, ramping up to full operation in January 1994. The groundwater treatment system consists of 16 extraction wells and 13 injection wells (Figures 2 and 3). TCE-contaminated groundwater passes through an air-stripping treatment plant with a design capacity of 8,000 gpm (1.54×10^6 ft^3/d). The average extraction rate of the system currently is approximately 6,200 gpm (1.2×10^6 ft^3/d).

From 1993 to the present, the U.S. Army Corps of Engineers – Hydrologic Engineering Center (HEC) has developed a series of computer models for simulating groundwater flow conditions at TEAD. The primary objective of these modeling efforts was to provide a tool for determining optimum pumping rates and locations that will ensure the hydrodynamic containment of the TCE plume emanating from the former wastewater ditches and the closed IWL. The primary objective of this study is to develop a flow and transport model that can be used as a decision-making tool for various specified design scenarios.

This report begins with an overview of the TEAD site including its history, geology, hydrology, and a summary of past modeling studies. The report then discusses conceptual model formulation, numerical model design, calibration, and TCE transport predictions. The

report concludes with recommendations for improving site understanding and minimizing uncertainty.

1.2 Methodology

In this study, the hydrogeologic system is represented numerically within a finite-difference grid. The model domain outline appears in Figure 1 (other map figures in the report are oriented with the model grid). The groundwater flow simulator MODFLOW (McDonald and Harbaugh, 1988) and the contaminant transport simulator MT3DMS (Zheng and Wang, 1998) calculate hydraulic head and TCE concentration. The hydrogeologic properties and boundary conditions are adjusted in the model to achieve calibration to observed hydraulic head, drawdown, and TCE concentration. Once calibrated, the model is used to predict the future migration of TCE under two scenarios: 1) continued operation of the pump-and-treat system and 2) no further operation of the pump-and-treat system.

2. SITE BACKGROUND

This section presents information about TEAD that is pertinent to groundwater flow and transport modeling. Information comes from a variety of sources, including regional United States Geological Survey (USGS) studies (Gates, 1965; Razem and Batheloma, 1980; Razem and Steiger, 1981; Stolp, 1994; Lambert and Stolp, 1999), site assessments and investigations by James M. Montgomery Consulting Engineers, Inc. (JMM 1986a-d, 1987a-d, 1988) and Kleinfelder, Inc. (1996, 1997, 1998a-f, 2000, 2002a, 2002b), and numerous other reports.

Over 200 monitoring wells and piezometers have been installed at TEAD for environmental characterization. A comprehensive database has been developed to store all the lithologic, chemical, water level, and well construction data from environmental investigations at TEAD. This data is available to site personnel and consultants via a secure internet site maintained by Synectics, Inc.

2.1 History of Tooele Army Depot

The U.S. Army Ordnance Department established the Tooele Ordnance Depot in 1942. In 1949, the Depot assumed command of the Deseret Chemical Depot, which became known as the south area. The Ordnance Depot was renamed Tooele Army Depot (TEAD) in 1962. In October 1996 the Deseret Chemical Depot separated from TEAD and retained its original name. TEAD is a TIER 1, Industrial Operations Command, ammunition storage site, responsible for storing training ammunition and war reserve ammunition. Tooele's Ammunition Equipment Directorate designs and manufactures ammunition and equipment for all of the U.S. Department of Defense (DOD).

TEAD has historically had a joint mission. The first was to provide storage, maintenance, and demilitarization of topographic equipment, troop support items, construction equipment, power generators, and various wheeled vehicles. The second was to provide the same

functions for conventional weapons. From 1942-1966, a large quantity of hazardous materials were generated and used for the maintenance and storage of military vehicles and equipment. The waste chemicals were piped through the industrial complex into a set of four unlined drainage ditches. These ditches ended at land-spreading areas and gravel pits that were used as evaporation/infiltration areas. These gravel pits have been called the old industrial wastewater lagoon (OIWL). In 1966, a collector ditch was constructed to intercept the four existing ditches. This interceptor ditch ran north for 1.5 miles to an abandoned gravel quarry. This pit, the IWL, was used as an evaporation/infiltration pond until its closure in 1988. At that time, an industrial wastewater treatment plant was brought on-line.

In 1993, TEAD was placed on the Base Closure and Realignment (BRAC) list. All vehicle and equipment maintenance and storage duties were transferred to the Red River Army Depot, Texas under BRAC, and the base industrial area was incorporated by the city of Tooele. TEAD currently maintains only its conventional ammunition mission and has six active-duty personnel and 657 civilian personnel.

2.2 Groundwater Contamination and Contamination Sources

Hazardous waste disposal practices at TEAD led to groundwater contamination in the industrial area and northward. The primary contaminant of concern is the solvent TCE, which is used in the service and repair of military vehicles and equipment.

The IWL and wastewater ditches were closed in 1988. A Resource Conservation and Recovery Act (RCRA) post-closure permit was subsequently issued for the site on January 7, 1991. After several phases of environmental assessment and remedial field investigations (JMM, 1988), a pump-and-treat system to contain and remediate TCE contamination in the groundwater was designed, and construction of initial injection and extraction wells was completed. Full-scale operation of the pump-treat-inject system began in January 1994. TCE-contaminated groundwater is passed through an air-stripping treatment plant capable of treating up to 8,000 gpm (1.54×10^6 ft^3/d).

A second groundwater contaminant plume was discovered in 1994-1996 at wells located along the TEAD boundary to the northeast of the IWL (Kleinfelder, 1996). Levels of TCE contamination in excess of 280 µg/L have been measured at one of these wells (C-10). High levels of TCE contamination have also been measured in a well (D-04, 197 µg/L) located on property owned by the Bolinder Companies to the northeast of well C-10. The primary source of this plume – an oil/water separator near Building 679 – was recently identified (Kleinfelder, 2000). The groundwater concentration of TCE near this source is 3430 µg/L (well C-33) (Parsons, 2002).

A sanitary landfill southwest of the industrial area (Figures 2 and 3) was used for solid waste disposal, beginning around 1965. Soil gas samples (Rust, 1995; Kleinfelder, 2002a) and several groundwater samples from wells within and north of this landfill (e.g., C-40, N-119-88, N-150-97, N-116-88) indicate that the landfill is also a TCE source to groundwater, particularly on the northeastern side.

Currently, 61 wells are sampled semi-annually for TCE and other contaminants. Figure 4 shows the approximate location of TCE contamination in groundwater based on samples collected in March 2003. Two plume lobes are apparent. The wide plume lobe originating at the ditches and in the industrial area near the ditches is called the main plume and merges with the plume originating from the sanitary landfill. The narrow concentrated plume lobe originating near building 679 is called the Northeastern Boundary plume. Note that the depiction of these plumes is a subjective interpretation of the data and groundwater flow/transport processes.

2.3 Geology

The Tooele Valley covers approximately 250 square miles within a 400 square mile drainage basin. It is bordered by the Oquirrh Mountains on the east, by the Stansbury Mountains on the west, and by South Mountain and Stockton Bar on the south (Figure 1). To the north, the valley borders the Great Salt Lake.

The north-trending Oquirrh Mountains rise sharply from the an elevation of about 5000 ft (MSL) at the valley floor to over 10,000 ft at the southeast corner of the drainage basin. The Stansbury Mountains, also north-trending, rise more gradually against the valley fill and attain an altitude over 11,000 ft in the southwest corner of the drainage basin. South Mountain, a relatively low transverse divide, and Stockton Bar, a bar-like feature deposited by Lake Bonneville during the Pleistocene Epoch, separate Tooele Valley from Rush Valley to the south.

The Tooele Valley floor gently slopes from about 5000 ft (MSL) near the base of the Oquirrh and Stansbury Mountains to 4200 ft at the Great Salt Lake. In the TEAD model area, the topographic elevation ranges from over 4600 ft in the southeast to 4400 ft in the northwest (Figure 1). The water table elevation in the model area ranges from about 4475 ft to 4285 ft. The depth to water in this area is generally between 120 ft and 375 ft.

The Tooele Valley is typical of the Basin and Range physiography in which fault-block mountains rise above flat, intermontaine valleys. The valley floor is underlain mostly by a thick sequence of unconsolidated sediments of the late Tertiary and Quaternary age. The bulk of this valley fill consists of interfingered clay, silt, sand, and gravel. Some volcanic material is present in the southeastern part of the valley. The fill was emplaced in a complex sedimentation pattern of lake bottom, lake shore, stream, and alluvial fan deposits, making it difficult to correlate beds from one part of the valley to another. The interbedded nature of the alluvial, wave-worked, and deep-water fine-grained sediments likely has a substantial influence on the vertical and lateral hydraulic conductivities at the TEAD site (Kleinfelder, 1998a). Though not well defined, the valley fill thickness ranges from zero at the mountain fronts to greater than 8,000 ft at the north-central parts of the Tooele Valley near Great Salt Lake (JMM, 1986a).

The Oquirrh Mountains and South Mountain are composed mainly of the Oquirrh Formation of Late Mississippian, Pennsylvanian, and Early Permian age. This unit consists mostly of

alternating quartzite and limestone beds, with much of the limestone containing chert. Numerous formations outcrop in the Stansbury Mountains, but the thickest are the Oquirrh Formation and the Tintic Quartzite of Cambrian age, which is exposed along most of the crest of the range. The rocks in all three of the mountain ranges bordering the valley have been extensively folded and faulted (Tooker and Roberts, 1970).

Two physiographic features dominate site geology – an uplifted bedrock block of quartzite, sandstone, limestone, dolomite, siltstone, and mudstone; and unconsolidated, poorly sorted, alluvial deposits of varying thickness. The bedrock block protrudes above the water table in areas beneath and to the north of the IWL (Figure 2). It extends to the surface and forms outcrops about 1000 to 3000 ft north of the IWL. The bedrock block consists of thinly bedded to massive sedimentary and metamorphic rocks striking roughly east-northeast and dipping sharply to the north-northwest.

The alluvium lies above bedrock and varies greatly in thickness. Alluvial deposits below the water table are located to all sides of the bedrock block. Geophysical surveys (Stollar, 1986) estimated the depth to bedrock at approximately 200-400 ft below ground in the southern alluvial area, and approximately 700 ft below ground in the northern alluvium. However, data from a single boring in the far northern alluvium suggest a depth to bedrock of 1,500 ft (Ryan et al., 1981). The unconsolidated alluvium is heterogeneous at the project scale and generally consists of coarser grained sand/gravel deposits with interfingered layers of clay and silt. Cross-sections of the subsurface geology of the study area are presented in Kleinfelder (1998a).

Extensive, yet highly variable fracturing exists throughout the bedrock system. Fault gouge was encountered during the drilling of borings on the northern end of the bedrock block (Dean Armstrong, personal communication, 7 December 1993). This fault system is believed to trend northeast-southwest. Additional evidence of faulting is found in sudden, dramatic drops in water levels recorded at several locations in the study area.

2.4 Hydrology

The climate of the Tooele Valley drainage basin ranges from semi-arid in the salt flats near the Great Salt Lake to humid in the higher mountains. The average annual precipitation at the town of Tooele for the period 1893-present is 17.59 in (http://www.wrc.dri.edu). The normal mean annual air temperature at Tooele (1941-1970) is 51°F and the average annual freeze-free period at Tooele is 209 days.

Gates (1965) hypothesized that annual, average precipitation in the Tooele Valley declines gradually across the valley, from approximately 18 in/yr at the mountain fronts to approximately 10 in/yr near the Great Salt Lake. Gates (1965) estimated the average precipitation in the study area to decrease from 13 in/yr at its southern boundary to 11 in/yr at the northern boundary. Stolp (1994) estimated annual precipitation at the southern boundary to be 17 in/yr, 4 in/yr greater than estimated by Gates (1965). A range of infiltration estimates has been published for the study area. Razem and Steiger (1981) estimated that the

percentage of precipitation that infiltrates to groundwater ranges from 1% to 3%. Hood and Waddell (1969) estimated that 8% of precipitation infiltrates to the water table.

Ephemeral and perennial streams carry approximately 17,000 ac-ft/yr (2×10^6 ft^3/d) from the mountains toward Tooele Valley. The largest perennial streams in the study area are in Settlement, Middle, and Soldier Canyons. Most of the stream flow from these canyons is diverted for irrigation and public supply uses. The average stream flow in Settlement Canyon Creek is about 6,000 ac-ft/yr (Stolp, 1994). The average stream flow in Middle Canyon Creek is about 2,100 ac-ft/yr (Stolp, 1994). The average stream flow in Soldier Creek is about 3,900 ac-ft/yr (Stolp, 1994).

No perennial streams flow across TEAD, although evidence of ephemeral gully flow exists along the southwest boundary of the model area. A small storage impoundment exists at the southwestern corner of the model area. However, groundwater recharge from this impoundment was determined to be insignificant relative to the volume of groundwater flow beneath this part of the study area (HEC, 1994).

2.5 Hydrogeology

The basin-fill aquifer is the principal source of groundwater in the study area. In this alluvial aquifer and in the underlying bedrock, groundwater flows away from the mountains and toward the central and northern parts of the Tooele Valley. In the unconsolidated valley fill, groundwater flows under unconfined and confined conditions. Deep water-table aquifers are found near the mountains, many hundreds of feet below the land surface. These deep aquifers merge with locally semi-confined to confined aquifers toward the center of the valley and are essentially a lateral extension of the same aquifer system.

Groundwater inflow to the southeastern Tooele Valley is predominantly subsurface flow from consolidated rock and stream channel deposits at the fronts of the Oquirrh Mountains. A model calibrated by Razem and Barthaloma (1980) estimated inflow to the southeastern Tooele Valley to be about 44,000 ac-ft/yr (5.3×10^6 ft^3/d). This includes 5,000 ac-ft/yr of inflow to Tooele Valley from Rush Valley underneath the Stockton Bar. Stolp (1994) estimated the average sub-surface inflow to the basin fill deposits in southeastern Tooele Valley to be about 41,800 ac-ft/yr (5.0×10^6 ft^3/d). These estimates were based on a regional water balance studies and contain significant uncertainty.

Groundwater flows toward the northwest across the TEAD site. The elevation of the water table drops from 4475 ft (MSL) on the southeastern boundary to 4285 ft on the northwestern boundary over a distance of 33,000 ft (average hydraulic gradient of 0.0058). Over most of the site, the hydraulic gradient is relatively flat (approximately 0.001), but large head changes occur over short distances where faults are either known to exist or suspected to exist. The depth to water at TEAD generally ranges from 120 ft to 375 ft. Inflows into the groundwater system consist of subsurface flow from the Oquirrh Mountains and Rush Valley and, to a much lesser extent, recharge from precipitation.

Broadly speaking, the TEAD study site can be divided into four separate hydraulic units: 1) fractured bedrock which dominates the central and southern portion of the site, 2) highly transmissive alluvium to the north, 3) shallow alluvium at the southern (upgradient) end of the site, and 4) fault zones.

In several locations at the site, large head changes occur over short distances. These abrupt head changes occur at the locations of known or suspected fault zones. The fault zones are therefore the hydraulically controlling features of the model area. The steep hydraulic gradients are evidence of relatively low hydraulic conductivities. Compaction, cementation, and mineral deposition in the fault zones may have led to the lower conductivities.

On a local scale, the uplifted bedrock block exhibits strongly heterogeneous hydrogeology typical of fracture-flow environments. The bedrock block consists largely of fractured limestone. The hydraulic gradient is relatively flat within the bedrock block but very steep on the upgradient (southern) and downgradient (northern) edges. Movement of groundwater into and out of the bedrock block is controlled by narrow, low-conductivity structures, likely the result of calcification and clay-filled fractures in conjunction with fault gouge. Smearing of fines and offset of beds may also impede flow across fault zones.

The northern alluvium is composed of several interconnected aquifer systems loosely bounded by discontinuous fine-grained aquitards. Vertical hydraulic gradients have been measured at several locations in the northern alluvium. Observed potentiometric head differences of about 10 ft over a vertical distance of 300 ft (0.03 hydraulic gradient) suggest semi-confined to confined conditions in lower portions of the aquifer. However, from review of the boring logs in this area, it is difficult to delineate any continuous low permeability aquitards.

The vertical head differences in the northern alluvium could also be a result of upward groundwater flow due to density and temperature gradients. Vertical hydrothermal gradients of up to 10°C per 400 ft have been observed (JMM, 1988). Concentrations of total dissolved solids in the northern saturated alluvium also show large variations from approximately 10,000 mg/L at a depth of 500 ft below the water table to under 1000 mg/L near the water table (JMM, 1988). The saline water at depth is associated with the Great Salt Lake to the north. The fresh water at shallower depths is derived from mountain-front inflow. The upward vertical gradient in this area may therefore be partially due to a ramping of fresh water near the interface with the saline water body.

The shallow alluvium at the southern (upgradient) end of the site has a very flat gradient most likely resulting from a damming effect of the low-conductivity fault system downgradient, along with the high percentage of high-conductivity gravels and sands noted in this area.

Field measurements of hydraulic conductivity show a broad variance from less than 1 ft/d in the bedrock areas, to over 1,000 ft/d in the northern alluvium (JMM, 1988; Papadopulos, 1987; Metcalf and Eddy, 1993). A long-term aquifer test indicated a hydraulic conductivity value of 200 ft/d and a specific yield of 0.3 for the northern alluvium (Papadopulos, 1987). In the northern alluvial area, the average hydraulic conductivity derived from 65 short-term

pumping tests averaged approximately 90 ft/d (JMM, 1988). The wide range of hydraulic conductivity values derived from these tests suggests significant heterogeneity in the alluvium. In the bedrock area, the average hydraulic conductivity derived from 32 pressure tests and short-term pumping tests was 30 ft/d (JMM, 1988). A preliminary flow-net analysis of the alluvial areas yielded a hydraulic conductivity range of 100 ft/d to 300 ft/d for the northern and southern alluvial areas (HEC, 1994). Well-development data from the installation of the 16 extraction and 13 injection wells across the site provided additional information on hydraulic conductivity. Based on these data, the hydraulic conductivity of the alluvium ranges from 50 ft/d to 1,000 ft/d and the hydraulic conductivity of the bedrock ranges from 6 ft/d to 150 ft/d.

2.6 Prior Groundwater Modeling Studies

Razem and Barthaloma (1980) developed a two-dimensional digital model of groundwater flow in the Tooele Valley. The model was calibrated to 38 years of water usage and water level data. Lambert and Stolp (1999) developed a three-dimensional regional model of the Tooele Valley groundwater flow system. The numerical model was calibrated to match steady-state water levels measured in 1968, and transient conditions during 1968 to 1994.

Over the past eleven years, United States Army Corps of Engineers (USACE) has developed a series of computer models for simulating groundwater flow conditions at the Tooele Army Depot. This included the initial flow model (HEC, 1994), a transient application/analysis using the initial model (HEC, 1995), a post-pumping steady-state calibration (HEC, 1998), an initial contaminant transport model (HEC, 1999), a reconstructed model with additional layers (HEC, 2002), and an expanded flow and transport model (HEC and GeoTrans, 2003). Since the initial study, the model area has progressively expanded from 8,595 ac (15,600 ft by 24,000 ft) in 1994 to the present size of 25,123 ac (32,000 ft by 34,200 ft). Over the same period, the number of model layers has increased from 3 to 9.

The primary objective of these modeling efforts was to optimize pumping rates and locations for plume containment and cleanup. A recent objective of the modeling was to simulate alternative source conceptualizations. Brief synopses of the prior USACE modeling analyses at TEAD are provided in Appendix A.

TEAD was one of three sites evaluated in a study of potential cost savings at pump-and-treat remediation sites (Greenwald, 1999). That study, which included a screening evaluation and hydraulic optimization modeling, suggested that significant cost savings at TEAD could be achieved by adjusting pumping locations and rates.

In 2002, U. S. Environmental Protection Agency (EPA) and DOD co-sponsored a study of transport model optimization using the TEAD site as a test case (Minsker et al., 2003). The purpose of the study was to determine whether automatic optimization algorithms could be practically applied with transport models to determine an optimum remediation strategy (lowest cost that meets pre-specified remediation criteria). Two prominent researchers in the fields of groundwater modeling and optimization – Dr. Chunmaio Zheng of the University of

Alabama and Dr. Richard Peralta of Utah State University – applied their own independently-developed nonlinear optimization techniques, along with an existing HEC model of groundwater flow and TCE transport, to determine the best locations and rates for extraction and injection wells. Modelers at GeoTrans, Inc. served as the control group by using a standard trial-and-error approach to optimization. Each group used the same lowest-price objectives, the same constraints (containment and cleanup criteria), and the same unit costs. The demo group results were meant to be a starting point for future evaluations since the project did not allow the interaction between the researchers and the installation.

The optimization study indicated that a pump-and-treat strategy with fewer wells and lower pumping rates could achieve the property-boundary cleanup goals at significantly reduced cost, relative to current operation. The automatic algorithms produced lower-cost solutions (3% to 13% lower) than did the trial-and-error approach. In Dr. Zheng's optimal configuration, some cost savings were achieved by injecting treated water within the TCE plume to dilute concentrations. All three groups noted that in order to achieve specified concentration goals at the southern edge of the bedrock block within a few years, treated water would have to be injected south of the bedrock block within the TCE plume.

3. HYDROGEOLOGIC CONCEPTUAL MODEL

The first step in the modeling process is development of a Hydrogeological Conceptual Model (HCM). The HCM assimilates the information that is known about the site (much of which is presented in Section 2) into a framework that can be used to build a numerical model of the site (model construction is presented in Section 4). The HCM describes the hydrogeologic units that are modeled, the groundwater flow boundary conditions that are imposed, and the transport model sources that are applied. The HCM also describes the processes of groundwater flow and transport that are simulated.

3.1 Hydrogeologic Units

3.1.1 Bedrock and Bedrock Encasing Zones

The majority of the southern and central portions of the study area are underlain by shallow bedrock. The bedrock location was delineated using information from boring logs and geophysical surveys (Sheley, 1999; Sheley and Yu, 2000; Sternberg et al., 2000; Zhdanov, et al. 2002). Additional interpretation of geophysical and bore log data was conducted by Benvenuto (written communication, January 2004) and Cole (written communication, February 2004). Groundwater levels indicate that the bedrock should be divided into two distinct units – the bedrock basement and an "encased", uplifted bedrock block located in the center of the study area.

3.1.1.1 Bedrock Basement

According to boring logs and geophysical surveys, the upper surface of the bedrock basement below the southern alluvium is approximately 4425 ft (MSL) in elevation. The bedrock basement drops abruptly to the northwest of the bedrock block to an approximate elevation of 3,000 ft (MSL).

Pumping tests in the bedrock indicate significant heterogeneity, with values of hydraulic conductivity ranging from 6 to 481 ft/d (JMM, 1988; Kleinfelder, 2000). Flow net analyses relating estimated regional inflows and measured water levels with hydraulic conductivity values suggest hydraulic conductivity values of approximately 100 ft/d (HEC, 1994). A comparison of water-level gradients in the bedrock with water-level gradients in the alluvial areas, where estimated hydraulic conductivities are much higher, resulted in an estimated hydraulic conductivity of 140 ft/d for the bedrock (HEC, 1994).

3.1.1.2 Uplifted Bedrock Block

Figure 2 presents the approximate location of the uplifted bedrock block. The upper surface of this local bedrock high crops out at land surface (4,600 ft MSL), approximately 250 ft above the water table. The measured water level in the bedrock high was approximately 4,380 ft (MSL) before the commencement of groundwater pumping and approximately 4,340 ft (MSL) in 2001, following 8 years of pumping from the pump-and-treat system.

In the bedrock area, the average hydraulic conductivity derived from 32 pressure and short-term pumping tests was calculated to be approximately 30 ft/d (JMM, 1988). HEC (1994) analyzed well development data for extraction wells E-4, E-5, and E-10 located in the uplifted bedrock block. Results indicated an average hydraulic conductivity of approximately 50 ft/d.

3.1.1.3 Uplifted Bedrock Block Encasing

Current (2003) groundwater levels across the study area decrease from 4475 ft MSL at the southeastern end of the site to 4285 ft MSL at the northwestern end – a total drop of 190 ft. Water levels drop 120 ft at the upgradient edge of the encased bedrock, and approximately 30 ft at the downgradient edge of the encased bedrock. The sharp changes in groundwater levels at the north and south edges of the bedrock block suggest the presence of a narrow, low-permeability zone that encases the entire bedrock block (labeled Fault A in Figure 2). During the drilling of borings on the northern end of the uplifted bedrock, fault gouge (clayey material resulting from the crushing and weathering of rock) was encountered (Dean Armstrong, personal communication, 7 December 1993). One geologic hypothesis is that the uplift of the bedrock resulted in the creation of low-permeability fault gouge, which encases the uplifted bedrock block. Another hypothesis is that the encasement results from weathering of bedrock into clay, and clay filling of fractures and joints.

A primary concern regarding the 2003 model was the location of extraction well E-3-2. The 2003 model located this well in the encased bedrock block in accordance to the gravity survey

provided by SPK (2002). However, the boring log of this well indicated E-3-2 was located in alluvium. In August 2003, a recovery test at well E-3-2 was conducted (Carl Cole, written communication, August 2003). Well E-3-2 was shut down and a static water level was taken at the well. The measured water level of about 4304 ft MSL was similar to alluvial monitoring wells in the vicinity and 35 ft lower than measured water levels in the adjacent bedrock block. A small response to the shutdown in well B-12, which is located in the alluvium, was also noted. These findings provided conclusive evidence that well E-3-2 was screened in alluvium to the north, and adjacent to, the encasing zone. The bedrock block and encasing zone in the vicinity of E-3-2 was reconfigured in the model.

Following the commencement of pumping at the site in fall 1993, the measured water levels in the uplifted bedrock dropped approximately 35-40 ft. Water levels on the outside of the bedrock dropped generally less than 2 ft in response to pumping in adjacent alluvial areas. The large drop in water levels within the bedrock block provides evidence that the bedrock block is completely encased by low-permeability material. There are no direct field measurements of the hydraulic conductivity of the bedrock encasing zones. Prior estimates were the results of model calibration to the measured hydraulic gradients in the area.

3.1.2 Additional Fault Zones

The conceptualization of fault zones in this study is dependent upon evidence of abrupt water level changes typical of faults in both bedrock and alluvium. In bedrock, the formation of low-permeability fault gouge and weeathered clay products is hypothesized to be the cause of the sharp gradients across bedrock faults. In alluvium, the offset of flow paths and the formation of low-permeability material are hypothesized to be two possible explanations for the sharp gradients associated with faults. Similar observations have been made at other sites. According to a recent study at Fort Irwin, California, "water-quality data…indicates that this fault may be acting as at least a partial barrier to groundwater flow. Minor compaction and deformation of the water-bearing deposits immediately adjacent to the faults and cementation of the fault zone by the deposition of minerals from groundwater are believed to cause the barrier effect of the faults" (USGS, 2000). A similar hypothesis was made in a study of the hydrologic influence of faults near Milford, Utah (Becker, J.D. and D.D. Blackwell, 1993).

In the conceptual model, fault zones, including the uplifted bedrock block encasing, are defined to be narrow, linear bands of low-permeability material. The typical thickness, in plan view, of a fault zone is conceptualized to be less than 200 ft, which is the grid size of the numerical model (see Section 4). The hydraulic conductivities of the conceptualized fault zones are determined by calibration to measured water levels.

To the southwest of the bedrock block, an abrupt drop in water levels occurs between wells/piezometers P-40, P-41, and B-36, and wells/piezometers P-13S, P-13D, and B-28. For example, the water level at piezometer P-40 is 4446 ft MSL, and the water level at piezometer P-13S, screened at approximately the same elevation, is 4315 ft MSL. This is a drop of 135 ft over less than 600 ft. Although there has not been direct evidence of fault gouge encountered in this area, the abrupt changes in measured water levels suggest the presence of a fault in this

area that connects with the bedrock block encasing faults. This fault is called Fault B in Figure 2. An additional fault (labeled Fault C in Figure 2) is suspected to be about 2,000 ft southeast of Fault A in deeper model layers. This fault was conceptualized during past model calibration.

To the northeast of the uplifted bedrock block, an abrupt change in water levels occurs between the area of wells D-5 and D-7, and the area of wells D-3 and D-8. For example, the measured water level at well D-5 is 4374 ft (MSL), and the water level at well D-3 is 4356 ft, a drop of 18 ft over approximately 800 ft. The head gradient in areas upgradient and downgradient of these wells is relatively flat. Furthermore, the low rate of seepage observed during installation of well D-3 may be indicative of anomalous, low-conductivity material in the proximate area (Carl Cole, personal communication, January 2003). The fault labeled Fault D in Figure 2 is included in the conceptual model based on this information.

An additional fault is hypothesized based on several abrupt changes in water levels measured across the site. This fault runs from southeast to northwest across the model area (labeled as Fault E in Figure 2). The abrupt water-level drops occur between wells C-13 and D-2, between C-10 and D-4, between D-3 and C-8, and between D-10 and D-9. The locations of these abrupt water level changes occur in a line roughly parallel to the dip of the bedrock basement and directly adjacent to the northeast edge of the uplifted bedrock block. Low-conductivity zones for Fault E are helpful for model calibration (see Section 5).

3.1.3 Alluvium and Lacustrine Deposits

The unconsolidated sediments, which underlie most of the study site, is heterogeneous at the project scale and generally consists of coarser grained sand/gravel deposits with some cemented areas and with inter-fingered layers of clay and silt typical of alluvial and lacustrine deposits. The deposition of fine-grained strata between coarse-grained depositional events results in an effective horizontal hydraulic conductivity that is much greater than the effective vertical hydraulic conductivity. The alluvium on the site is conceptualized as two separate units: the southern alluvium, located to the southeast of the uplifted bedrock block; and the northern alluvium located to the northwest of the uplifted bedrock block.

The shallow upgradient alluvium at the southern end of the site has a very flat gradient most likely resulting from a damming effect produced by the low conductivity fault/bedrock system downgradient. Additionally, a high percentage of permeable gravels and sands were noted in borings in the southern alluvium, relative to the northern alluvium. One hypothesis for this is that the southern alluvium is closer to the mountain front where coarser material would be deposited from alluvial outwash. At the southern end of the model area, the alluvium is very shallow with approximately 50 ft of saturated thickness between the bedrock basement and the water table. Additionally, a shallow zone of fine-grained material located in the southern alluvium directly upgradient and adjacent to the encased bedrock block was delineated based on interpretation of geologic processes (Carl Cole, verbal communication, February 2004). In this interpretation, the weathering of the uplifted bedrock block resulted in erosion and deposition of fine-grained materials.

The northern alluvium is composed of several interconnected aquifer systems loosely bounded by discontinuous fine-grained aquitards. Significant vertical hydraulic gradients have been measured at several locations in the northern alluvium. Hydraulic head differences of approximately 10 ft over a vertical distance of approximately 300 ft indicate potential semi-confined to confined conditions. However, from review of the boring logs in this area, it is difficult to delineate any continuous low permeability aquitards. Perhaps the most reliable field estimate of hydraulic conductivity in the study area (Papadopulos, 1987) was derived from a long-term aquifer test at WW-7 in the northern alluvium. Results from this test estimated the horizontal hydraulic conductivity to be 200 ft/d.

3.2 Description of Groundwater Flow

The primary source of groundwater in the study area is from subsurface inflow from the Oquirrh Mountain front. Other sources of groundwater are infiltration of precipitation on the valley floor and subsurface inflow from Rush Valley, to the south of the study area.

The model area encompasses the entirety of potential subsurface inflow pathways from the Oquirrh Mountains at the southeastern Tooele Valley. Lambert and Stolp (1999) estimated the volume of recharge from the Oquirrh Mountains to be 43,400 ac-ft/yr (5.2×10^6 ft^3/d). This inflow figure is based on a 2-dimensional flow model of the Tooele Valley by Razem and Bartholoma (1980). According to Lambert and Stolp (1999), Razem and Bartholoma (1980) used an equation to calculate the inflow (32,000 acre-ft/yr) based on precipitation, altitude, geology and land gradient. Razem and Bartholoma (1980) then adjusted the inflow (to 40,000 acre-ft/yr) in order to calibrate their model. Lambert and Stolp (1999) increased their assumed recharge rate to 43,400 ac-ft/yr (5.2×10^6 ft^3/d) to achieve model calibration .

Groundwater levels across the study area decrease from 4475 ft (MSL) at the southern end of the site to 4285 ft at the northern end of the site; a drop of 190 ft over a distance of 33,000 ft. The study area is characterized by a very heterogeneous hydraulic gradient distribution where groundwater levels are relatively consistent across most of the site, and drop abruptly across fault areas. For example, measured water levels drop approximately 120 ft across the upgradient bedrock encasing fault zone, measured water levels drop approximately 30 ft across the downgradient bedrock encasing fault zone, and measured water levels drop approximately 145 ft across the fault zone southwest of the bedrock. To the northeast, abrupt water level drops ranging from 30 to 80 ft were measured.

Measured vertical gradients across the study area are insignificant except near pumping wells and at the northwestern end of the site. In the northern alluvium, potentiometric surface differences of approximately 10 ft over a vertical distance of 300 ft were measured (head increasing with depth). This is indicative of semi-confined to confined conditions. Upward flow due to temperature and salinity gradients is likely a contributing factor to the large vertical gradients measured in the area. HEC (1994) demonstrated that effects of temperature dominate the effect of salinity when determining density changes in the Tooele Valley groundwater. The upward vertical gradient in this area may also be related to a ramping of fresh water near the interface with the saline water body.

3.3 Contaminant Sources

Prior characterization studies identify several known and suspected TCE sources at TEAD (e.g., Kleinfelder 2002a). In the industrial area, several unlined wastewater ditches were used between 1942 and 1988 (Figures 2 and 3). These ditches ran to the northwest, parallel to the roads – one was between Avenues A and B (called Ditch B) and three more were located along Avenues C, D, and E (Ditches C, D, and E). Originally, these ditches drained to a spreading area, which is now called the OIWL. In 1965, an unlined gravel pit was converted into the IWL. An unlined collector ditch was constructed to carry effluent from Ditches B, C, D, and E to the IWL, where the wastewater evaporated and infiltrated to groundwater. In 1988, the ditches were closed, lined, filled, and capped and the IWL was closed, filled, and capped. Wastewater is now piped to a treatment plant.

TCE has been observed in the vadose zone beneath the ditches and the lagoons, and in the saturated groundwater near the ditches and lagoons (Kleinfelder, 2002a), indicating that these features were significant TCE contamination sources to groundwater at TEAD. Even though the system of ditches and lagoons are no longer in use, the vadose-zone contamination beneath these features continues to be a potential source of TCE to the groundwater.

In addition to the ditches, significant vadose-zone and saturated-zone TCE has been observed in other locations within the industrial area. The highest recorded TCE concentration in groundwater at TEAD (3430 µg/L) was from well C-33, near building 679 (Figure 3). Recent investigations (Kleinfelder, 2000) have determined that an oil/water separator near building 679 was the primary source of this contamination. The oil/water separator was removed and a soil vapor extraction system pilot test has been conducted. This system may have removed significant mass from the Building 679 source area. Vadose-zone soil-gas concentrations (Kleinfelder, 2002a) and groundwater concentrations also suggest that a source of TCE exists near buildings 619, 615, 613, 612, and 611.

The sanitary landfill southwest of the industrial area is another probable source of TCE in groundwater. Soil-gas samples indicate elevated TCE levels in the vadose zone at the northern end of the landfill (Kleinfelder, 2002a), and a groundwater sample from well C-40 indicates a groundwater concentration of up to 885 µg/L beneath this portion of the landfill.

The industrial-area soil-gas survey (Kleinfelder, 2002a) also indicates elevated vadose-zone TCE concentrations in a portion of the former Defense Reutilization and Marketing Office (DRMO) area (Figure 2). However, there have been no high concentrations of TCE observed in the groundwater near this location.

3.4 Description of Contaminant Transport

Pure liquid-phase TCE and/or TCE-laden wastewater seeped into the vadose zone at TEAD through the wastewater ditches, wastewater lagoons, and at other locations discussed above. In the vadose zone, TCE may adsorb to the alluvial soils, volatilize to gas phase, dissolve into vadose-zone water, or remain in pure liquid phase. (Note that no direct evidence at TEAD

indicates that TCE currently exists in pure liquid phase in the subsurface.) The TCE that is dissolved in water or that remains in non-aqueous liquid phase drains downward to the water table. The vadose zone in the industrial area is approximately 150 ft thick.

TCE thus infiltrates to groundwater along with precipitation recharge. Conceptually, the recharge water at the source areas carries a certain concentration of TCE, providing a mass flux of TCE to the water table. In the numerical groundwater model, TCE recharge concentrations are specified for the source areas discussed in Section 3.3. The setting of concentrations and timing for the TCE sources are described in Sections 4.2.4 and 5.2.3.

In the groundwater, TCE moves northwestward along with groundwater flow (advection), creating a TCE plume. The plume spreads and plume-center concentrations are reduced as the plume moves downgradient, due in large part to the process of dispersion (molecular diffusion is unimportant compared to dispersion at the site scale). Figure 4 presents an interpretation of the TCE plume in groundwater at TEAD.

TCE can adsorb to soil and rock materials, effectively slowing its movement. The degree of TCE sorption depends largely on the organic content of the soil and rock. TCE will more readily adsorb to material with a higher organic content. Often, sorption is assumed to be a linear-equilibrium process, wherein the groundwater concentration of TCE (µg/L) is always proportional to the soil concentration of TCE (µg/kg). The proportionality constant is the sorption coefficient, or K_d (L/kg or similar units), which is a property of the contaminant (TCE) and soil/rock material. No site-specific estimates of K_d have been published for TEAD.

TCE may undergo chemical transformation during transport. Most commonly, TCE is biologically degraded into cis-1,2-dichloroethylene (cDCE) or (less commonly) trans-1,2-dichloroethylene (tDCE). The cDCE and tDCE may be subsequently degraded to vinyl chloride then ethylene (innocuous), or oxidized to form carbon dioxide and water (also innocuous). These degradation steps remove chlorine atoms from the organic compounds, creating chloride ions. TCE dechlorination generally requires anaerobic conditions, certain biological organisms, and an organic substrate for biological growth. At TEAD, there is no evidence of significant TCE dechlorination in the saturated groundwater.

4. NUMERICAL MODEL CONSTRUCTION

4.1 Numerical Methods

In the saturated groundwater, a combination of continuity (mass conservation) and Darcy's Law leads to the following mathematical description of steady-state groundwater flow:

$$\frac{\partial}{\partial x}\left(K_x \frac{\partial h}{\partial x}\right)+\frac{\partial}{\partial y}\left(K_y \frac{\partial h}{\partial y}\right)+\frac{\partial}{\partial z}\left(K_z \frac{\partial h}{\partial z}\right)=0 \qquad (1)$$

In this equation, the dependent variable is the hydraulic head, *h*, which is defined in the traditional (*x*, *y*, *z*) Cartesian coordinate system. The horizontal and vertical hydraulic conductivities (K_x, K_y, and K_z) are known functions. Boundary conditions must also be specified to solve equation 1. The boundary conditions may be specified head (Dirichlet), specified flux (Neumann), or head-dependent flux (Cauchy). It is assumed that groundwater flow is unchanging in time (steady state).

The United States Geological Survey (USGS) groundwater flow modeling software MODFLOW (McDonald and Harbaugh, 1988) provides a means to solve equation 1 for *h* in a chosen domain, with specified values for hydraulic conductivity and specified boundary conditions. MODFLOW uses the finite-difference method to approximate the groundwater flow equation as a set of algebraic equations in a discretized three-dimensional grid of rectangular cells.

The transport of contaminants in groundwater is governed by the advection-dispersion-reaction equation, which can be written as follows:

$$\left(\theta + \rho_b K_d\right)\frac{\partial c}{\partial t} + \frac{\partial}{\partial x_i}\left(\theta v_i c\right) = \frac{\partial}{\partial x_i}\left(\theta D_{ij}\frac{\partial c}{\partial x_j}\right) - \lambda\left(\theta + \rho_b K_d\right)c + q_s c_s \qquad (2)$$

In this equation, the Cartesian coordinates are represented by x_i (i = 1, 2, 3), and the dependent variable is the contaminant concentration in groundwater, *c*. The velocity field (v_i) is determined from the flow solution and Darcy's Law. The effective porosity is θ, and the porous medium bulk density is ρ_b. First order (exponential) decay is assumed at a rate of λ (in this study, λ is set to zero since TCE degradation in groundwater appears insignificant). Equilibrium linear sorption is also assumed, with a sorption coefficient of K_d. Contaminant sources and sinks are represented by the source/sink groundwater flow rate per unit volume of the aquifer (q_s) and the source/sink concentration (c_s). The dispersion coefficient tensor, D_{ij}, is dependent on the groundwater velocity and specified length scales for dispersion, called dispersivities. Dispersivities are usually specified as longitudinal (along the direction of flow, α_L), horizontal-transverse (α_H), and vertical-transverse (α_V). The initial value of *c* must also be specified in order to solve equation 2.

MT3DMS (Zheng and Wang, 1998) is a software program for solving equation 2 that uses the same finite-difference framework as MODFLOW. Once the steady-state values of *h* are determined from MODFLOW, and the independent variables of equation 2 are specified, MT3DMS can be used to solve for contaminant concentration (*c*) as a function of space and time in the modeled domain. For the simulations presented in this report, the total-variation-diminishing (TVD) solution method is used to simulate solute advection. This method is more accurate than standard finite-difference techniques (though more computationally intensive) and is inherently mass-conservative. The MT3DMS simulator automatically chooses model time steps that are small enough to limit numerical error.

4.2 Model Design

4.2.1 Model Grid

The model grid consists of 171 rows and 160 columns (Figure 5), encompassing an area of 34,200 ft by 32,000 ft. Relative to the 2003 model, the current model is expanded by 51 columns (10,200 ft) to the northeast, and 6 rows (1,200 ft) to the southeast. The expansion of the model grid was facilitated by new water-level data from a U.S. Geological Survey regional hydrologic study (Lynette Brooks, written communication, January 2004). The expansion of the model grid allows for a more accurate representation of the regional flow domain, and facilitates the modeling of the northeastern flank of the Northeastern Boundary plume. The model is oriented towards the northwest parallel to the direction of regional groundwater flow. The lower left corner of the grid is at 1,402,613.5 ft E, 7,351,854.1 ft N in state-plane coordinates (Utah Central Zone, NAD83), and the grid is rotated 39.5 degrees counterclockwise relative to this coordinate system (Figure 1).

The horizontal discretization is selected to be: 1) fine enough to represent various hydrologic zones with a precision commensurate with the ability of the data to represent the system, 2) fine enough to exhibit a measurable sensitivity to various pumping scenarios, 3) fine enough to allow for the accurate simulation of particle tracking and contaminant transport, and 4) coarse enough to allow for maximum computational efficiency without compromising the above considerations. A cell size of 200 ft square is selected to best meet the grid criteria.

The model consists of 9 layers covering a vertical dimension of 780 ft (Figure 6). Layer bottom elevations are specified as constant throughout the model domain. Layer thickness varies from 25 ft in the upper two layers (approximate depending on water table elevation) to a bottom layer thickness of 200 ft. The finer discretization in the upper layers allows for more accurate simulation of vertical gradients and contaminant transport.

In MODFLOW, the layers that are completely above the water table are flagged as dry and become inactive. Consequently, large portions of the top four layers are inactive. The exact location of the water table in the model is determined by MODFLOW, which can automatically dry and re-wet cells as necessary. However, some portions of layers one through four are pre-specified as inactive (dry) to speed the flow solution process.

4.2.2 Hydrogeologic Properties

The numerical simulation of groundwater flow requires the assignment of hydrogeologic properties at all grid cells. Generally, these assignments are made using property zones, where each zone has uniform hydrogeologic properties. The location and areal extent of property zones in this model are specified in accordance with the conceptual model discussed in Section 3. Hydraulic conductivities and other properties are initially assigned to each zone based upon measured field parameters discussed in Sections 2 and 3.

Data sources were evaluated for model-scale reliability. For example, pumping tests (Papadopulos, 1987 and HEC, 1994) were given more weight than slug and pressure tests. Based on the field evidence, values of horizontal hydraulic conductivity of the northern alluvium are estimated to be in the range of 100 ft/d to 300 ft/d. Values of horizontal hydraulic conductivity of the southern alluvium are estimated to range from 150 ft/d to 500 ft/d. Values of hydraulic conductivity of the bedrock are assumed to range from 20 ft/d to 150 ft/d.

The number of zones used in the model is based on a subjective evaluation of appropriate complexity. The complexity of a model should be commensurate with the ability of the data to represent the hydrologic system. Freyberg (1988) analyzed the results of nine separate groups that developed a groundwater model from a common data set. The group that achieved the best prediction of future conditions chose to zone the hydraulic conductivity field into relatively few homogeneous regions. The group that produced the worst prediction chose to "tweak" the conductivity field on a cell-by-cell basis to achieve the best calibration to observed data. The conclusion of this study was "good calibration, in this sense, does not equal good prediction" (Freyberg, 1988, p 360).

Sixteen zones representing unique, homogeneous hydrogeologic units were used in the 2003 model (HEC and GeoTrans, 2003). Two additional zones were added in the 2004 model: a zone of fine-grain sediments in the upper alluvium located adjacent and upgradient of the encased bedrock block, and an additional fault zone that represents a specified value of hydraulic conductivity within the vertical fault (Fault D-2). The 18 homogeneous zones used in the 2004 model are presented in Figures 6 through 15. Note that some of the zones shown in these figures may have different properties in different layers. The location and properties of these zones were determined through model calibration as described in Section 5.2.1.

For simplicity, properties affecting TCE transport –dispersivity, bulk density, and sorption coefficient – are assumed to be uniform values in the model. The dispersivities are set to 100 ft longitudinal (α_L), 10 ft horizontal-transverse (α_H), and 1 ft vertical-transverse (α_V). These values are appropriate for a plume that extends about 15,000 ft. As a practical rule of thumb, the longitudinal dispersivity should be less than or equal to one tenth of the length of the plume (lower values are more conservative in that they produce higher simulated concentrations), the horizontal-transverse dispersivity should be one tenth of the longitudinal dispersivity, and the vertical-transverse dispersivity should be one hundredth of the longitudinal dispersivity.

The effective porosity (θ) was initially set to 20% across the model domain (a reasonable value for alluvial deposits and highly-fractured bedrock), and the sorption coefficient (K_d) to 0.06 L/kg (giving a reasonable retardation factor ($1 + K_d(\rho_b/\theta)$) of 1.5). These values can be adjusted during calibration, as described in Section 5.2.4. The bulk density (ρ_b) is set to 1.7 kg/L.

4.2.3 Groundwater Flow Boundary Conditions

4.2.3.1 Recharge

A range of precipitation and infiltration estimates have been published for the study area. Gates (1965) estimated average precipitation at the study area to decrease from 13 in/yr at the southern boundary to approximately 11 in/yr on the northern boundary. Stolp (1994) estimated precipitation at the southern boundary as approximately 17 in/yr. Hood and Waddell (1969) estimated that the fraction of precipitation that recharges groundwater is 8%. Razem and Steiger (1981) estimated this fraction to range from 1% to 3%.

For the model study, precipitation is specified to range from 16 in/yr at the southern boundary to 14 in/yr at the northern boundary. The fraction of precipitation that infiltrates to groundwater was specified to range from 5% to 3%. Three zones are used to represent the specified flux of recharge from infiltration on the uppermost active model layer. Zone 1 is located in the Industrial Area at the southern of the site, zone 2 encompasses the central area of the site, and zone 3 covers the northwestern portion of the site (Figure 16). The specified recharge for zone 1, 2×10^{-4} ft/d (0.876 in/yr), assumes an average precipitation rate of 16 in/yr, of which 5% infiltrates to the water table. The recharge for zone 2, 1×10^{-4} ft/d (0.438 in/yr), assumes an average precipitation rate of 15 in/yr, of which 3% infiltrates to the water table. The recharge for zone 3, 1×10^{-4} ft/d (0.438 in/yr), assumes an average precipitation rate of 14 in/yr, of which 3% infiltrates to the water table.

4.2.3.2 Lateral Edge and Model Bottom Boundaries

No-flow conditions are specified at the model bottom, along the southwest grid boundary, and along the center of the northeast grid boundary. The construction of the model into 9 layers with constant layer bottom elevations presented challenges in attaining an acceptable numerical solution for the flow model. Water levels within and downgradient of the bedrock block were lower than layer bottom elevations in layers 1-4. This resulted in a large number of model cells going dry (becoming inactive) during the iterative numerical solution. The solution to this challenge was to specify as inactive cells that are clearly dry (head below layer bottom elevation).

Constant head boundary conditions are specified along the southeast boundary, the northwest boundary, and the upper and lower ends of the northeast boundary in all model layers, where active (Figure 5). The model grid was expanded to a distance where the effect of stresses from extraction wells was minimal at the model boundary. Constant heads at the model boundaries are largely based upon measurements at off-site wells made by the U.S. Geological Survey (Lynette Brooks, written communication, January 2004). Values of constant head were adjusted during model calibration, as discussed in Section 5.

4.2.3.3 Well Extraction and Injection

The pump-and-treat system consists of 16 extraction wells and 13 injection wells. Additionally, three City of Tooele wells, located south of the Industrial Area (Brad Call, written communication, January 2004) are simulated by the model (Figure 17).

In past model studies, extraction and injection rates at the pump-and-treat system were determined by dividing the total volume of water pumped since the beginning of operation by the total days since the beginning of operation. This produced a long- term average pumping rate. However, variations in pumping rates can result in localized fluctuations away from this long-term trend. The water levels taken at a certain time are more dependent on the pumping rates in the period immediately preceding the measurements.

A study was performed to better represent the influence of more recent pumping rates on water levels. This study included the development of a representative model to assess the influence of pumping over time on calibration target locations. An algorithm was then developed to provide a more physically based estimation of representative steady-state pumping rates. A discussion of this study is presented in HEC and GeoTrans (2003).

Extraction and injection rates used in the current model are presented in Table 1. Note that some wells extract from more than one model layer – in these cases, the percentage of well screen length in a layer was used to determine the portion of extraction assigned in that layer.

4.2.4 TCE Sources

Thirteen source zones are used in the model (Figure 18). These source zones represent known and suspected locations where TCE has discharged (and may continue to discharge) to the water table. The recharge concentration for these source zones was specified based on the prior model (HEC and GeoTrans, 2003). The recharge concentrations in these source areas are treated as calibration parameters that are adjusted to achieve the best match to the observed TCE plume. Note that the DRMO source is not active in the current model since there is no evidence that this potential source has led to groundwater contamination.

It is assumed that the treatment system removes all of the TCE from the extracted groundwater. Therefore, the injection concentrations are assumed to be zero in the transport simulations. Effluent concentrations are tested routinely and provide support for this assumption.

Table 1. Specifications for Extraction Wells and Injection Wells

Well	Layer	Row	Column	Rate* (gpm)
E-01	6	63	48	-165.25
E-02-1	6	76	41	-145.64
E-02-2	7	77	41	-489.88
E-03-1	5	88	49	-308.59
E-03-2	8	88	48	-227.24
E-04	6	102	37	-123.98
	7	102	37	-289.29
E-05	7	104	45	-555.63
E-06	5	115	37	-147.81
	6	115	37	-147.81
E-08	6	109	45	-82.59
	7	109	45	-82.59
E-09	6	94	48	-156.66
	7	94	48	-313.34
	8	94	48	-313.34
E-10	6	95	53	-753.19
E-11	6	57	45	-531.92
E-12	7	45	45	-0.11
E-13	6	84	28	-507.36
E-14	7	90	32	-497.52
E-15	6	64	34	-537.08
I-01	6	72	65	37.82
I-02	6	62	61	15.78
	7	62	61	15.78
I-03	5	58	60	471.83
I-04	6	53	58	546.49
I-05	5	45	56	443.66
	6	45	56	295.77
I-06	6	40	54	154.02
	7	40	54	154.02
I-07	5	35	49	169.17
	6	35	49	338.35
	7	35	49	338.35
I-08	6	32	43	522.59
I-09	6	31	37	276.25
	7	31	37	276.25
I-10	6	37	33	271.64
	7	37	33	271.64
I-11	6	42	28	283.63
I-12	5	48	20	43.27
	6	48	20	100.95
I-13	6	54	15	55.09
City of Tooele 6	3,4	157	66	-190.33 &
City of Tooele 7	3,4,5,6	161	57	-528.21 &
City of Tooele 8	3,4,5,6	166	50	-541.22 &

*Negative rates signify extraction, positive injection. & Total across all layers

5. MODEL CALIBRATION

Model calibration is the process of adjusting model specifications until the model reasonably reproduces observed conditions. Once calibrated, the model can more reliably be used to predict future conditions.

5.1 Calibration Procedure

The calibration of the TEAD model includes five steps:

- calibration to observed current head conditions, with the pump-and-treat system on,
- calibration to estimated subsurface inflows under current conditions,
- calibration to observed drawdown in the bedrock block caused by the extraction wells,
- calibration to observed TCE concentrations, and
- calibration to the measured TCE mass removed by the extraction system.

Three separate simulations are required in order to evaluate the calibration:

- a steady-state flow simulation with extraction and injection,
- a steady-state flow simulation without extraction and injection, and
- a (steady-state) flow and (transient) TCE transport simulation of the period from 1942 to present (extraction and injection beginning in January 1994).

These simulations and the calibration targets are discussed further in the subsections below.

Initial values for hydraulic conductivity and other parameters are identical to those in the 2003 model (HEC and GeoTrans, 2003) in areas of similar conceptualization. Values of hydraulic conductivity were initially specified as 400 ft/d in the southern alluvium, 200 ft/d in the northern alluvium, 120 ft/d in the southern bedrock, and 80 ft/d in the uplifted bedrock block. The initial hydraulic conductivities of faults and encasing zones ranged from 0.01 ft/d to 4 ft/d. The location of the bedrock block and adjacent uplifted bedrock zone was adjusted in accordance with recent interpretations of geophysical and borehole data (Gary Benvenuto and Carl Cole, written communications, January 2004 and February 2004 respectively).

Section 5.2 presents the specific model adjustments that were made to achieve the best calibration in all five calibration steps. These adjustments were made in trial-and-error fashion. The process is an iterative procedure involving many simulations of the model, with the final result being a set of hydrogeologic-unit property values, boundary conditions, and

TCE source specifications that make up the final calibrated model. The calibration quality is discussed in Section 5.3.

5.1.1 Steady-State Flow Calibration to Current Conditions

Flow model calibration assumes steady-state conditions. In other words, stresses, flow rates, and water levels are assumed to be constant in time. As discussed in previous model studies (HEC, 1995), simulated water levels across the site approach steady-state conditions after approximately 3 years of pumping.

5.1.1.1 Current Observed Water-Level Calibration Targets

Five water-level data sets are used for water-level calibration: local study area water levels measured in spring 2002, fall 2002, spring 2003, and fall 2003; and regional water levels measured in spring 2003 by the U.S. Geological Survey (Lynette Brooks, written communication, January 2004). As discussed in Appendix B, a complete analysis was performed on these data sets. This analysis included the influence of climate variations on water levels, measurement discrepancies, and identification of localized data anomalies. The 2002 data set was judged to provide the best representation of long-term, average water levels. As a result of this analysis, 195 water-level calibration targets are identified. The water-level calibration targets are presented in Figure 2 and Appendix C.

5.1.1.2 Estimated Subsurface Inflow Target

As discussed in Section 3.2, studies by Lambert and Stolp (1999) and Razem and Steiger (1981) estimated the total pre-pumping inflow into the study area to be approximately 5.2×10^6 ft^3/d. The groundwater extraction rate at the study area averages approximately 6,230 gpm (1.2×10^6 ft^3/d). These extraction wells, located upgradient from the injection wells, create a partial increase in subsurface inflow. The estimated pre-pumping inflow was used as a target for the calibration involving simulation of pre-pumping conditions.

5.1.2 Steady-State Flow Calibration to Bedrock-Block Drawdown

For the pre-pumping simulation, extraction and injection wells are removed from the model. The difference (or drawdown) between simulated steady-state water levels with pumping and without pumping is calculated. A comparison is then made between the simulated drawdown in the encased bedrock zone and the drawdown measured in the field. The difference between measured water levels in June 1992, before pumping started, and August 1998, about 5 years after the system became operational, is about 40 ft in the encased bedrock. In the alluvial deposits, measured drawdown from the extraction system is much smaller (a few feet or less).

5.1.3 Calibration of TCE Transport

The next step in the model calibration process is comparison of model-predicted TCE plume development to observed TCE concentrations in groundwater. For this step, a transport

simulation is made that begins in 1942 and continues through 2003. During the first model period – 1942 through 1964 – Ditches B, C, D, and E are active, as well as the OIWL, the spreading area, and the source at building 619 (Figure 19). Between 1965 and 1988, the IWL and IWL interceptor ditch are active sources, as are the sanitary landfill and Building 679 sources. A lower mass input is assumed for the spreading area that is no longer in use (contamination is assumed to remain in the vadose zone). After 1988, the mass input from the ditches and IWL are reduced dramatically to account for closure and remediation. The extraction and injection wells begin operation in 1994, at which time the flow field is changed. Note that steady-state flow is assumed – the effect of the extraction and injection is assumed to be instantaneous.

5.1.3.1 TCE Concentration Targets

The goodness-of-fit for this calibration step is determined primarily through visual matching of model plumes with posted-symbol plots of observed concentrations. A few TCE concentration measurements were made in the early 1980s, but the first significant groundwater characterization effort took place in October 1986 with the installation of the A-series and B-series wells. Based on available TCE data and TEAD operational history, the following six calibration time-frames are used for transport calibration: 1) before 1988, 2) 1988 through 1990, 3) 1991 through 1993, 4) 1994 through 1996, 5) 1997 through 1999, and 6) 2000 through 2002. A final calibration was completed with March 2003 data (see Figure 4). Within each time frame (all but the first and last are three years in duration), the average observed TCE concentration at each well is used as the target concentration.

5.1.3.2 TCE Mass Extracted Target

The transport model simulation results can also be processed to indicate the cumulative amount of TCE mass removed by the extraction system between system startup and any time during the simulation. This modeled value can be compared to the measured cumulative value of 2187 lb (992 kg) that was totaled through June 2002, with 107 lb extracted from Jan – June 2002 (Kleinfelder, 2002b).

5.2 Model Adjustments Made During Calibration

During calibration to flow and transport conditions, several changes were made to the parameter values in the model, and small changes were made to the locations of the property zones in the model. Those changes and the final model specifications are discussed below.

Over 200 steady-state flow model runs were made during the calibration process. The calibration process specifically involved: 1) the adjustment of hydraulic conductivity values to attain an improved match with measured water levels, 2) the adjustment of zones of homogeneous aquifer parameters to better fit hydrogeological conditions, and 3) the adjustment of boundary conditions to attain an improved match with both measured water levels and estimated regional subsurface inflows. Simulation of current groundwater flow conditions initially focused on matching calibration targets described in Appendices B and C.

Additionally, over twenty 60-year transport model simulations were made. In these simulations, the TCE source concentrations were modified until the simulated plume best matched the observed TCE concentrations. When the transport calibration suggested that a change in the flow field was required, the flow calibration steps were made again and adjustments were made as necessary.

5.2.1 Adjustments to Property Zones and Hydraulic Conductivity

The calibration process included both the adjustment of hydrogeologic parameters and the minor adjustment of the location of hydraulic conductivity zones. Additionally, a new zone of fine-grained material, located upgradient of the encased bedrock zone in shallow alluvial areas, was added to the model based on geologic interpretation of the boring log of well T-4 (Carl Cole, verbal communication, February 2004). Zones along the faults were also added in order to attain better calibration to the observed water levels. Figures 6 through 15 show the final property zone configurations. Calibrated values of hydraulic conductivity are presented in Table 2. These values provided the best match to observed conditions.

Table 2. Calibrated Values of Hydraulic Conductivity

Hydrogeologic Unit	Model Zone No.	Layers	Hydraulic Conductivity (ft/d)	
			Horizontal	Vertical
Southern Alluvium	1	1	300	15
	2	2-9	300	0.75
Northern Alluvium	3	All	200	1
Far Northern Alluvium	4	All	200	0.01
Bedrock	6	1-2	80	0.75
	7	3-9	100	20
Upgradient Fines of Encased Zone	18	1-3	0.75	0.075
Encased Bedrock Block	5	All	60	15
Fault A-1	12	All	0.25	1e-5
Fault A-2	11	All	0.12	0.12
Fault B	13	All	0.18	0.18
Fault C	14	All	2	2
Fault D-1, D-3	16	All	0.3	0.3
Fault D-2	15	All	0.3	0.03
Fault D-4	17	All	2.5	2.5
Fault E-1	10	All	0.1	0.1
Fault E-2	9	All	0.12	0.12
Fault E-3	8	1-7	0.8	0.8
	9	8-9	0.12	0.12

Across most of the site, the measured change in water levels induced by pumping is less than 2 ft; however, in the encased bedrock block zone, the measured long-term change is 35-40 ft.

The model was calibrated to produce a simulated change in water levels of 35-40 ft, matching the target.

The purpose of the low vertical conductivity in the far northern alluvium zone is to allow for the simulation of significant upward vertical gradients measured in the area. The purpose of the vertical conductivity differences in the southern alluvium and upper (vs. lower) bedrock are to simulate low-permeability layers believed to be located at the alluvium/bedrock interface in the southern portion of the site (Carl Cole, personal communication, January 2003).

Flow is horizontal across the low-conductivity fault zones. The faults are assumed to be isotropic (vertical conductivity equals horizontal conductivity), except for the northern bedrock encasement zone (Fault A). Since this fault changes location in a stair-step fashion as model layers increase (Figure 6), the vertical conductivity is set to an arbitrarily low value. This forces horizontal flow through this fault, consistent with the conceptual model.

5.2.2 Adjustments to Constant-Head Boundaries

Values of constant head for the lateral-boundaries were calibrated to two primary targets as described in Section 5.1: measured water levels near the grid boundary, and regional estimates of subsurface inflow (Razem and Steiger, 1981; HEC, 1994; Lambert and Stolp, 1999).

At the Tooele site, groundwater generally flows in a southeast to northwest direction. At the southeast model boundary where the water enters the domain, constant head values were set equal to measurements taken in off-site wells by the U.S. Geological Survey (Lynette Brooks, written communication, January 2004) (Figure 5). Constant head values were also adjusted to produce a good match with on-site wells adjacent to the grid boundary. No constant head boundary is used where faults intersect the model boundary. Constant head values at the northwest boundary were adjusted to produce a good match to on-site well measurements. Head values increase with depth to simulate the measured vertical gradients at the northern end of the site. Along the northeast boundary, a constant head boundary is used along rows 1-31 and rows 121-171. Along rows 32-120, a no-flow boundary was specified. In this area, it is assumed that flow is parallel to the model grid boundary. In areas where head is specified, values of head were set equal to measurements taken at off-site wells by the U.S. Geological Survey (Lynette Brooks, written communication, January 2004).

The regional contour map of groundwater elevations in the southeast Tooele Valley developed by the U.S. Geological Survey (Lynette Brooks, written communication, January 2004) was used as a general guide for a regional representation of the flow regime. Analysis of the U.S. Geological Survey map indicated that significant inflows transect the southeast corner of the model grid, and significant outflows transect the northeast corner of the model grid. Figure 20 presents a vector map of groundwater flow simulated by the model.

Table 3 presents the final specifications for the constant heads in the calibrated groundwater model.

Table 3. Specifications for Model-Edge Constant Head Boundaries

		Layer	Head (ft)
Southeast Boundary	Southwest of Fault E	1-9	4482-4475
	Northeast of Fault E	1-2	*No Flow*
		3-9	4389-4393
Northwest Boundary	Northeast of Fault E	1-4	*No Flow*
		5-6	4284
		7	4289
		8-9	4311
	Southwest of Fault E	1-9	4314
Northeast Boundary	Southern Alluvium Rows 121-171	1-2	*No Flow*
		3	4393-4379
		4	4393-4379
		5-9	4393-4379
	Northern Alluvium Rows 1-31	1-2	*No Flow*
		3	*No Flow*
		4	*No Flow*
		5-9	4322-4314

5.2.3 Adjustments to TCE Source Area and Concentrations

Passive and active soil-gas sampling in the vadose zone at the industrial area (Kleinfelder, 2002a) provides a good indication of the source locations and a reasonable indication of current, relative source concentrations. However, the soil-gas concentrations cannot be translated into reliable estimates of TCE mass flux to the water table. Additionally, the soil-gas results provide very limited information about the historical pattern of TCE source release, which probably began over 60 years ago. Therefore, the recharge concentrations of the TCE sources and to some extent the timing of TCE releases are treated as adjustable parameters in the transport model. Initial estimates of source concentrations were based on the prior transport model (HEC and GeoTrans, 2003). After making many transport simulations, with adjustments to recharge concentration values in the source zones, a final best-estimate set of TCE recharge concentrations was determined. These concentrations are presented in Table 4. The main difference between the 2003 model and the 2004 model is the mass flux from the Building 679 source. The source area was increased by a factor of two and recharge concentrations were decreased by 25 percent (from 1,100,000 µg/L to 825,000 µg/L). This modification results in increasing the mass flux by a factor of 1.5 (from 249,000,000 µg/d to 374,000,000 µg/d). Note that the solubility of TCE is approximately 1,100,000 µg/L.

Table 4. Calibrated Model Source Concentrations

Source Name	Model Area (ft^2)	Recharge Rate (ft/d)	Recharge Concentration (µg/L)			
			Pre IWL (1942-64)	IWL (1965-87)	Post IWL (1988-93)	Pumping (1994-2003)
Ditch B	3.2×10^5	0.0002	13,000	13,000	8,500	8,500
Ditch C	3.2×10^5	0.0002	13,000	13,000	8,500	8,500
Ditch D	3.2×10^5	0.0002	6,500	6,500	4,500	4,500
Ditch E	5.2×10^5	0.0002	6,500	6,500	4,500	4,500
IWL Ditch	8.8×10^5	0.0001	0	13,000	7,800	7,800
OIWL	6.0×10^5	0.0002	13,000	13,000	7,800	7,800
IWL	2.0×10^5	0.0001	0	19,500	5,850	5,850
East Landfill	11.6×10^5	0.0002	0	20,000	20,000	30,000
West Landfill	9.6×10^5	0.0002	0	1,000	1,000	1,000
Building 619	3.6×10^5	0.0002	10,000	10,000	10,000	10,000
Building 679	0.8×10^5	0.0002	0	825,000	825,000	825,000
Spreading Area	9.2×10^5	0.0001	13,000	6,500	4,500	4,500

Note that the pattern of source activity matches what is known about site history. Ditches B, C, D, and E are active (higher source concentration and mass input) from 1942 until 1988. The concentration at the spreading area is large between 1942 and 1964 (when it was likely in use) and lower after that (some source is remaining in the vadose zone). The OIWL remains active from 1965 until 1988 because of its proximity to the other ditches (it effectively represents part of the IWL interceptor ditch). The IWL and IWL interceptor ditch become active sources in 1965. In 1988, concentrations at all of the ditches and the IWL are lowered to signify their closure (again, TCE is remaining in the vadose zone). The sanitary landfill sources (east and west) begin in 1965, approximately when solid waste disposal began there. The Building 679 source also begins in 1965 – this part of the industrial area was apparently not used heavily in the early years of site operation (Kleinfelder, 2002a) and this start time resulted in a reasonable calibration to the Northeastern Boundary plume lobe. For lack of historical information, the Building 619 source is assumed to be a constant concentration from 1942 to present. For all source areas, TCE travel time in the vadose zone is neglected. In reality, there could be many years between a change in source behavior at the surface and the realization of that change at the water table.

Figure 19 presents the mass inflow from the four general source areas – the entire wastewater system (including ditches, lagoons, and the spreading area), the sanitary landfill (eastern and western sources added), the building 619 area, and building 679. The mass input to the water table is calculated as the source concentration times the source area times the recharge rate. Prior to 1965, the wastewater system is the main source in the model. After that time, the main source becomes Building 679, and the sanitary landfill source is also important.

5.2.4 Adjustments to Effective Porosity and Sorption Coefficient

Minor adjustments were made to parameters that affected transport of TCE in the model. The sorption coefficient (K_d), was kept at the value that was calibrated in the 2003 model (HEC and GeoTrans, 2003. This value is 0.06 L/kg and results in a retardation coefficient of 1.5.

Effective porosity was adjusted from its calibrated value of 0.20 in the 2003 model (HEC and GeoTrans, 2003). Three zones of porosity were used, representing the bedrock block, the faults, and all other areas. An effective porosity of 0.20 was used across much of the model domain; however, this needed to be adjusted downward in certain discrete areas. Effective porosity in the bedrock block was set to 0.1. This is a reasonable value given the lithology and fractured nature of the bedrock block. An effective porosity of 0.04 was used in the faults, which is also consistent with their hypothesized makeup.

5.3 Calibration Results

5.3.1 Calibration to Current Conditions – Observed Water Levels

The model matches current water levels very well (Figure 21). The table in Appendix C presents model residuals for individual wells. Statistical results of the model calibration are presented in Table 5. Figure 22 compares modeled and observed heads to the ideal 1-to-1 fit and Figure 23 presents a histogram of model residuals (residual = modeled head – observed head). Figure 24 shows the simulated potentiometric surfaces for layer 5.

Table 5. Steady-State Model Head Calibration Statistics

Statistic	Value (ft)
Mean Absolute Residual	1.36
Mean Residual	0.08
Root Mean Square Residual	2.07
Minimum Residual	-10.04
Maximum Residual	7.65

The Mean Absolute Residual (MAR) represents the average difference between simulated and measured water levels. In the 2003 model study (HEC and GeoTrans, 2003), the MAR was 1.76 ft for a smaller data set of 184 calibration targets. The current model produces a MAR of 1.55 using the data set from the 2003 calibration study. A complete discussion of calibration statistics and target selection is presented in Appendix B. The residual mean represents the sum of all residuals (positive and negative) divided by the total number of calibration targets. A residual mean near zero indicates that there is little overall bias toward over-prediction or under-prediction of heads.

5.3.2 Calibration to Estimated Subsurface Inflow

The total simulated steady-state subsurface inflow, without pumping, is 4.9×10^6 ft^3/d. This is within 5% of that estimated by regional studies and well within the margin of error of the

estimate. The good match between estimated inflows and simulated inflows provides additional validation of model parameters. The total simulated subsurface inflow into the model domain with pumping is 5.4 x 10^6 ft^3/d. This increase in flow is induced by increasing the hydraulic gradient between the model boundaries and the central part of the model. Approximately 80% of the subsurface inflow occurs through the upper 100 ft (upper 3 layers) of the model.

5.3.3 Calibration to Observed Drawdown in the Bedrock Block

Across the most of the site, the measured change in water levels induced by pumping is less than 2 ft; however, in the encased bedrock block zone, the measured long-term change was 35-40 ft. During calibration, the configuration of the bedrock block was modified, the bedrock-block hydraulic conductivity was raised, and the total inflow into the model domain was decreased by over 25%. The calibrated model was run with and without extraction wells. The model produced a simulated drawdown of 35 to 40 ft in the bedrock block, consistent with measured drawdown between 1992 and 1998.

5.3.4 Calibration to Observed TCE Concentrations

Figures 25 through 32 show the simulated TCE transport plume in 1965, 1986, 1989, 1992, 1995, 1998, 2001, and 2003. In all of these figures, the contoured concentration is the maximum concentration simulated in any of the nine model layers (generally the uppermost active layer). The 1965 plume is shown to give a sense of the early-time plume development in the model. The later times correspond with the midpoints of the six calibration time frames presented in Section 5.1.3. In each of Figures 25 through 32, the observed (averaged within the time frame) concentrations are plotted along with the simulated plume for direct comparison. Note that similar colors are used to represent observed (symbols) and modeled (color flood) concentrations. In making this comparison it is assumed that the midpoint of the screened interval of a well has the maximum observed concentration in the vertical sequence represented by the well. It is also assumed that the midpoint of the screened interval corresponds to the model layer where the maximum concentration is simulated.

These figures are from the final best-calibrated TCE transport simulation. The modeled results match the observed concentrations fairly well in the source areas, and in most parts of the downgradient plume. There are some weaknesses with the calibration quality, however. For instance, there is a line of wells in the northern alluvium south of extraction well E-11 and northwest of the bedrock block where concentrations have been consistently measured above 25 µg/L. All model simulations consistently underestimated these observed concentrations. Note however, that the observed concentration distribution is complicated: it does not show a consistent pattern of decreasing away from the source. This observation suggests complex source term behavior that is difficult to conceptualize and represent in a model. Calibration to observed concentrations is also complicated by the effectiveness of the groundwater extraction system. There are other differences between simulated and observed concentrations, primarily on the edges of the model plumes. Note that some non-detect points that appear on these figures are from depths below (or above) the simulated TCE plume.

In general, the model reproduces observed concentrations and changes in concentrations better than the prior model (HEC and GeoTrans, 2003). An area of particular improvement is with the trajectory and concentrations in the Northeastern Boundary plume. It should also be noted that the calibration to observed conditions in 2003 is particularly good. An accurate representation at the end of the calibration period is important because this period represents the initial conditions for ensuing predictive simulations.

5.3.5 Calibration to Measured TCE Mass Extracted

Figure 33 shows the amount of mass removed by each extraction well in the simulation. The totals are presented in Table 6. Note that a few wells in the bedrock block are removing much of the mass in the simulation. The cumulative mass removed during the simulation between startup and the end of 2002 is 1000 kg (2199 lb); between startup and the end of 2003 is 1135 kg (2499 lb). The cumulative TCE extracted that is modeled to the end of 2002 is within 10 percent of the cumulative TCE removal amount of 992 kg (2187 lb) measured through June 2002. Note that the current model matches this quantity significantly better than the 2003 model (HEC and GeoTrans, 2003) which overestimated TCE removal by 44 percent.

Figure 34 compares the total mass extracted with the total mass input (all source zones). Figure 35 shows the TCE mass in the aquifer over the course of the simulation. The extraction system does have an immediate effect on aquifer mass, but the amount of mass continues to rise at a slower rate. This happens in part because the significant mass sources that are modeled at Building 679 and at the eastern portion of the landfill are not targeted by the current extraction system.

Table 6. Simulated TCE Mass Removed by Each Extraction Well (1994-2003)

Well ID	Location	Extraction Rate (gpm)	Mass Extracted (kg)
E-04	Bedrock Block	413.25	211
E-10	Bedrock Block	753.14	190
E-02-2	Northern Alluvium	489.85	129
E-14	Northern Alluvium	497.48	122
E-05	Bedrock Block	555.58	113
E-09	Bedrock Block	783.28	101
E-03-1	Bedrock Block	308.57	72
E-02-1	Northern Alluvium	145.63	50
E-11	Northern Alluvium	531.89	46
E-15	Northern Alluvium	537.04	37
E-06	Southern Alluvium	295.60	34
E-08	Bedrock Block	165.16	17
E-13	Northern Alluvium	507.33	9
E-03-2	Northern Alluvium	227.22	3
E-01	Northern Alluvium	165.24	3
E-12	Northern Alluvium	0.11	0

5.4 Notes on Numerical Convergence and Water Balance

The MODFLOW Preconditioned Conjugate Gradient (PCG2) algorithm was used for the final numerical simulations. Head closure criterion was set to 0.0005 ft. Simulated water levels in the uplifted bedrock were very sensitive to the mass balance error of the numerical solution. Mass balance errors as low as 0.1% resulted in head changes in the bedrock of greater than 1 ft. The final numerical simulation attained a mass balance error of less than 0.01%. Water balance information for the current-conditions simulation is presented in Table 7. The flow from inflow in Table 7 is slightly greater than cited in Section 5.3.2. This is due to flow into and out of the model between constant head cells along the grid boundary. The total simulated subsurface inflow into the model domain with pumping is 5.4×10^6 ft^3/d. The total simulated subsurface inflow into the model domain without pumping is 4.9×10^6 ft^3/d.

Table 7. Steady-State Flow Model Volumetric Water Balance

Boundary	Inflow (ft^3)	Outflow (ft^3)
Wells (Injection & Extraction)	9.7835×10^5	1.4700×10^6
Recharge	1.4026×10^5	0
CH Boundaries	6.3812×10^6	6.0296×10^6
Total	7.4998×10^6	7.4997×10^6
Difference (Inflow – Outflow)	112.5	

5.5 Capture Zones

The particle-tracking processor MODPATH (Pollock, 1989) is used to delineate the simulated capture zones for each extraction well (Figure 36). The different colors of the zones correspond with the well-symbol colors of the extraction well. The capture zones shown in this figure are for contamination in model layer 5. This layer is appropriate for viewing capture of contamination within and northwest of the bedrock block. The figure does not necessarily show which source areas would be captured as this contamination originates above layer 5.

6. TCE TRANSPORT PREDICTIONS

The calibrated model is used to predict TCE transport over the next five years with and without operation of the extraction/injection system. The five-year simulation period is selected to provide a reasonable horizon for near-term planning. For each case, three representations of the sources are modeled:

- all sources continuing at the current levels,

- all sources having a concentration of zero from present day, and
- all sources declining linearly from current levels to zero in five years.

The range of future mass flux represented by these scenarios is intended to provide a range of possible future plume migration. The zero concentration source term simulation also shows the movement of mass that is currently in place in the system.

6.1 Continued Operation of the Extraction/Injection System—Current Source

In the first scenario, another five years are simulated with the transport model. The initial concentrations for this simulation are the final (January 1, 2003) concentrations from the calibration model (Figure 32). The source concentrations for recharge and extraction/injection rates at wells remain the same as in the last part of the calibration simulation.

The predicted concentration plumes after three years (2006) and five years (2008) are shown in Figures 37 and 38, respectively. There are small, but observable differences in the plume locations and concentrations relative to present conditions. The main plume remains about the same, while the Northeastern Boundary plume continues to expand along and across Fault D.

6.2 Continued Operation of the Extraction/Injection System—No Source

The second scenario is similar to the first, except that all source concentrations for recharge are changed to zero at the onset of simulation. The initial concentrations for this simulation are also the final (January 1, 2003) concentrations from the calibrated model. This scenario therefore simulates plume migration of contaminants already in the system with no further addition of contamination from sources or the vadose zone.

The predicted concentration plumes after three and five years are shown in Figures 39 and 40, respectively. The front edge of the plume (within and northwest of the bedrock block) is nearly identical to the first scenario. However, concentrations in the former source area (southeast of the bedrock block) have decreased slightly. In addition, there is a small amount of migration away from the source areas.

6.3 Continued Operation of the Extraction/Injection System—Linearly Declining Source

The third scenario is intermediate to the first two, with source concentrations declining linearly with time from current conditions to zero in five years.

The predicted concentration plumes after three (2006) and five years (2008) are shown in Figures 41 and 42, respectively. As expected, based on the similarity between the first two scenarios, the results are very similar to both, with the largest differences in the source areas.

6.4 No-Further-Action—Current Source

In the fourth scenario, the extraction and injection rates are set to zero another five-year simulation is made. The pre-pumping flow field is used for this simulation, with initial concentrations from the end of the calibration run. All sources remain active at their current levels throughout the simulation.

Figures 43 and 44 show the plume after three and five years, respectively, with no extraction or injection. The front edge of the plume (northwest of the bedrock block) is slightly more advanced than the first scenario, which involved continued extraction/injection. Migration of the Northeastern Boundary plume is similar to the first scenario.

6.5 No-Further-Action—No Source

For the fifth scenario, the extraction and injection rates are set to zero while the source concentrations are set to zero, and another five-year simulation is made. The pre-pumping flow field is used for this simulation, with initial concentrations from the end of the calibration run.

Figures 45 and 46 shows the plume after three and five years, respectively, with no extraction or injection. The plume configuration northwest of the bedrock block is very similar to the simulation involving current sources (the previous scenario, Figures 43 and 44). However, concentrations in the source area are reduced and the plume has begun to migrate away from the source area.

6.6 No-Further Action—Linearly Declining Source Term

The sixth scenario is intermediate to scenarios four and five, with source concentrations declining linearly with time from current conditions to zero in five years.

The predicted concentration plumes after three (2006) and five years (2008) are shown in Figures 47 and 48, respectively. As expected, based on the similarity between scenarios four and five, the results are very similar to both, with the largest differences in the source areas.

6.7 Summary of Solute Transport Predictive Simulations

The six predictive solute transport simulations produce results that are very similar. The continued use of the extraction/injection system results in what appears to be slightly less mass and lower concentrations within and northwest of the bedrock block. The Northeastern Boundary Plume is unaffected by the extraction/injection system. The difference between a continuing source and no-source is limited to the source area itself: concentrations reduce slightly and some plume migration is noted for the no-source simulations. A linearly decreasing source term shows results that are intermediate to simulations involving the current source and no source.

Note that in each case, the TCE plume moves slowly – on the order of 100 ft/yr – in the simulation. These three- and five-year simulations support the hypothesis that only limited plume migration will take place during the period where the extraction/injection system is turned off.

7. ANALYSIS OF SENSITIVITY AND UNCERTAINTY

7.1 Sensitivity Analysis of Flow Model

Sensitivity analysis is used to estimate the uncertainty in a model caused by uncertainty in aquifer parameters and boundary conditions. During sensitivity analysis, model parameters are systematically changed, one at a time, within a predefined plausible range factor. The accompanying change in head values, relative to the calibrated head values, are then analyzed as a measure of the sensitivity of the model to that particular parameter. Factors of 2.0 and 0.5 were selected as plausible range factors. Model parameters on which sensitivity analysis was performed included horizontal and vertical hydraulic conductivity, and areal recharge.

The calibrated model produced a Mean Absolute Residual (MAR) of 1.36 ft between simulated and measured water levels. The MAR incorporates simulated water levels at all calibration targets across the study area. Sensitivity analysis was performed using this value as a basis for the effects of varying parameters on model results. Thus, in general terms, the greater the change in MAR, the more sensitive model results are to the simulated parameter. Because calibration targets are not evenly distributed throughout the model domain, care should be taken to evaluate the changes in MAR in the proper context.

As described in Table 8, the initial sensitivity analysis consisted of varying horizontal and vertical hydraulic conductivity across the site. Values of vertical hydraulic conductivity control leakance between model layers. Because the drop in water levels simulated in fault zones are as great as 120 ft across a 200 ft cell, the vertical hydraulic conductivity has a larger influence on flow in fault zones. In other words, groundwater flow direction has a larger vertical flow component across fault zones. Thus, a separate sensitivity analysis was performed on vertical hydraulic conductivity of alluvium and bedrock, and fault zones.

Table 8. Spatial Sensitivity Analysis of Simulated Hydraulic Conductivity

Hydrogeologic Parameter	K x 2.0 MAR (ft)	K x 0.5 MAR (ft)
Horizontal Hydraulic Conductivity (entire site)	3.02	10.78
Vertical Hydraulic Conductivity (alluvium/bedrock)	1.47	1.53
Vertical Hydraulic Conductivity (fault zones)	1.46	1.42

As described in Table 9, a more detailed sensitivity analysis was performed on various hydrologic units of the site. In this analysis, the hydraulic conductivity of specific structures were varied while all other values were held constant. This provided a basis for identifying structures that have the greatest control on flow and transport. Structure specific sensitivity analysis can also provide a guide for data calibration.

Table 9. Structure Specific Sensitivity Analysis

Geologic Structure	K_h x 2.0 MAR (ft)	K_h x 0.5 MAR (ft)
Southern Alluvium	2.09	3.04
Northern Alluvium	3.51	4.63
Bedrock	1.36	1.59
Fault Zones	6.52	6.95
Upgradient Encased Bedrock Fault	3.28	2.36
Downgradient Encased Bedrock Fault	2.10	1.96
North-South Trending Faults	2.02	1.41
Faults Adjacent to Encased Bedrock	2.73	2.25

From this analysis, the hydraulic conductivity of fault zones, specifically the upgradient encased bedrock fault are the most sensitive parameters. Simulated results were also sensitive to changes in hydraulic conductivity in the northern alluvium.

As described in Table 10, values of recharge were also varied within the plausible range factor. Because of the relatively large volume of estimated subsurface inflow (greater than 5 x 10^6 ft/day) into the model domain relative to the estimated recharge (0.14 x 10^6 ft/day), changes in recharge values do not significantly impact water levels across the site.

Table 10. Sensitivity Analysis of Areal Recharge

Model Parameter	R x 2.0 MAR (ft)	R x 0.5 MAR (ft)
Areal Recharge (R)	1.35	1.37

7.2 Uncertainty of Flow Model

Darcy's law describes groundwater flow through a porous medium:

$Q = -KA\ (\partial h/\partial l)$

where Q is the volumetric flow (ft^3/day), A is the flow area (ft^2), K is the hydraulic conductivity (ft/day) and $\partial h/\partial l$ is the hydraulic gradient.

Values of flow (Q) and hydraulic conductivity (K) are interdependent. For a steady state application, without stresses (such as recharge and pumping), calibrated values of hydraulic

conductivity can vary greatly. For example, identical heads and gradients can be simulated by doubling or dividing by half both flow and hydraulic conductivity. Measurements of the water level gradient ($\partial h/\partial l$) at the site have been conducted semi-annually since 1992. In the current calibration, 195 water elevation data points are used. An accurate description of water levels and their spatial distribution has been developed. The uncertainty in the flow model lies primarily in the uncertainty of estimated values of hydraulic conductivity (K) and subsurface inflow (Q).

Lambert and Stolp (1999) estimated inflows into the study area to be 5.2×10^6 ft^3/day. This estimate was based on a regional water balance model. Data used in this study was gathered prior to the commencement of operation of the TEAD pump-and-treat system in December 1993. This value is currently being adjusted based on recently gathered data and will likely be lowered slightly (Bert Stolp, phone conversation, March 2004). The "pre-pumping" inflow simulated by the 2004 model is 4.9×10^6 ft^3/day. The uncertainty in values of hydraulic conductivity (K) is reduced by multiple pumping tests and slug tests that have been performed across the site. The most reliable estimates of hydraulic conductivity were determined to be a long-term pump test performed by Papadopulus (1987) in the northern alluvium, and numerous pump tests conducted in the encased bedrock block (HEC, 1994). Measured values were incorporated into the calibrated model. The model was additionally calibrated to long-term measured drawdown in the encased bedrock zone. The ability of the model to successfully integrate three independent data sets i.e. inflow, hydraulic conductivity, and drawdown, increases the reliability of model predictions.

Groundwater flow in the study area is highly heterogeneous. Relatively thin zones of low conductivity largely control the flow regime, and therefore, contaminant transport. The simulated location and permeability of these zones is determined primarily by measured water level gradients. Additionally, geophysical analysis has been performed to provide a more geologic basis for fault delineation. The uncertainty in the flow model is largely determined by uncertainty in estimates of subsurface inflow and hydraulic conductivity. The calibrated model produced a good correlation of these two values, which were estimated from independent data. This correlation reduces the uncertainty and increases the predictive reliability of the model.

7.3 Sensitivity Analysis of Transport Model

Sensitivity analysis was conducted informally on the transport model as a part of the calibration process. This analysis involved observing the model response to changes to porosity, distribution coefficient, and source term magnitude and temporal behavior. These simulations were conducted by making changes that were believed to provide a better calibration; therefore a structured sensitivity analysis was not conducted. A structured sensitivity analysis is planned to be included in an addendum to this report.

8. CONCLUSIONS AND RECOMMENDATIONS

8.1 Overall Model Assessment

This model calibration study includes several changes and additions to the prior models of TEAD. The model grid was extended 10,200 ft to the northeast and 1,200 ft to the southeast to allow for a more accurate representation of the regional flow regime. A revised conceptualization of the bedrock, based upon recent geophysical studies and analysis of bore logs, was integrated into the model. Three new City of Tooele pumping wells were input into the model. The incorporation of a larger calibration data set allowed for a more complex and accurate numerical representation of the site. Transport-model calibration was also included in this analysis.

The model was calibrated to 195 water levels. Additionally the model was calibrated to regional estimates of subsurface inflow, measured drawdown in the uplifted bedrock block, and the migration of the TCE plume. The final model head calibration produced an absolute mean error of 1.36 ft. The absolute mean error of the prior (2003) calibration study was 1.76 ft. The prior study used 184 calibration targets. The model also reproduces the approximately 35-40 ft observed drawdown in the bedrock block due to groundwater pumping. The model matches prior estimates of groundwater inflow into the model domain, and simulates the general regional flow domain.

The TCE plume produced by the model is a reasonable match to the observed plume, both under current conditions and during the development of the plume. The modeled results compare better with observed results than the prior model (HEC and GeoTrans, 2003), particularly for the Northeastern Boundary plume area. There are a few noted exceptions where the model does not match observed conditions as well as other areas. In particular, the model under-predicts some concentrations in the northern alluvium, but may over-predict concentrations in other areas of the model. Approximately 992 kg of TCE have been removed by the groundwater extraction and treatment system since June 2002 (Kleinfelder, 2002b). The model simulates TCE removal of 1135 kg, which is within ten percent of measured.

8.2 Modeling Conclusions

Groundwater flow across the site can be conceptualized as consisting of relatively flat gradients located in broad areas between fault zones, where dramatic drops in water levels occur over a very short distance. Model results indicate that these fault zones are the controlling hydrologic structures in the model area. The volume and direction of subsurface inflow into the model domain controls the migration of the contaminant plume and the calibrated range of hydraulic conductivity values.

The transport model indicates a few important aspects of the TEAD site:

- The Building 679 (Northeastern Boundary plume lobe) and sanitary landfill sources contribute significantly to the overall size and extent of plumes at the TEAD.

- The existing pump-and-treat system contains the main lobe of the plume, and the lobe emanating from the sanitary landfill, but not the Northeastern Boundary plume.

- A few (six) of the wells in the existing pump-and-treat system are providing the majority of TCE mass removal.

- If pump-and-treat activities are halted, and the sources continue to contribute TCE to groundwater, then plume extent and concentrations do not appear to change significantly during the five-year simulation period.

- If the sources are no longer a factor, the plume north of the bedrock block will behave much like the scenario with a continuing source, however, the source areas will begin to diminish in concentration.

8.3 Recommendations for Improving Site Understanding and Minimizing Uncertainty

The model is sensitive to the location and hydraulic conductivity of fault zones. The location of fault zones were based largely on delineating areas of steep water level gradients. Future data gathering efforts should focus on further delineating the location, importance, and nature of these fault zones. In 2004, it is anticipated that 7-9 new monitoring wells will be constructed off-depot in the area of the potential migration of the Northeastern Boundary plume. Additionally, several new wells will be constructed on-site in source areas and deeper zones of the Northeastern Boundary plume. Data from these wells will provide a greater understanding of the flow regime and lateral and vertical extent of the plume in areas where minimal data currently exists.

The U.S. Geological Survey estimate of inflow in the study domain (Stolp, 1994) was based on a regional water balance study. There is significant uncertainty in this estimate. The model estimate of inflow is based on measured flow gradient and hydraulic conductivity from numerous pumping tests. There is also uncertainty in this estimate, especially in areas where there is little or no field measurement data of water levels and hydraulic conductivity. The U.S. Geological Survey is currently completing an update of a regional hydrologic model of the Tooele Valley, estimates of inflow from this study should be integrated into the current flow model.

The contaminant transport model predictions are subject to significant uncertainty, as transport-model results often are. Some of the difficulties encountered in calibrating this model to TCE plumes are mentioned in Section 8.1. Further investigation into the possibility of preferred flow paths could help to make TCE predictions more reliable. These investigations could be field studies or modeling analyses that specifically evaluate anomalous conditions.

A detailed sensitivity analysis that treats each source area independently could be useful for establishing the relative strength of each source. This information is useful for a better understanding of the solute transport processes at Tooele and for prioritizing source areas for additional characterization or remediation.

Additional characterization of the source areas could indicate that the mass flux to the vadose zone is already rapidly decreasing. This may be especially true at Building 679, where a soil-vapor extraction system may have removed much of the source and vadose zone contamination.

8.4 Suggestions for Future Analysis

Transient variability in water levels across the study area has been observed since the installation of monitoring wells. This variability has been addressed by computing average water levels for certain time periods and using these averages as calibration targets for steady state models. Although this is an appropriate and widely used procedure, it may be useful to conduct a transient simulation to better understand the effect of transient variability of water levels and pumping. To make this potentially complex analysis tractable, a generalized transient calibration that would simulate long-term changes in water levels, using long stress periods, and averaged pumping data is proposed. There are two largely unknown independent variables that will control this transient calibration: subsurface inflow, which varies with climatic variations; and porosity and specific yield, which are a function of the flow medium.

A period of reduced operations of the pump-and-treat system is proposed to begin in June 2004. The recovery of water levels following shutdown will be measured continuously at specified locations. This shutdown event will be will provide a unique and valuable opportunity to obtain physically based estimates of porosity, specific yield and their distribution across the study area.

The groundwater flow model should be calibrated to transient data from the shutdown of the pump-and-treat system. Results from this calibration should then be integrated into the transient calibration of long-term water level fluctuations. The transient groundwater flow model should be used for application of the transport model. The groundwater flow and contaminant transport models should continue to be developed simultaneously. Initial results of the contaminant transport model should be used in the calibration of the groundwater flow model. An updated transport model should then be developed. Possible modifications to the transport model include variations in mass input and zonation of transport parameters such as dispersivity and K_d.

The transport model could be used to investigate the sensitivity of results to the different source areas. This would allow restoration activities to be focused on the sources that are most likely to present environmental compliance issues or those that are likely to lead to the greatest ecological and health risks.

The transport model is used here to draw general conclusions about the plume and the current extraction/injection system. The calibration quality of the model is sufficiently good to draw such conclusions. A more detailed analysis of potential remediation alternatives, perhaps including different extraction configurations or alternative technologies, could significantly benefit TEAD.

9. REFERENCES

Becker, D.J., and D.D. Blackwell, 1993, "Gravity and Hydrothermal Modeling of the Roosevelt Hot Springs Area, Southwestern Utah", *Journal of Geophysical Research*, v. 98, n. B10, pp. 17,787-17,800.

Freyberg, David, 1988, "An Exercise in Ground Water Model Calibration and Prediction", *Groundwater*, Vol, 26, 3, pp. 350-360.

Gates, J.S., 1965, "Reevaluation of the Ground-Water Resources of Tooele Valley, Utah", Utah State Engineer, *Technical Publication* No. 12.

Greenwald, Rob, 1999. "Hydraulic Optimization Demonstration for Groundwater Pump-And-Treat Systems", HSI GeoTrans, Inc., Prepared for Dynamac Corporation and U.S. Environmental Protection Agency.

Hood, J.W., and Waddell, K.M., 1969, "Hydrologic reconnaissance of Rush Valley, Tooele County, Utah", Utah State Engineer Technical Publication 23, 63 p.

HEC, 1994, "Hydrogeologic Flow Model for the Tooele Army Depot, Utah", U.S. Army Corps of Engineers- Hydrologic Engineering Center *Project Report* PR-25, 87 p. plus app.

HEC, 1995, "Preliminary Transient Calibration of Hydrogeologic Flow Model for the Tooele Army Depot, Utah", U.S. Army Corps of Engineers- Hydrologic Engineering Center, 29 p. plus app.

HEC, 1996, "Tooele Army Depot Hydrologic Flow Model- FY96 Work Performed", U.S. Army Corps of Engineers- Hydrologic Engineering Center, 47 p.

HEC, 1998, "Tooele Groundwater Flow Model- 1997 Recalibration", U.S. Army Corps of Engineers- Hydrologic Engineering Center, 46 p.

HEC, 1999, "Hydrogeologic Flow Model and Accompanying Transport Model for the Tooele Army Depot, Utah", U.S. Army Corps of Engineers- Hydrologic Engineering Center *Project Report* PR-42, 136 p. plus app.

HEC, 2002, “Tooele Army Depot Groundwater Flow Model 2001/2002 Recalibration Study”, U.S. Army Corps of Engineers- Hydrologic Engineering Center, 57 p.

HEC and GeoTrans Inc., 2003, “Tooele Army Depot Groundwater Flow and Contaminant Model (2003)”, U.S. Army Corps of Engineers- Hydrologic Engineering Center *Project Report* PR-50, 80 p. plus app.

James M. Montgomery and Assoc., 1986a, “Final Geotechnical Report for the Ground-Water Quality Assessment at Tooele Army Depot, Utah”, Prepared for the U.S. Army Corps of Engineers, Contract No. DACA 87-86-C0038, August 1986.

James M. Montgomery and Assoc., 1986b, "Engineering Report for Closure of the Industrial Waste Lagoon at Tooele Army Depot, Utah", Prepared for the U.S. Army Corps of Engineers, Contract No. DACA 87-84-C-0054, March 1986.

James M. Montgomery and Assoc., 1986c, "Standard Operating Procedures for Aquifer Test and Evaluation, Monitoring Well Installation, Sampling and Analysis and Quality Control and Quality Assurance - Ground-Water Quality Assessment at the Industrial Waste Lagoon, Tooele Army Depot, Utah", Prepared for the U.S. Army Corps of Engineers, May 1986.

James M. Montgomery and Assoc., 1986d, "Final Geotechnical Report for the Ground-Water Quality Assessment at Tooele Army Depot, Utah", Prepared for the U.S. Army Corps of Engineers, Contract No. DACA 87-86-C-0038, August 1986.

James M. Montgomery and Assoc., 1987a, "Alternate Concentration Limit Position Paper for Tooele Army Depot, Utah", Prepared for U.S. Army Corps of Engineers, March 1987.

James M. Montgomery and Assoc., 1987b, "Ground-Water Quality Assessment Engineering Report for Tooele Army Depot, Utah", Prepared for the U.S. Army Corps of Engineers, March 1987.

James M. Montgomery and Assoc., 1987c, "Ground-Water Quality Assessment Engineering Report for Tooele Army Depot, Utah, Addendum No. 1", Prepared for the U.S. Army Corps of Engineers, August 1987.

James M. Montgomery and Assoc., 1987d, "Alternative Analysis Engineering Report for Tooele Army Depot, Utah", Prepared for the U.S. Army Corps of Engineers, July 1987.

James M. Montgomery and Assoc., 1988, “Ground-Water Quality Assessment Engineering report to Tooele Army Depot, Utah”, Prepared for the U.S. Army Corps of Engineers, Contract No. DACA 87-86-C0038, December 1988.

Kleinfelder Inc., 1996, “Technical Evaluation, Groundwater Conditions beneath the Northeast Boundary of the Tooele Army Depot”, prepared for U.S. Army Corps of Engineers, Sacramento District.

Kleinfelder, Inc., 1997, “Technical Memorandum: Conceptual Model for Groundwater Optimization Study, Tooele Army Depot”, prepared for the U.S. Army Corps of Engineers, November 1997.

Kleinfelder Inc., 1998a, “Draft Report, Northeastern Boundary Area Groundwater Investigation Report of Findings, Tooele Army Depot Utah, Vol. 1", prepared for U.S. Army Corps of Engineers, Sacramento District.

Kleinfelder Inc., 1998b, “Draft Report, Northeastern Boundary Area Groundwater Investigation Report of Findings, Tooele Army Depot Utah, Vol. 2", prepared for U.S. Army Corps of Engineers, Sacramento District.

Kleinfelder Inc., 1998c, “Draft Report, Southeastern Boundary Area Groundwater Investigation Report of Findings, Tooele Army Depot Utah, Vol. 1", prepared for U.S. Army Corps of Engineers, Sacramento District.

Kleinfelder Inc., 1998d, “Draft Report, Southeastern Boundary Area Groundwater Investigation Report of Findings, Tooele Army Depot Utah, Vol. 2", prepared for U.S. Army Corps of Engineers, Sacramento District.

Kleinfelder Inc., 1998e, “Draft Report, Eastern Boundary Area Groundwater Investigation Report of Findings, Tooele Army Depot Utah, Vol. 1", prepared for U.S. Army Corps of Engineers, Sacramento District.

Kleinfelder Inc., 1998f, “Groundwater Treatment System Optimization Study for the Main Plume, Tooele Army Depot, Tooele, Utah", prepared for U.S. Army Corps of Engineers, Sacramento District.

Kleinfelder Inc., 2000, “Northeast Boundary Investigation Source Determination Document, Tooele Army Depot, Tooele, Utah”, prepared for U.S. Army Corps of Engineers, Sacramento District.

Kleinfelder Inc., 2002a, “Phase I RCRA Facility Investigation Report for SWMU 58, On-Post Sources and Groundwater Contamination, Tooele Army Depot, Tooele, Utah”

Kleinfelder Inc., 2002b, “Semi-Annual Groundwater Quality Report and Voluntary SWMU Sampling, Spring 2002, Tooele Army Depot, Tooele, Utah”, prepared for U.S. Army Corps of Engineers, Sacramento District.

Lambert, P.M. and B.J. Stolp, 1999, “Hydrology and Simulation of the Ground-Water Flow System in the Tooele Valley, Utah”, U.S. Geological Survey *Water Investigations Report* 99-4014, 60 p.

McDonald, M.G. and Harbaugh, A.W., 1988, "A Modular Three-Dimensional Finite-Difference Ground-Water Flow Model", U.S. Geological Survey *Open-File Report* 83-875.

Metcalf and Eddy Inc., 1993, “Tooele Army Depot Ground-Water Remediation Project Well Completion Reports; Wells E-1, E-2-1, E-2-2, E-3-1, E-3-2, E-4, E-5, E-6, E-7, E-8, E-9, E-10, E-11, E-12, I-1, I-2, I-3, I-4, I-5, I-6, I-7, I-8, I-9, I-10, I-11, I-12, I-13”.

Minsker, B., Y. Zhang, and R. Greenwald, 2003, “Environmetal Security Technology Certification Program, Draft Final Technical Report for Application of Flow and Transport Optimization Codes to Groundwater Pump and Treat Systems”.

Papadopulos, S.S., 1987, “Analysis of Pumping Test Data at Tooele Army Depot”, prepared for James M. Montgomery Consulting Engineers Inc. 20 p.

Parsons, 2002, “Draft Final Addendum to Phase I RCRA Facilities Investigation Report for SWMU 58”

Pollock, D.W., 1989, "Documentation of Computer Programs to Compute and Display Pathlines Using Results from the U.S. Geological Survey Modular Three-Dimensional Finite-Difference Ground-Water Flow Model", U.S. Geological Survey *Open-File Report* 89-381.

Razem, A.C. and S.D. Barthaloma, 1980, "Digital Computer Model of Ground-Water Flow", U.S. Geological Survey *Open- File Report* 80-446.

Razem, A.C. and J.I. Steiger, 1981, "Ground-Water Conditions in Tooele Valley, Utah, 1976-1978", State of Utah Department of Natural Resources, *Technical Publication* No. 69.

Rust Environment and Infrastructure, 1995, “Final RCRA Facility Investigation Report, Phase II Study, Known-Releases SWMUs”, Prepared for U.S. Army Environmental Center, Contract No. DAAA15-90-D-0007, April 1995.

Ryan, K.H., B.W. Nance, and A.C. Razem, 1981, "Test Drilling for Fresh Water in Tooele Valley, Utah”, State of Utah Department of Natural Resources, Division Rights, *Information Bulletin* No. 26.

Sheley, David, 1999, “Pilot Reflection and Refraction Test at Tooele Army Depot (TEAD), Utah

Sheley, David and Jianhua Yu, 2000, “Bedrock Delineation by a Seismic Reflection and Refraction Survey at Tooele Army Depot, Utah”.

Sternberg, B. K., Henley, M. L., and Kay, J. T., 2000, “Geophysical Research at the Tooele Army Depot”.

Stollar, T.L. and Associates, Inc., 1986, "Gravity Survey of a Portion of Tooele Army Depot, Utah", June 1986.

Stolp, Bernard J., 1994, “Hydrology and Potential for Ground-Water Development on the southeastern Tooele Valley and adjacent areas in the Oquirrh Mountains, Tooele County, Utah”, State of Utah Department of Natural Resources *Technical Publication* No. 107, 67 p.

Tooker, E.W. and R.J. Roberts, 1970, "Upper Paleozoic Rocks in the Oquirrh Mountains and Brigham Mining District, Utah", U.S. Geological Survey *Professional Paper* 629-A.

U.S. Geological Survey, 2000, "Groundwater Flow Simulation of Irwin Basin Aquifer System, Fort Irwin NTC, CA", Water-Resources Investigations Report, preliminary draft, not public

Zhdanov, M., Golubev, N., and Pavlov D., 2001, “Gravity Data Interpretation to Determine the Depth to Bedrock in the Northeast Boundary Area of Tooele Army Depot (Additional Analysis of the Data)”

Zheng, C. and Wang, P., 1998, “MT3DMS- Documentation and User’s Guide”, U.S. Army Corps of Engineers Waterways Experiment Station *Technical Report*, 214 p.

(This page is intentionally blank. Figures follow.)

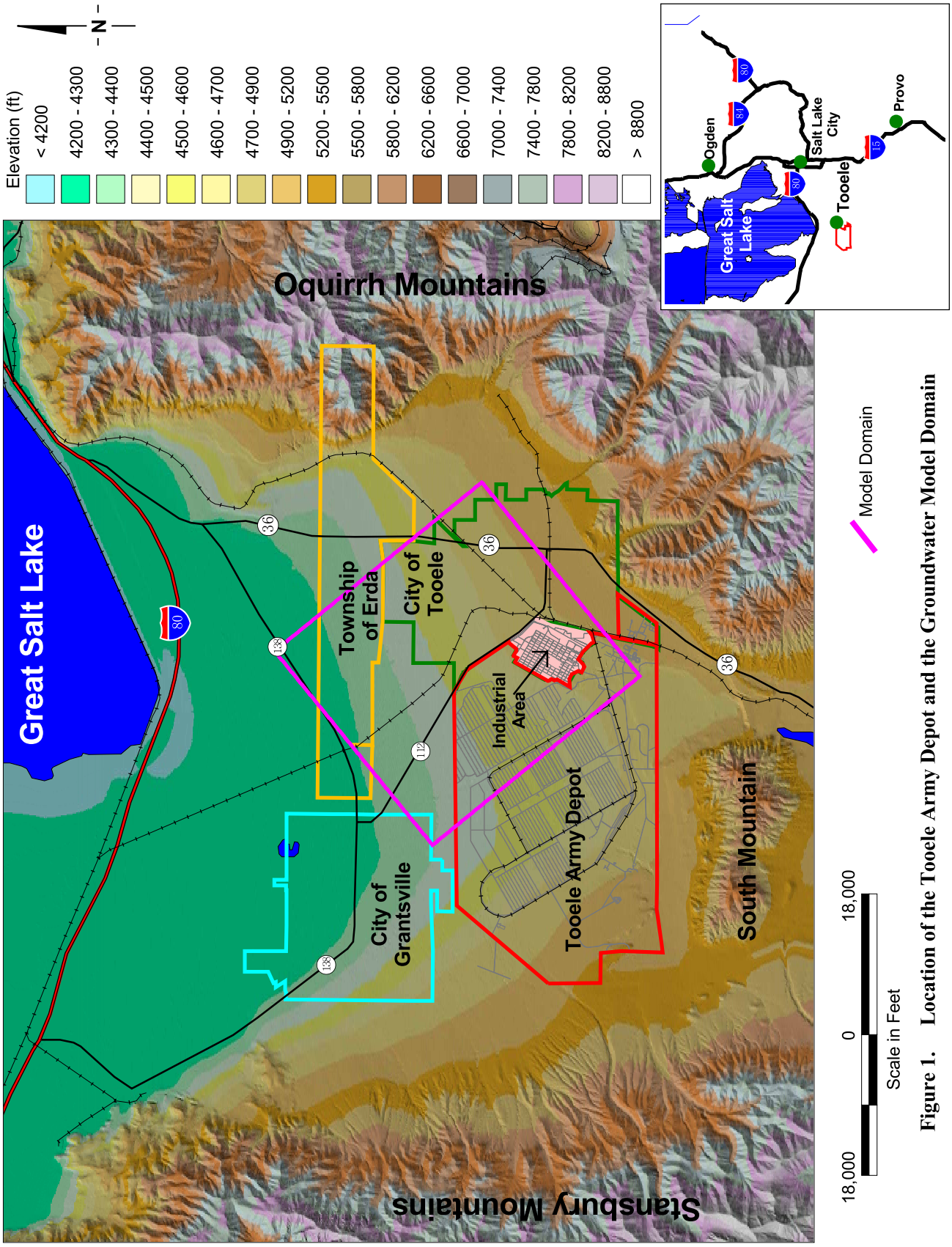

Figure 1. Location of the Tooele Army Depot and the Groundwater Model Domain

P:\tooele\model2004\mapinfo\figure1.apr,regional

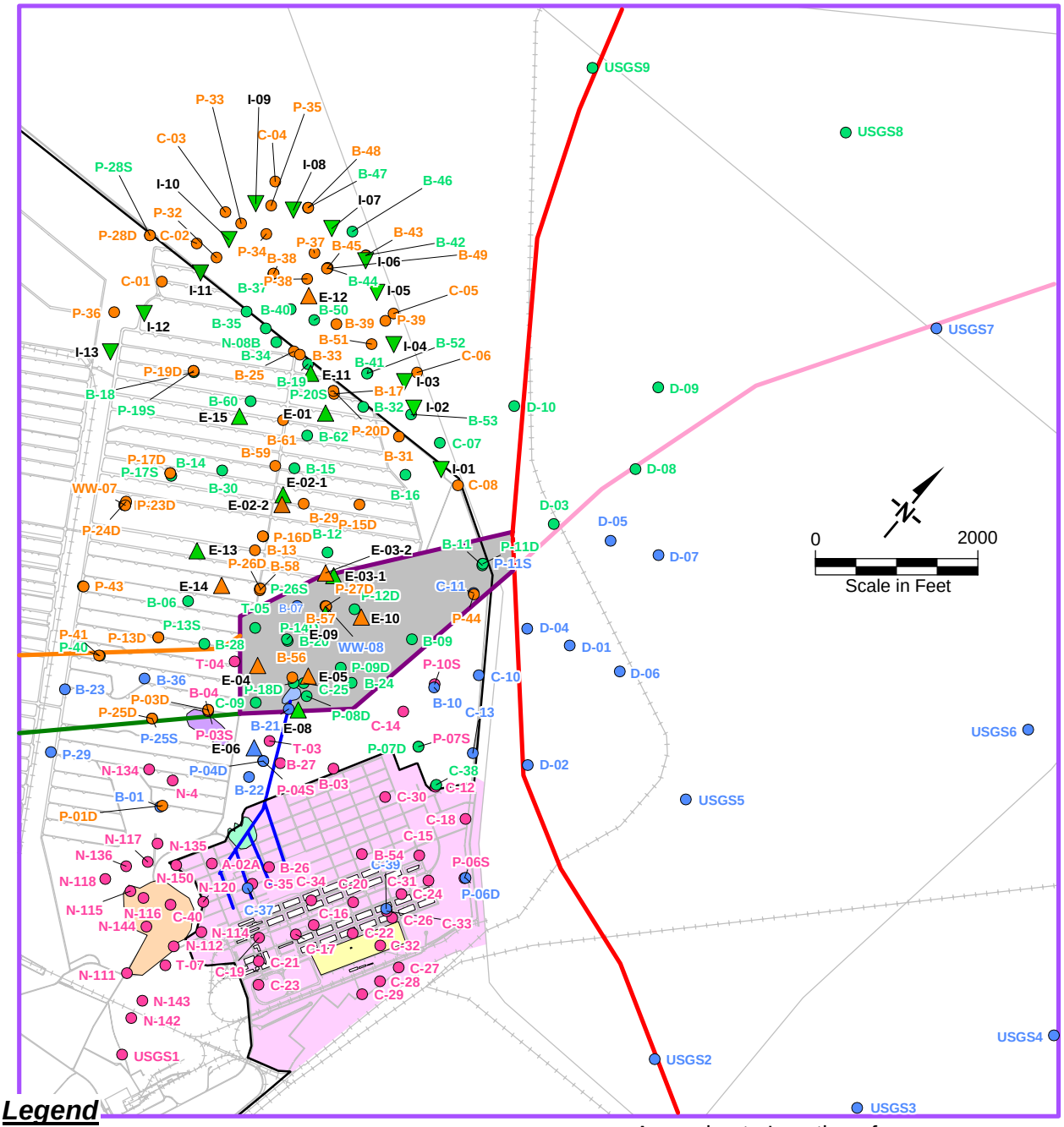

Figure 2. Map of the TEAD model Area including Source Locations, Wells, Bedrock Blocks, and Faults

p:\tooele\model2004\MapInfo\Tead2.wor

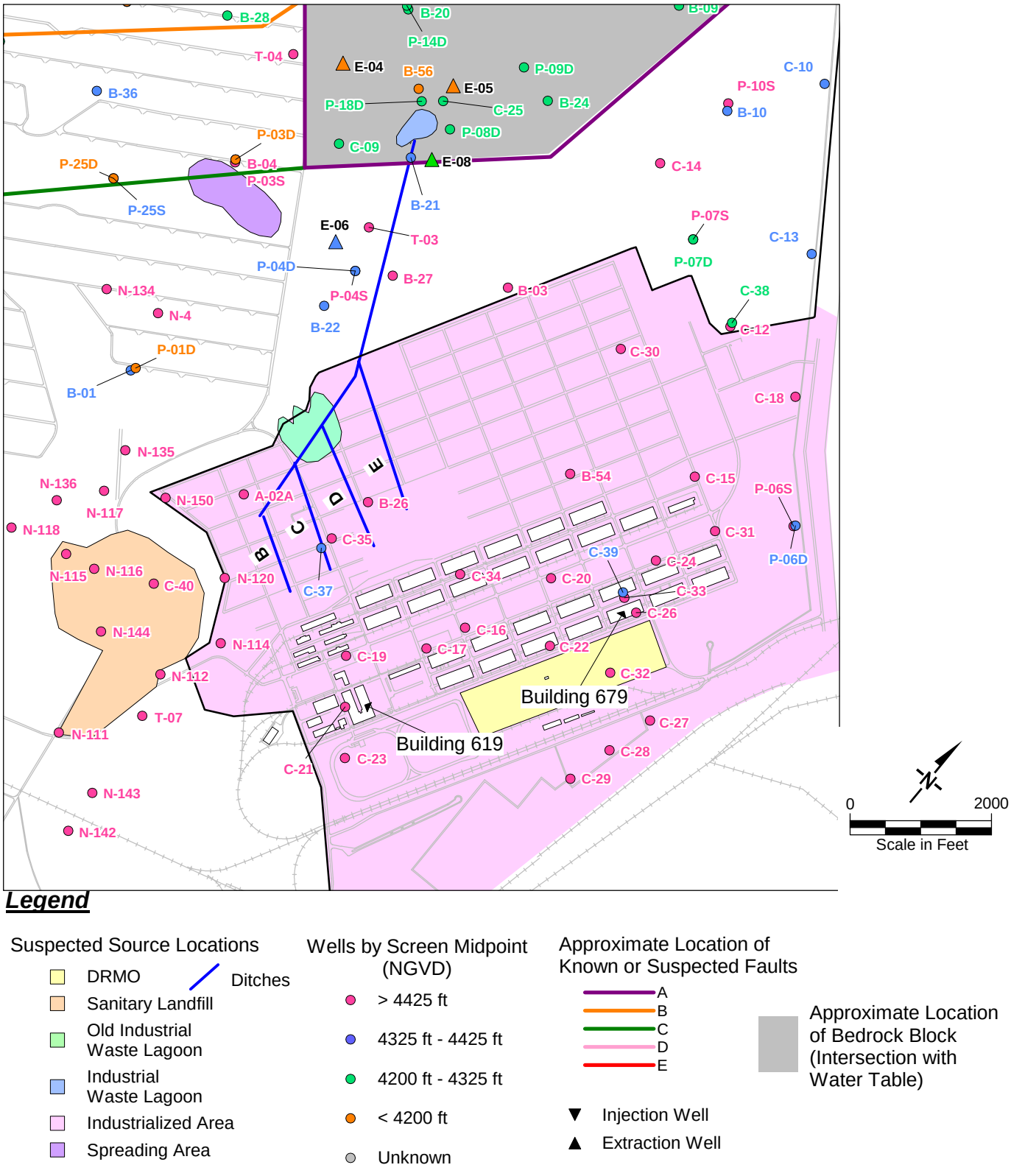

Legend

Suspected Source Locations
- DRMO
- Sanitary Landfill
- Old Industrial Waste Lagoon
- Industrial Waste Lagoon
- Industrialized Area
- Spreading Area
- Ditches

Wells by Screen Midpoint (NGVD)
- > 4425 ft
- 4325 ft - 4425 ft
- 4200 ft - 4325 ft
- < 4200 ft
- Unknown

Approximate Location of Known or Suspected Faults
- A
- B
- C
- D
- E

Approximate Location of Bedrock Block (Intersection with Water Table)

- Injection Well
- Extraction Well

Figure 3. Zoomed-In Map of the Industrial Area and Source Locations

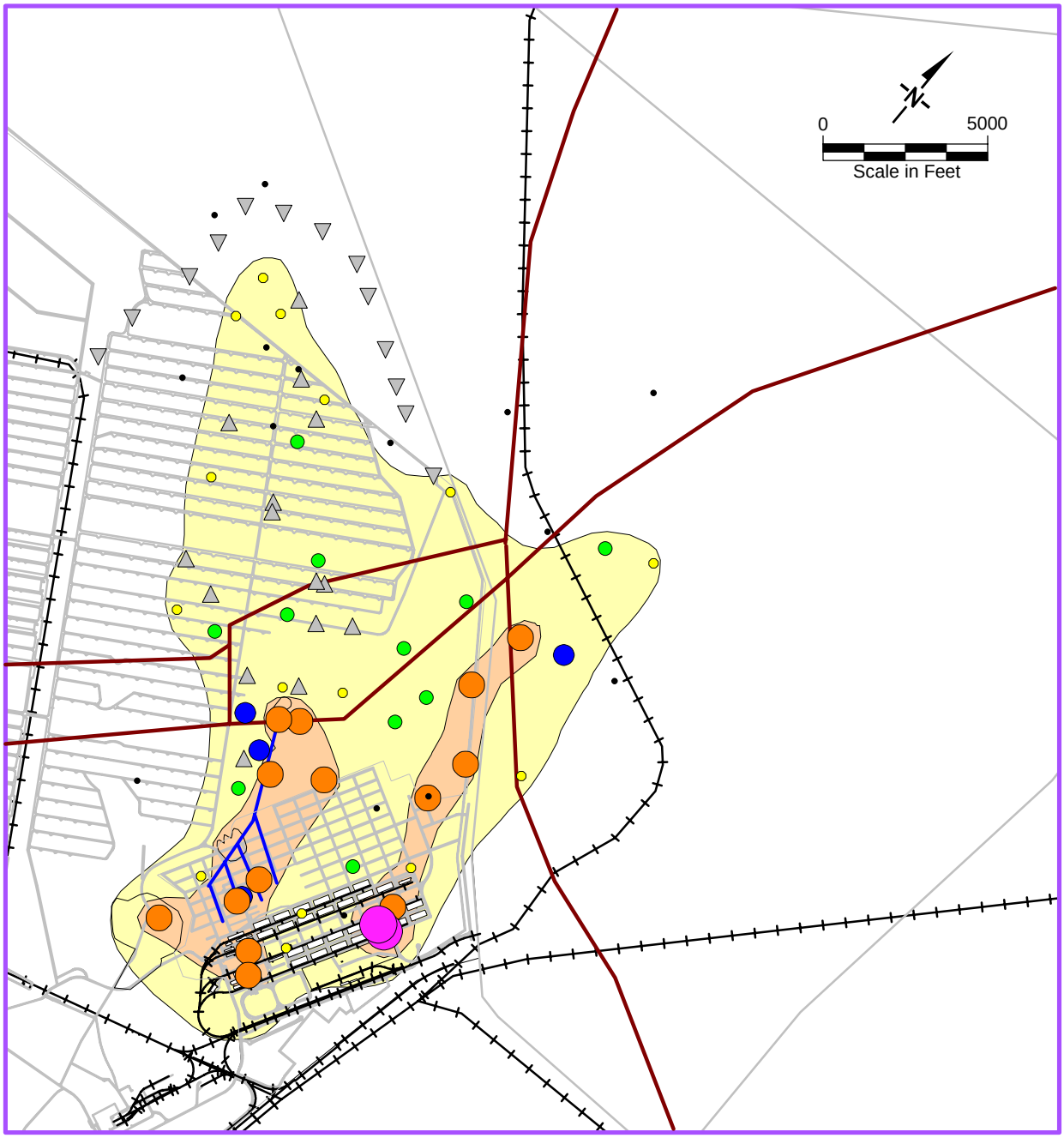

Legend

Interpreted Plume
> 5 µg/L

Interpreted Plume
> 100 µg/L

Observed TCE Concentration (µg/L)

> 1,000
500 to 1,000
100 to 500
50 to 100
25 to 50
5 to 25
< 5

Figure 4 TCE Plume Interpreted from 2003 Groundwater Observations

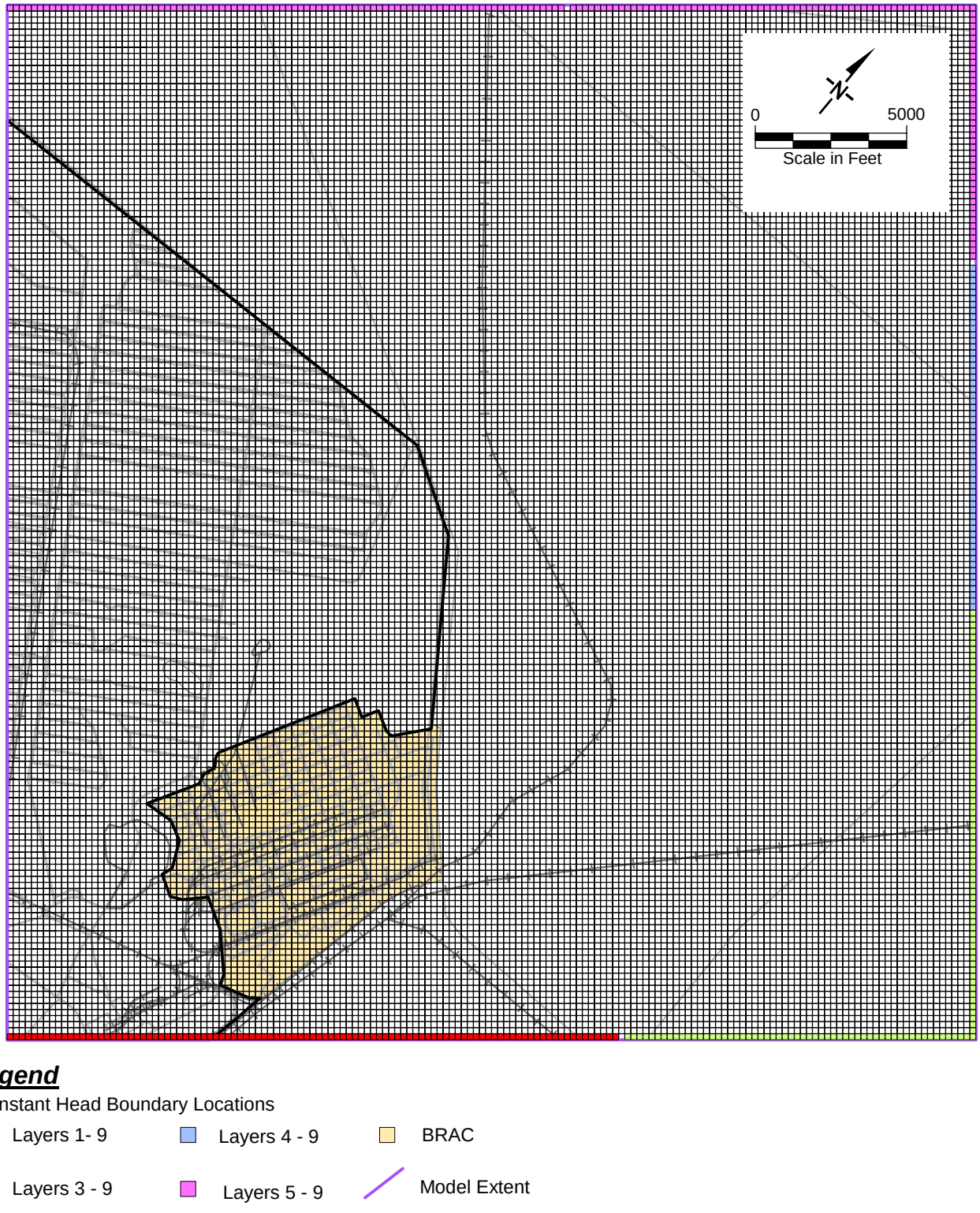

Figure 5. Model Grid and Constant Head Boundary Locations

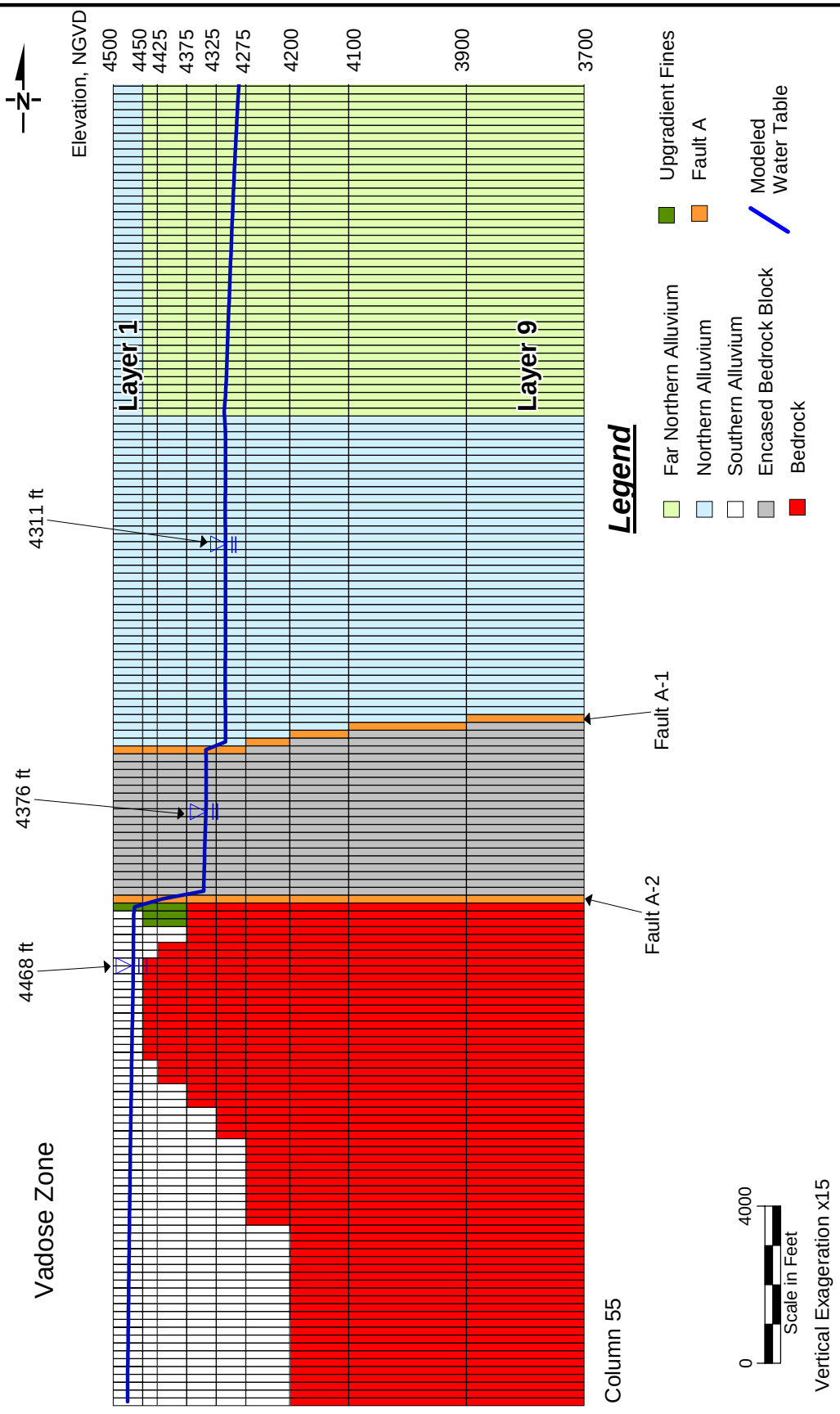

Figure 6. Model Cross Section Along Column 55

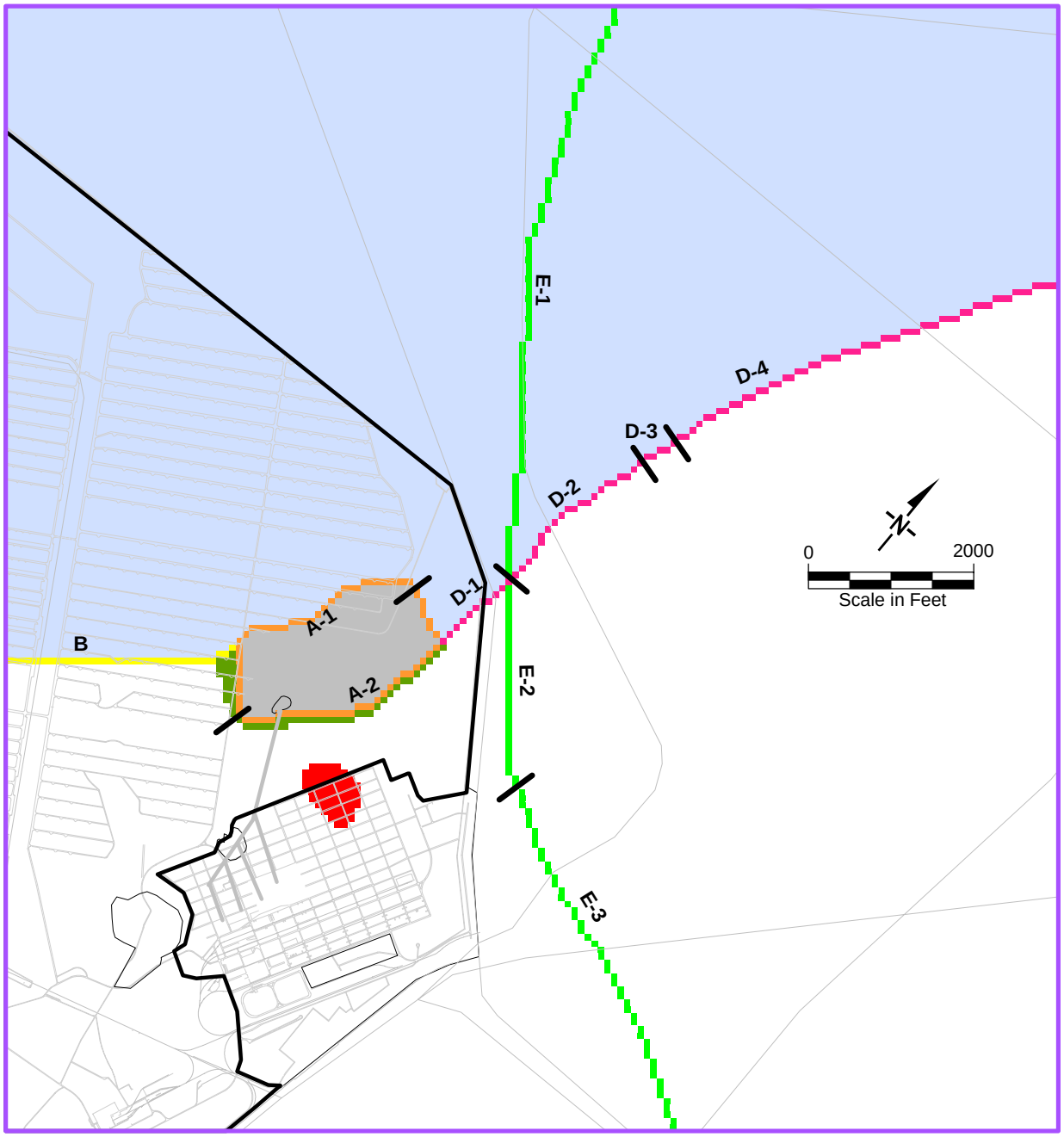

Legend

- Far Northern Alluvium
- Northern Alluvium
- Southern Alluvium
- Bedrock
- Upgradient Fines
- Encased Bedrock Block
- Fault A
- Fault B
- Fault C
- Fault D
- Fault E

Figure 7 Property Zones in Layer 1

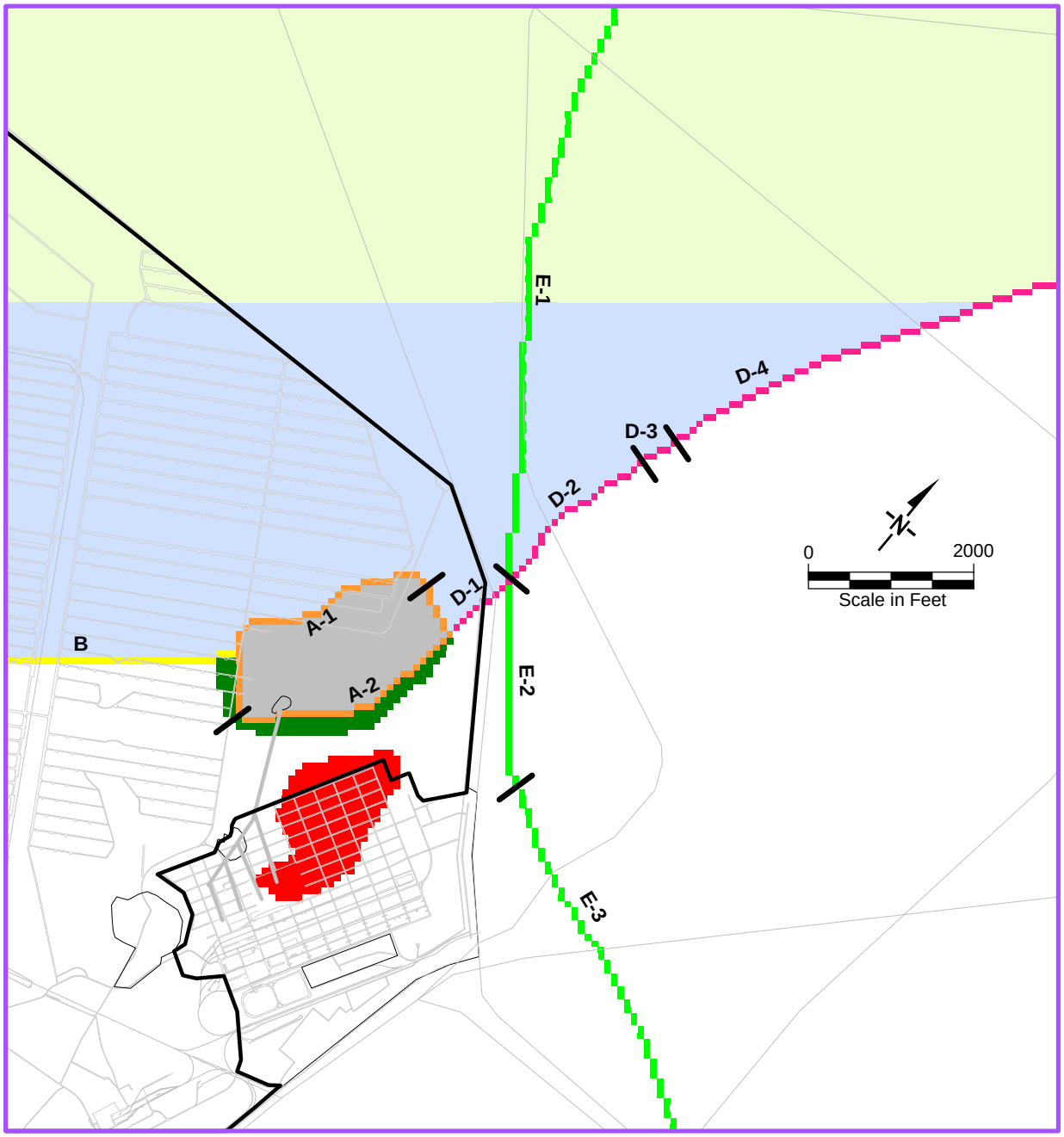

Legend

- Far Northern Alluvium
- Northern Alluvium
- Southern Alluvium
- Bedrock
- Upgradient Fines
- Encased Bedrock Block
- Fault A
- Fault B
- Fault C
- Fault D
- Fault E

Figure 8 Property Zones in Layer 2

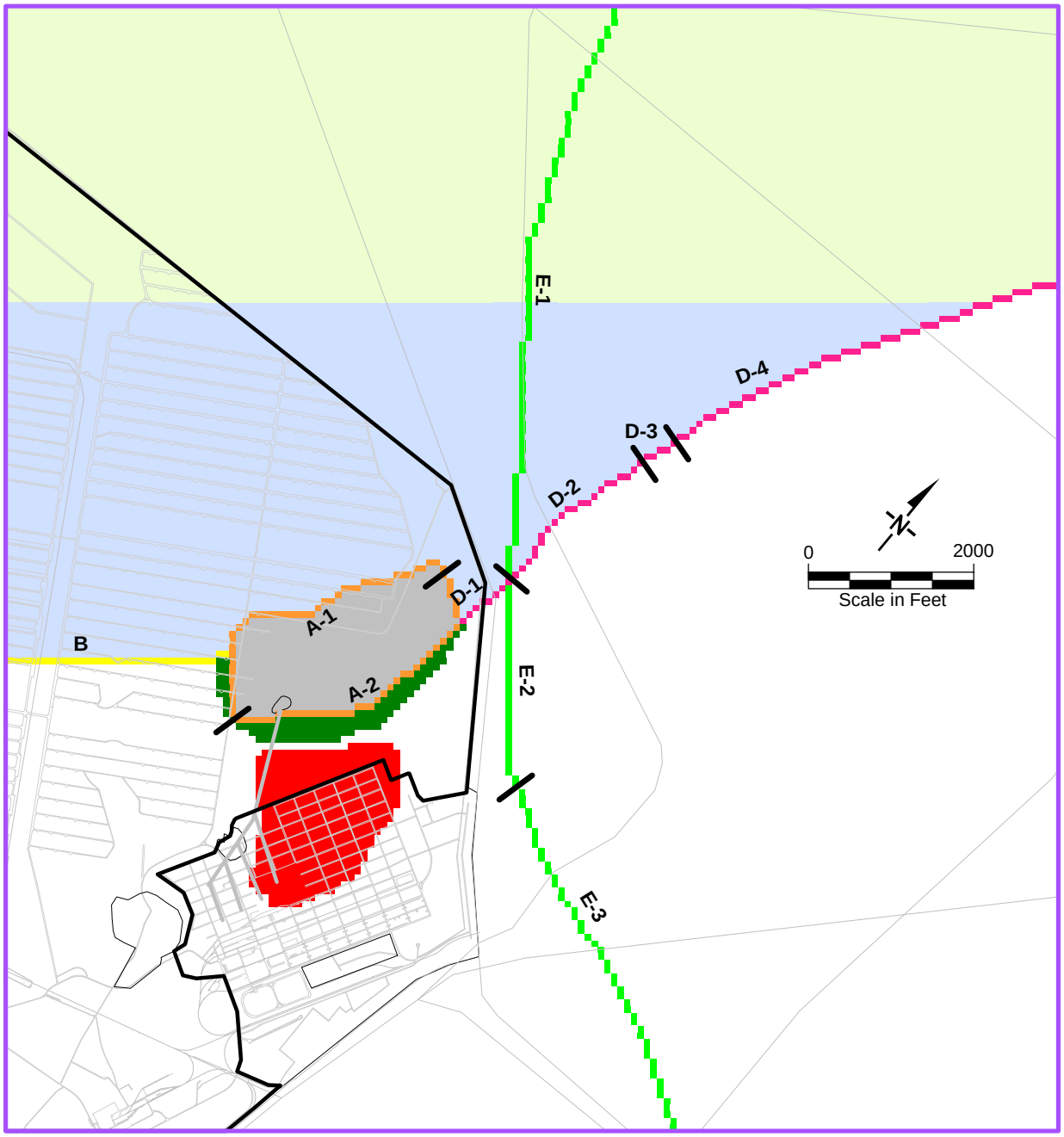

Legend

- Far Northern Alluvium
- Northern Alluvium
- Southern Alluvium
- Bedrock
- Upgradient Fines
- Encased Bedrock Block
- Fault A
- Fault B
- Fault C
- Fault D
- Fault E

Figure 9 Property Zones in Layer 3

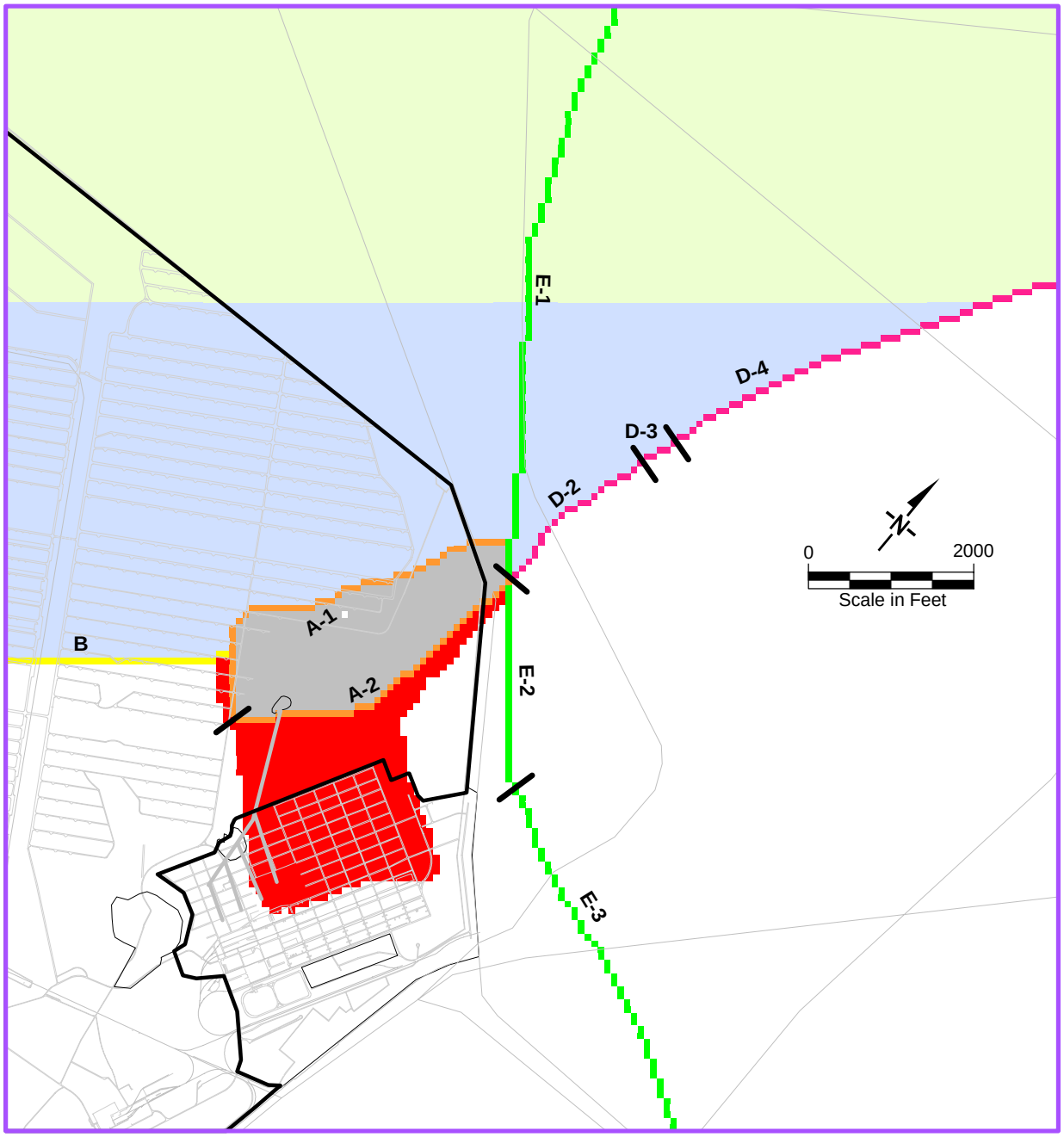

Legend

- Far Northern Alluvium
- Northern Alluvium
- Southern Alluvium
- Bedrock
- Upgradient Fines
- Encased Bedrock Block
- Fault A
- Fault B
- Fault C
- Fault D
- Fault E

Figure 10 Property Zones in Layer 4

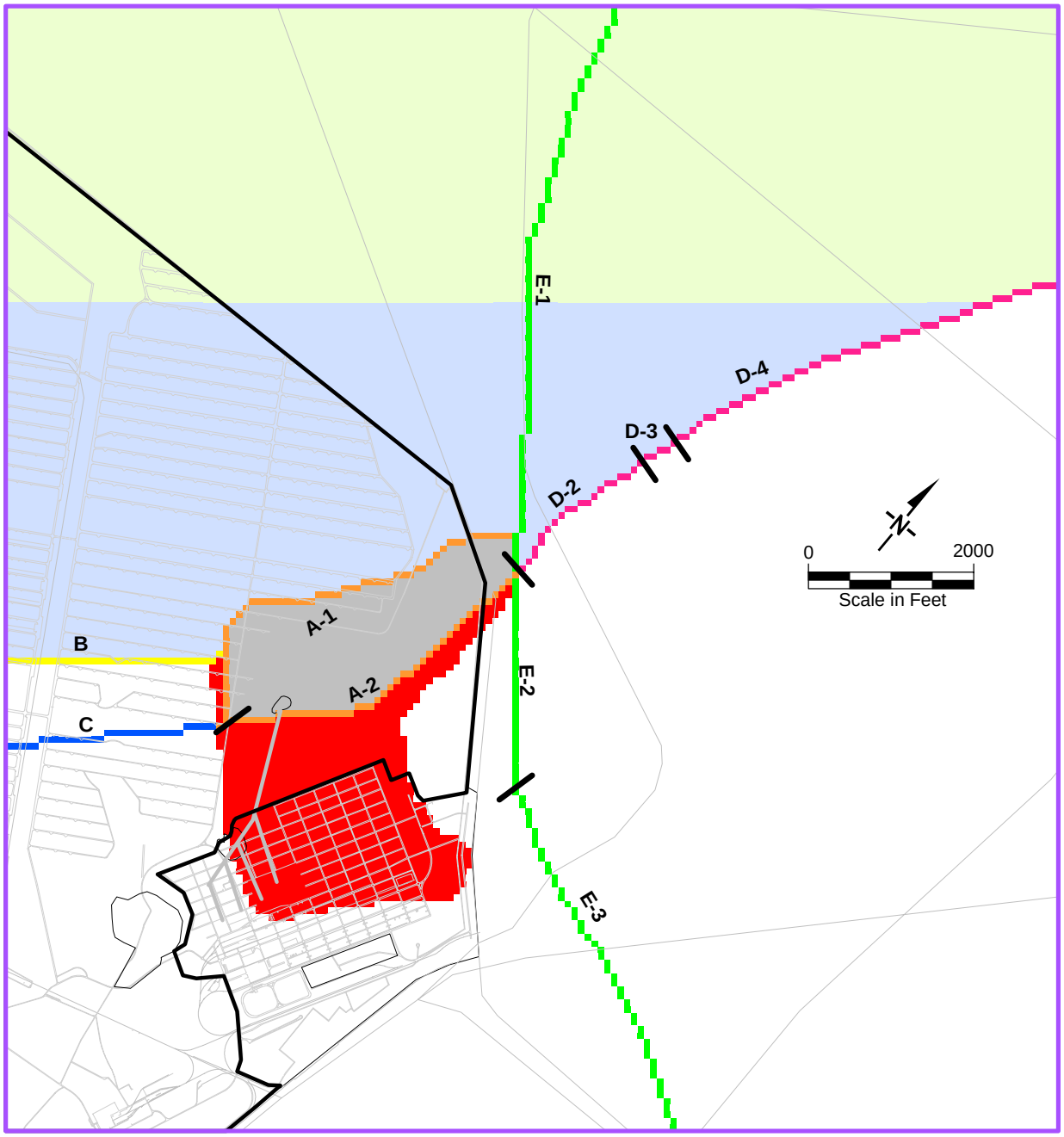

Legend

- Far Northern Alluvium
- Northern Alluvium
- Southern Alluvium
- Bedrock
- Upgradient Fines
- Encased Bedrock Block
- Fault A
- Fault B
- Fault C
- Fault D
- Fault E

Figure 11 Property Zones in Layer 5

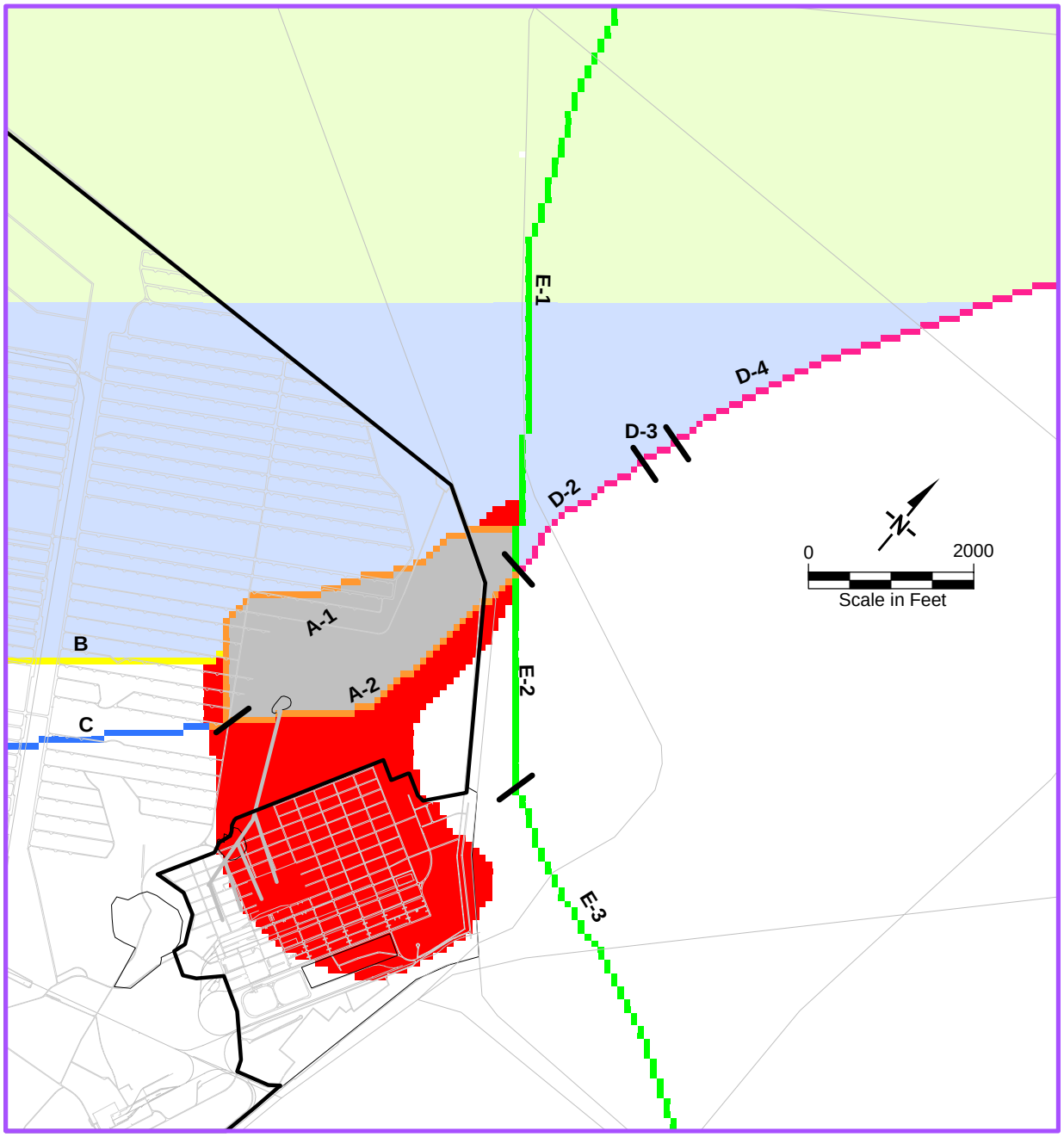

Legend

- Far Northern Alluvium
- Northern Alluvium
- Southern Alluvium
- Upper Bedrock
- Lower Bedrock
- Encased Bedrock Block
- Fault A
- Fault B
- Fault C
- Fault D
- Fault E

Figure 12 Property Zones in Layer 6

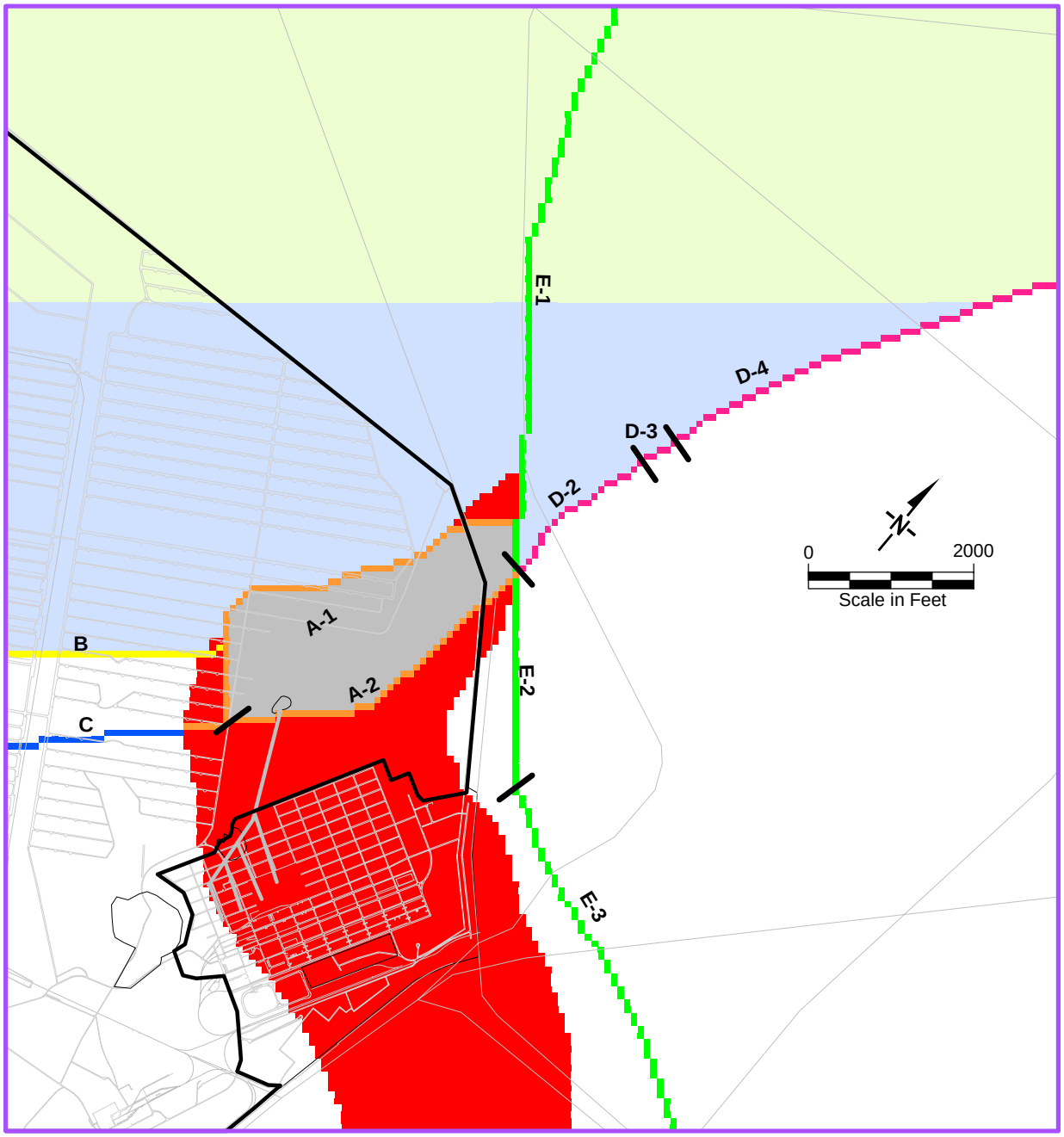

Legend

- Far Northern Alluvium
- Northern Alluvium
- Southern Alluvium
- Bedrock
- Upgradient Fines
- Encased Bedrock Block
- Fault A
- Fault B
- Fault C
- Fault D
- Fault E

Figure 13 Property Zones in Layer 7

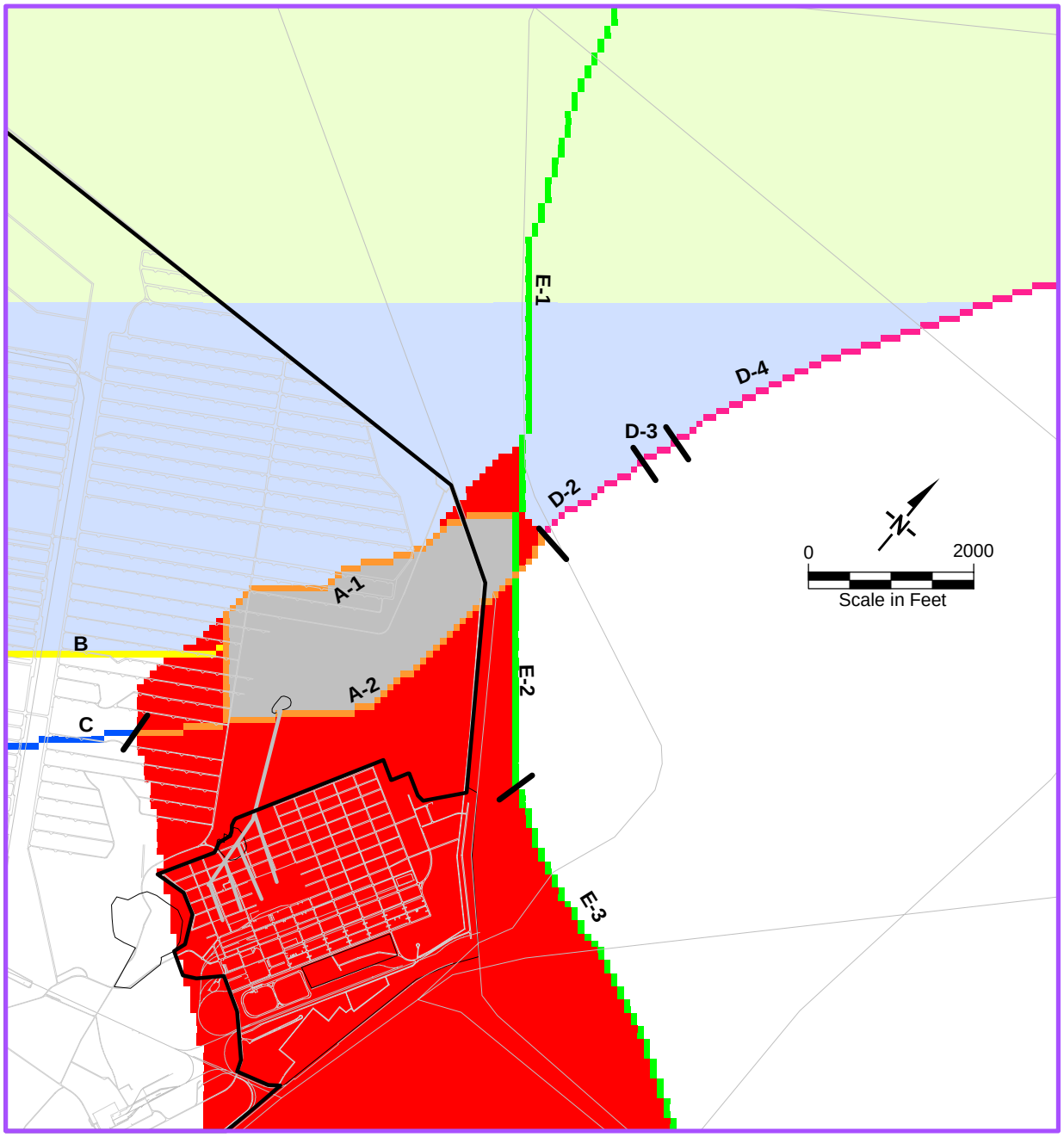

Legend

- Far Northern Alluvium
- Northern Alluvium
- Southern Alluvium
- Bedrock
- Upgradient Fines
- Encased Bedrock Block
- Fault A
- Fault B
- Fault C
- Fault D
- Fault E

Figure 14 Property Zones in Layer 8

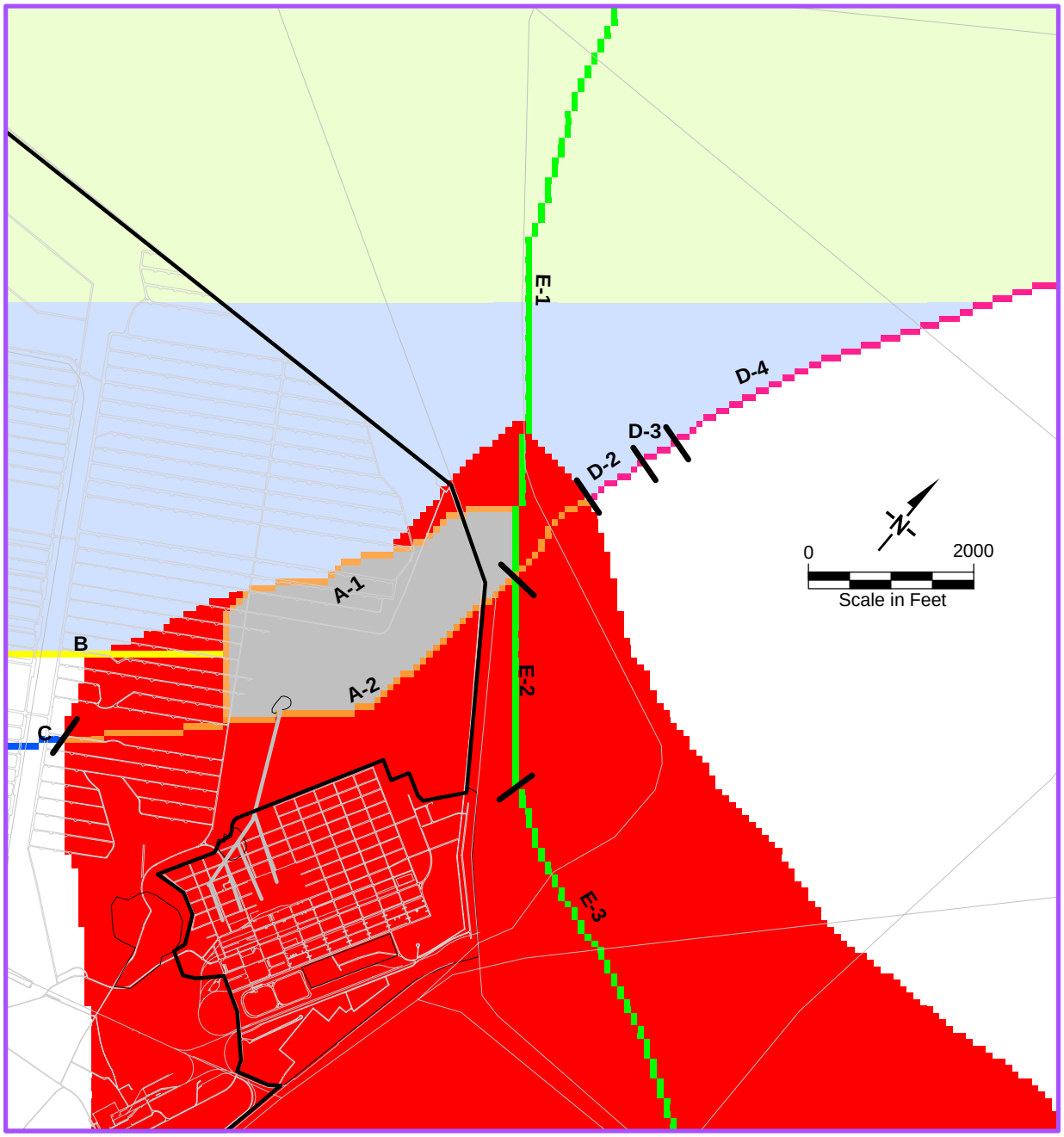

Legend

- Far Northern Alluvium
- Northern Alluvium
- Southern Alluvium
- Bedrock
- Upgradient Fines
- Encased Bedrock Block
- Fault A
- Fault B
- Fault C
- Fault D
- Fault E

Figure 15 Property Zones in Layer 9

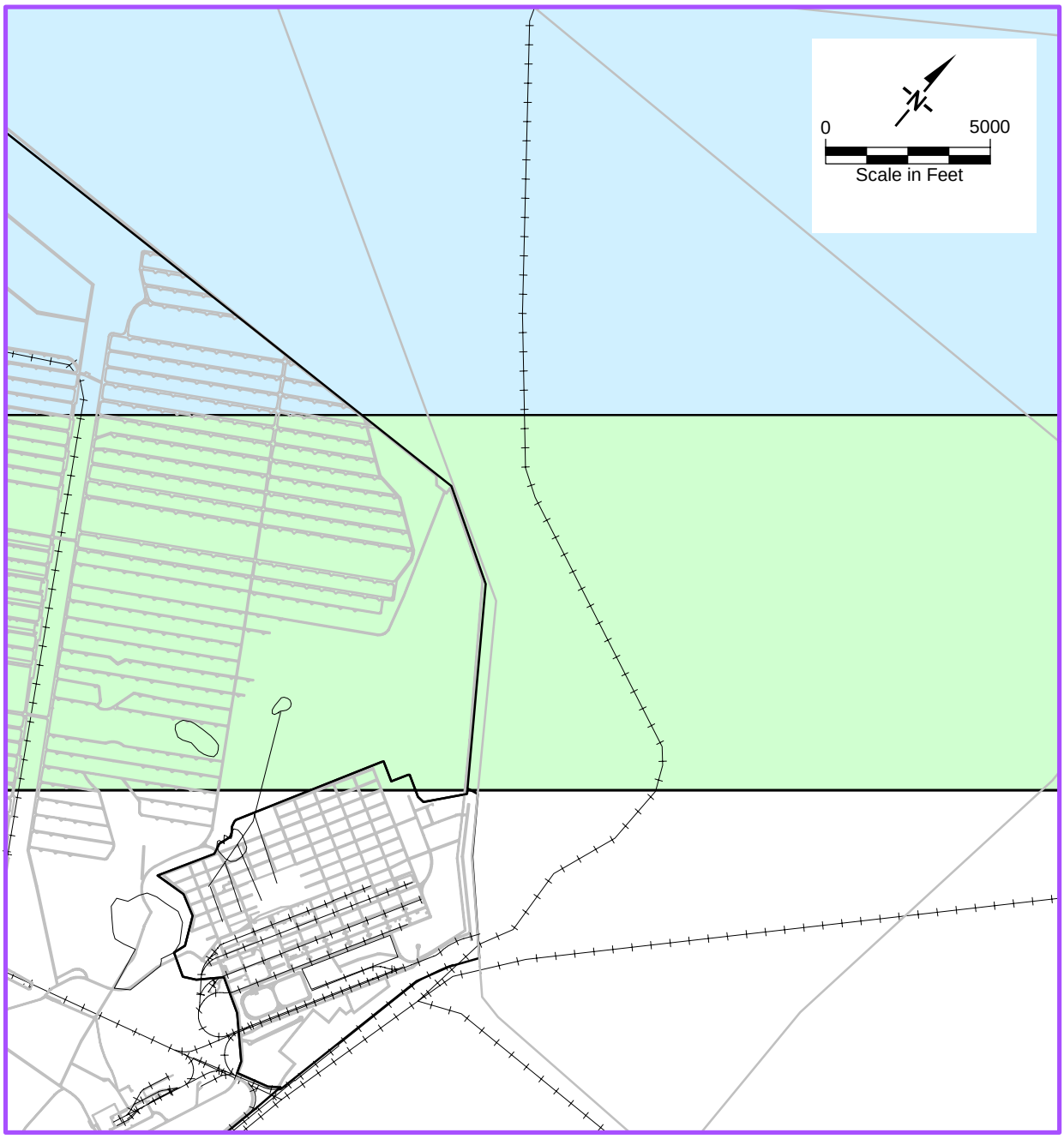

Legend

Northern Zone
Southern Zone
Central Zone
Model Extent

Figure 16. Recharge Zones

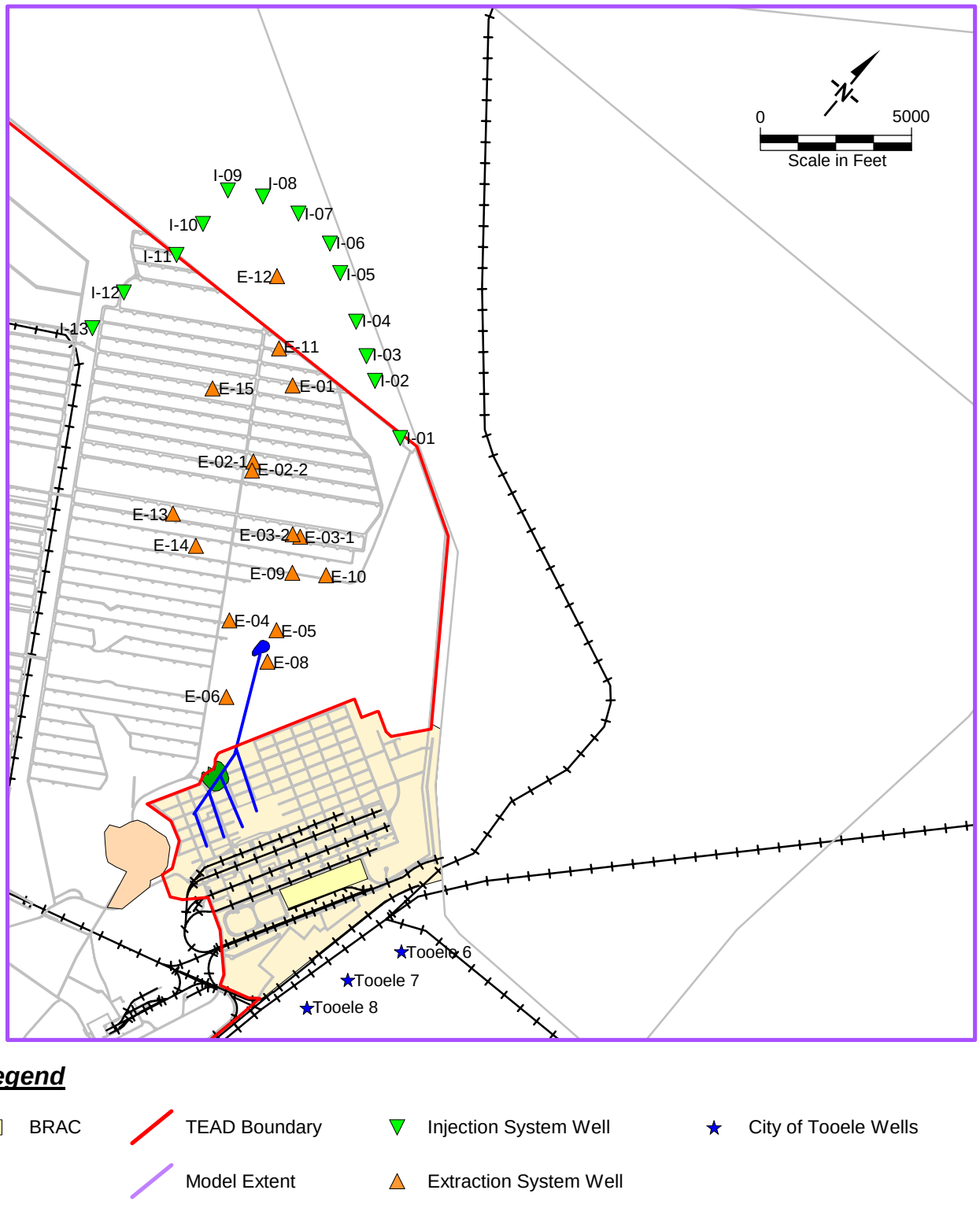

Figure 17. Extraction and Injection Well Locations

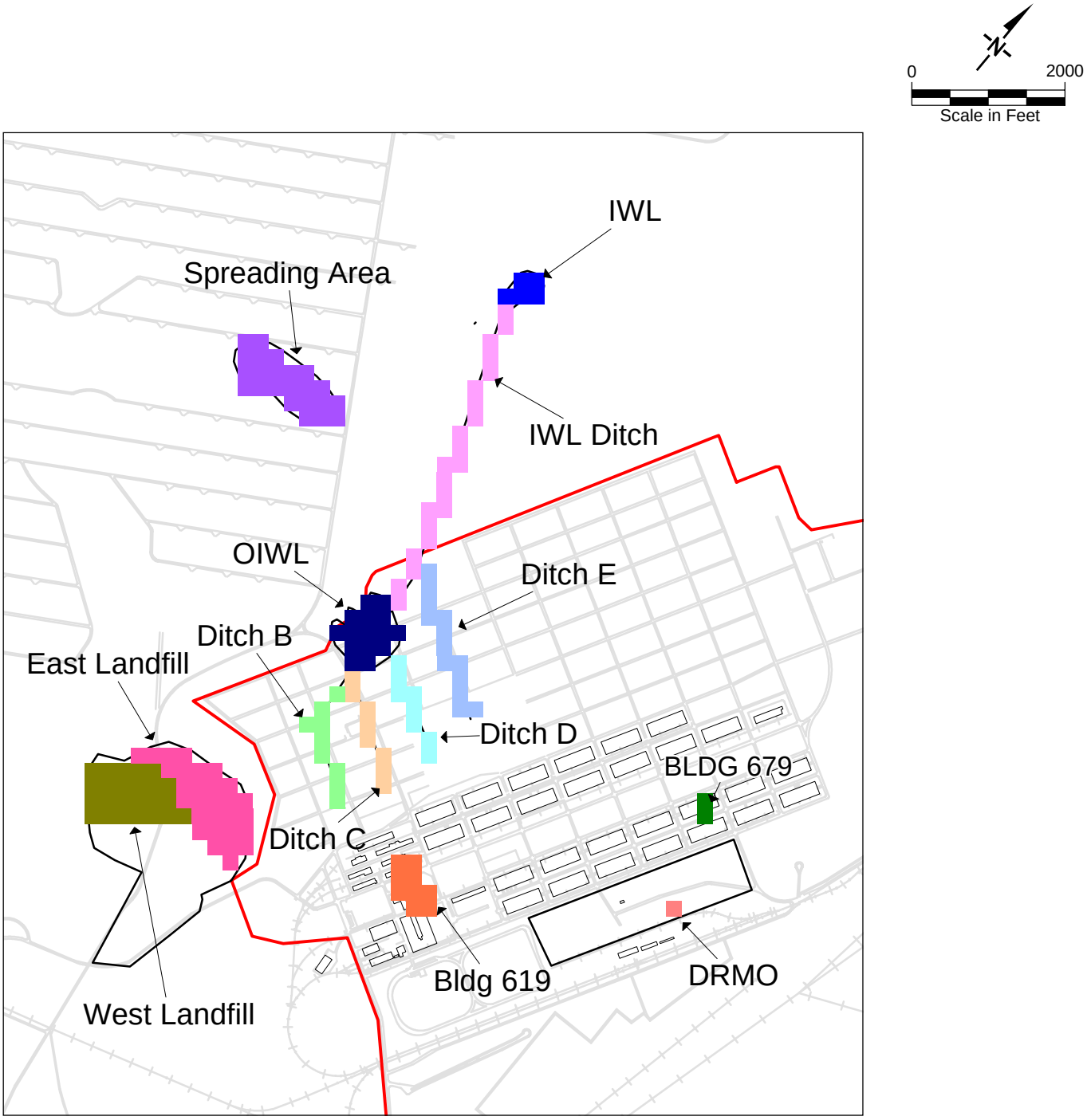

Figure 18. TCE Source Zones

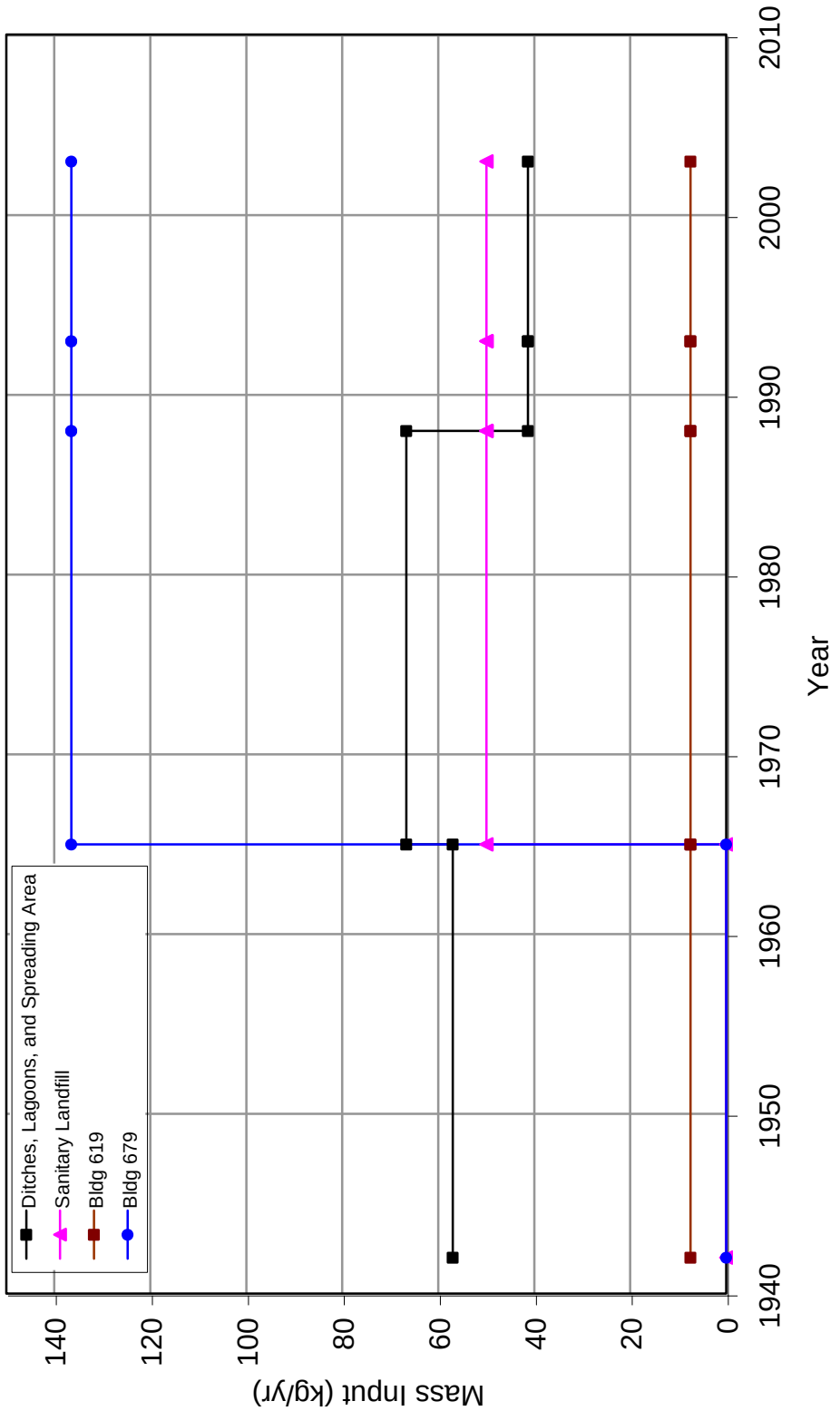

Figure 19. Mass Input in Source Zones

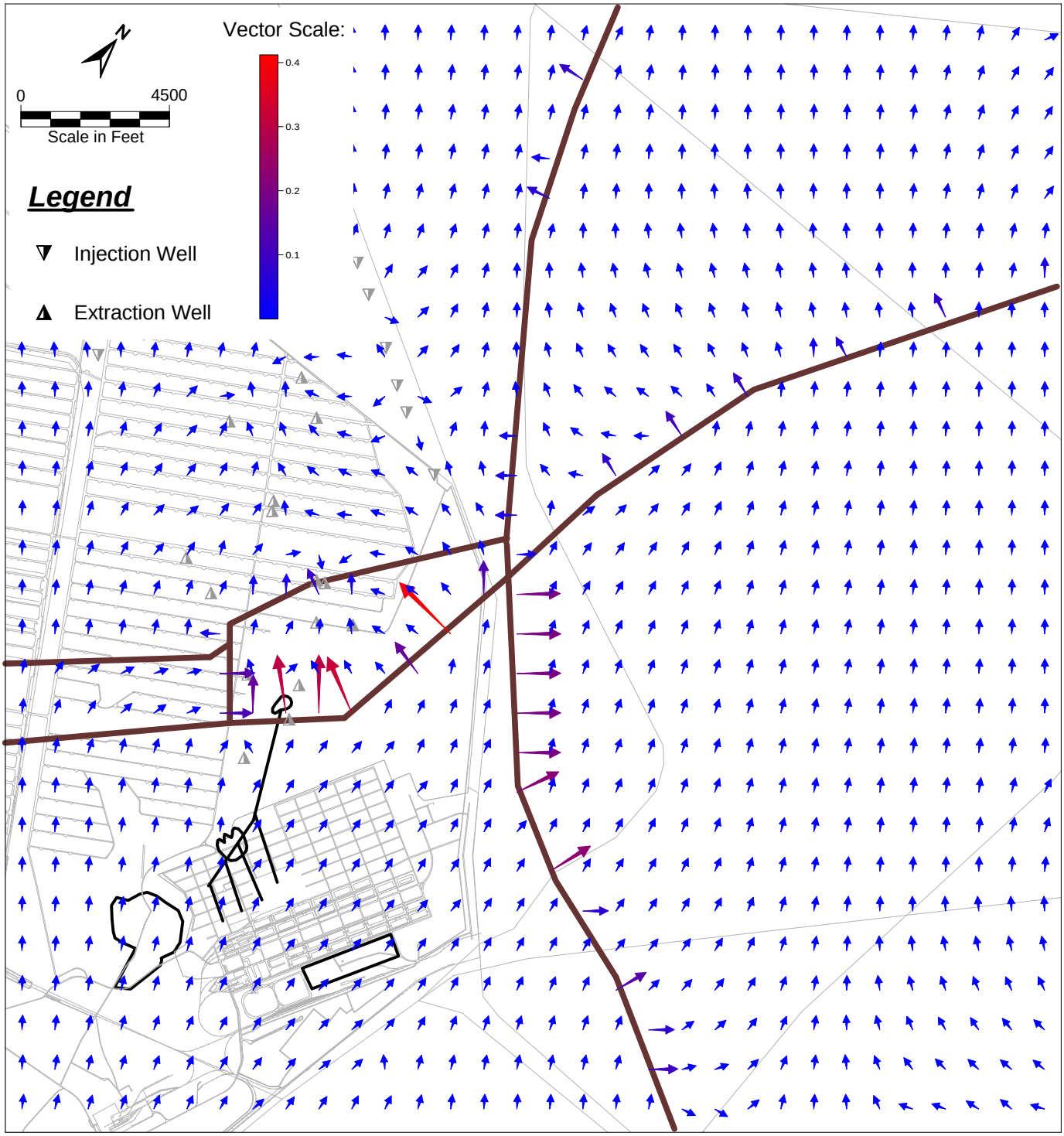

Figure 20. Vector Map of Groundwater Flow in Layer 5

P:\Tooele Modeling\Figures\WLlay5.srf

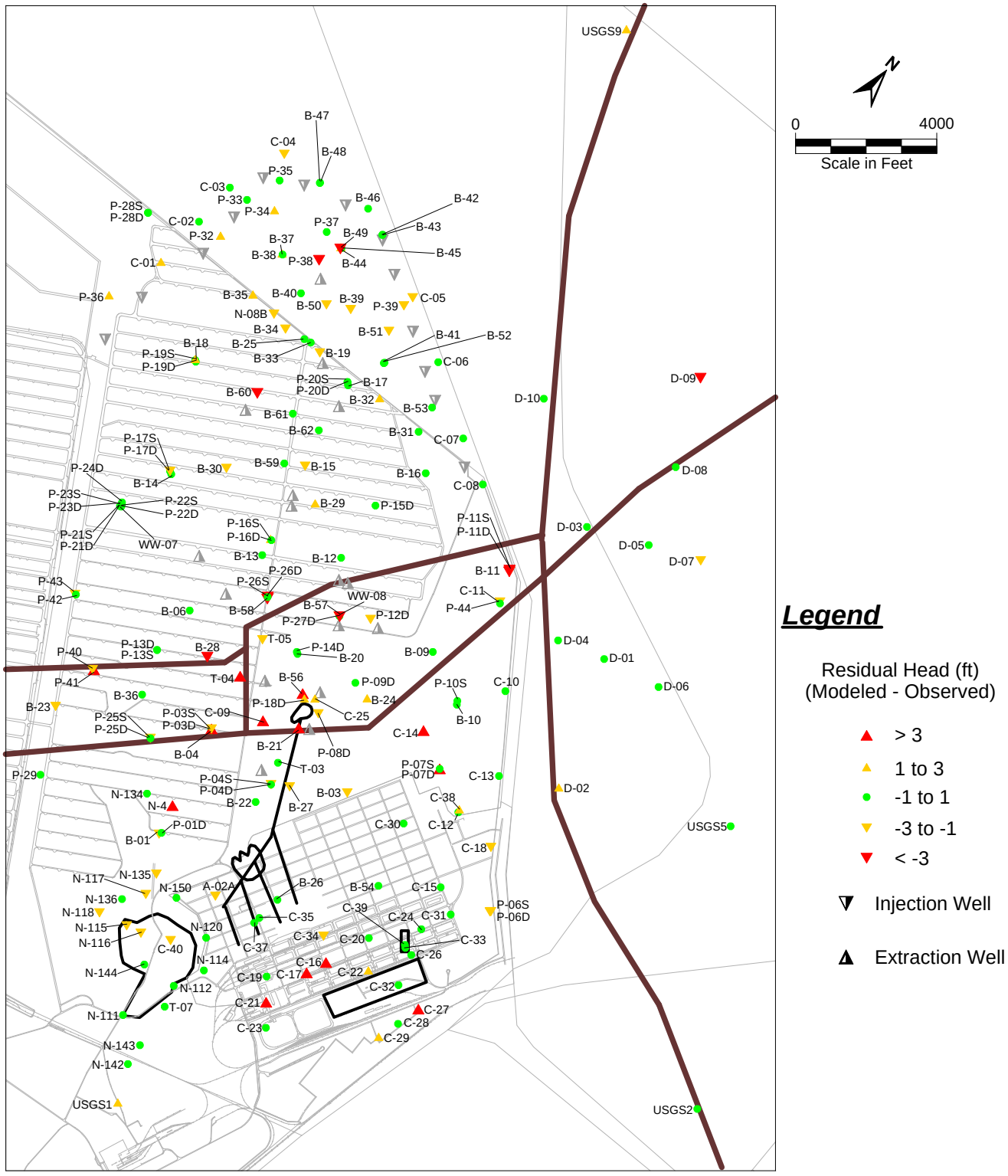

Figure 21. Water Level Residuals in All Layers

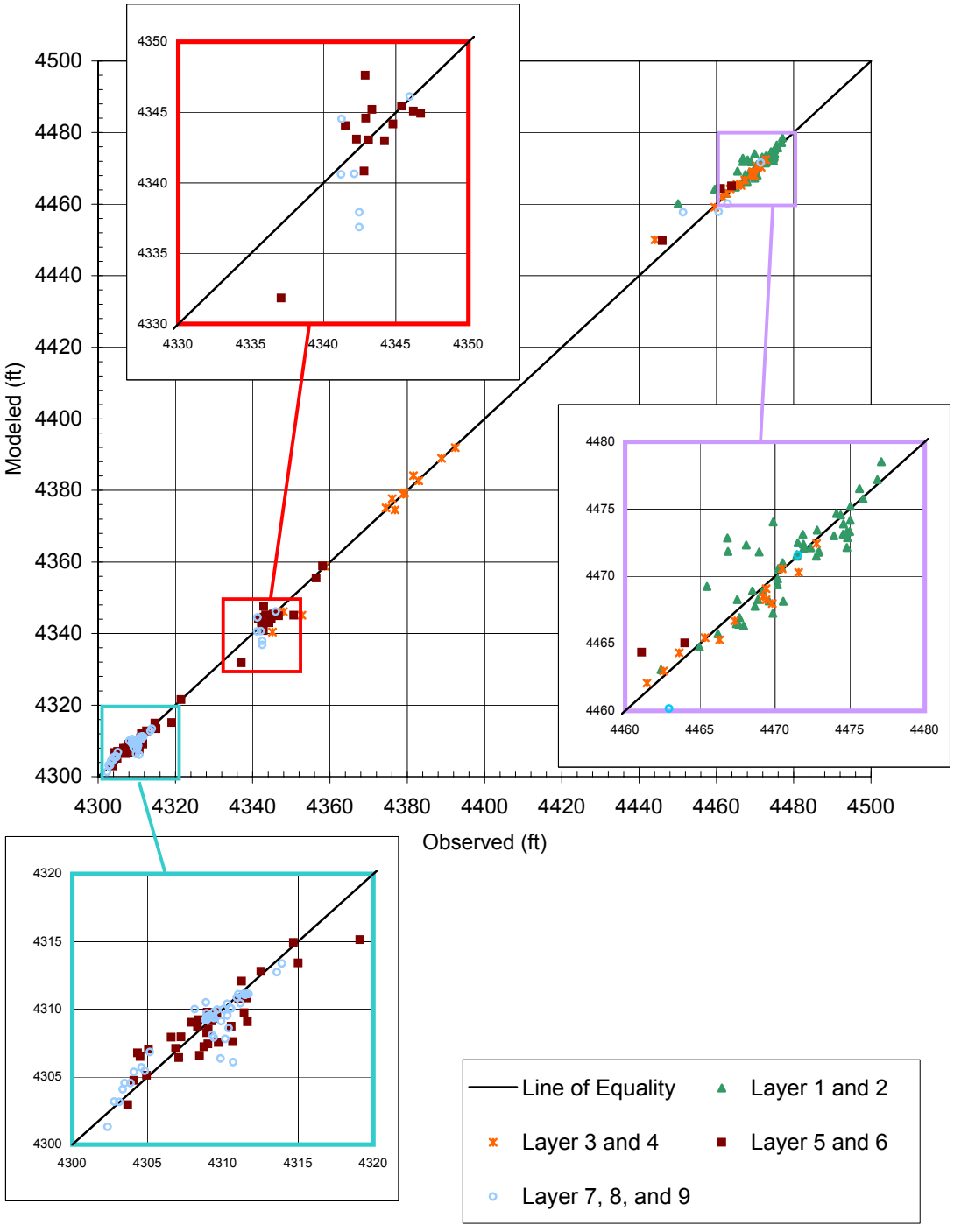

Figure 22. Steady State Calibration -- Modeled vs. Observed Head

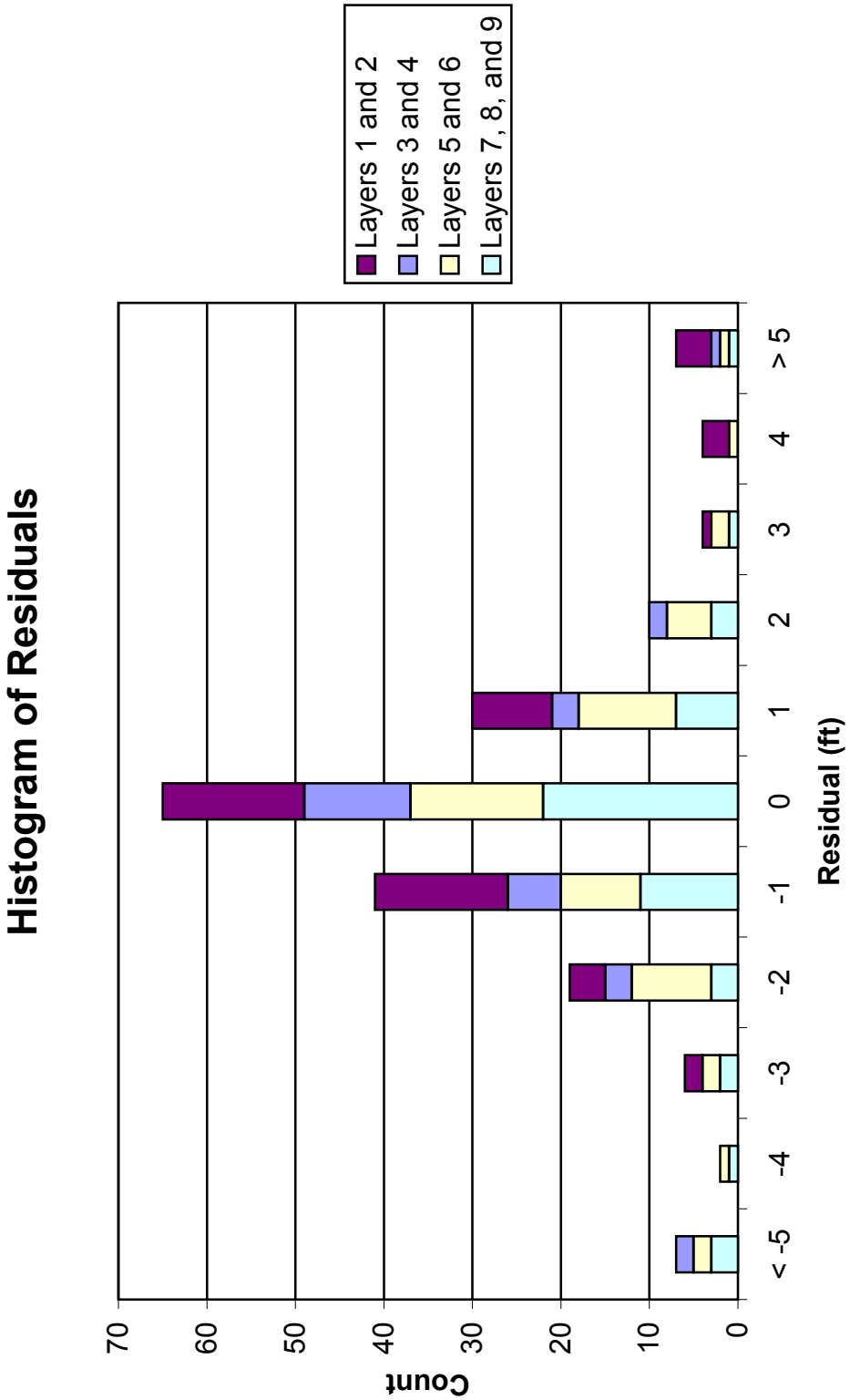

Figure 23. Steady State Calibration -- Residual Histogram

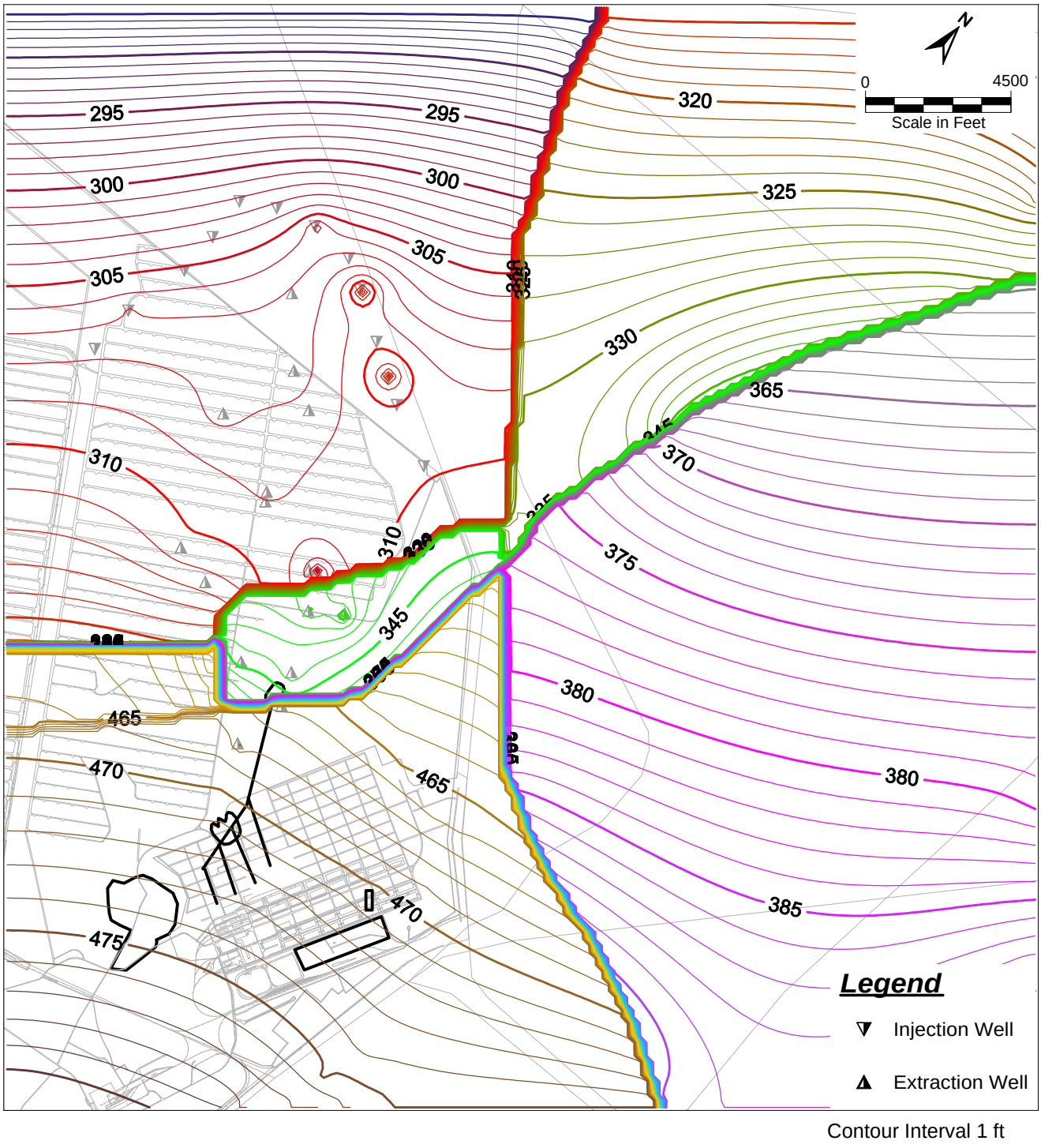

Figure 24. Modeled Head in Layer 5

P:\Tooele Modeling\Figures\WLlay5.srf

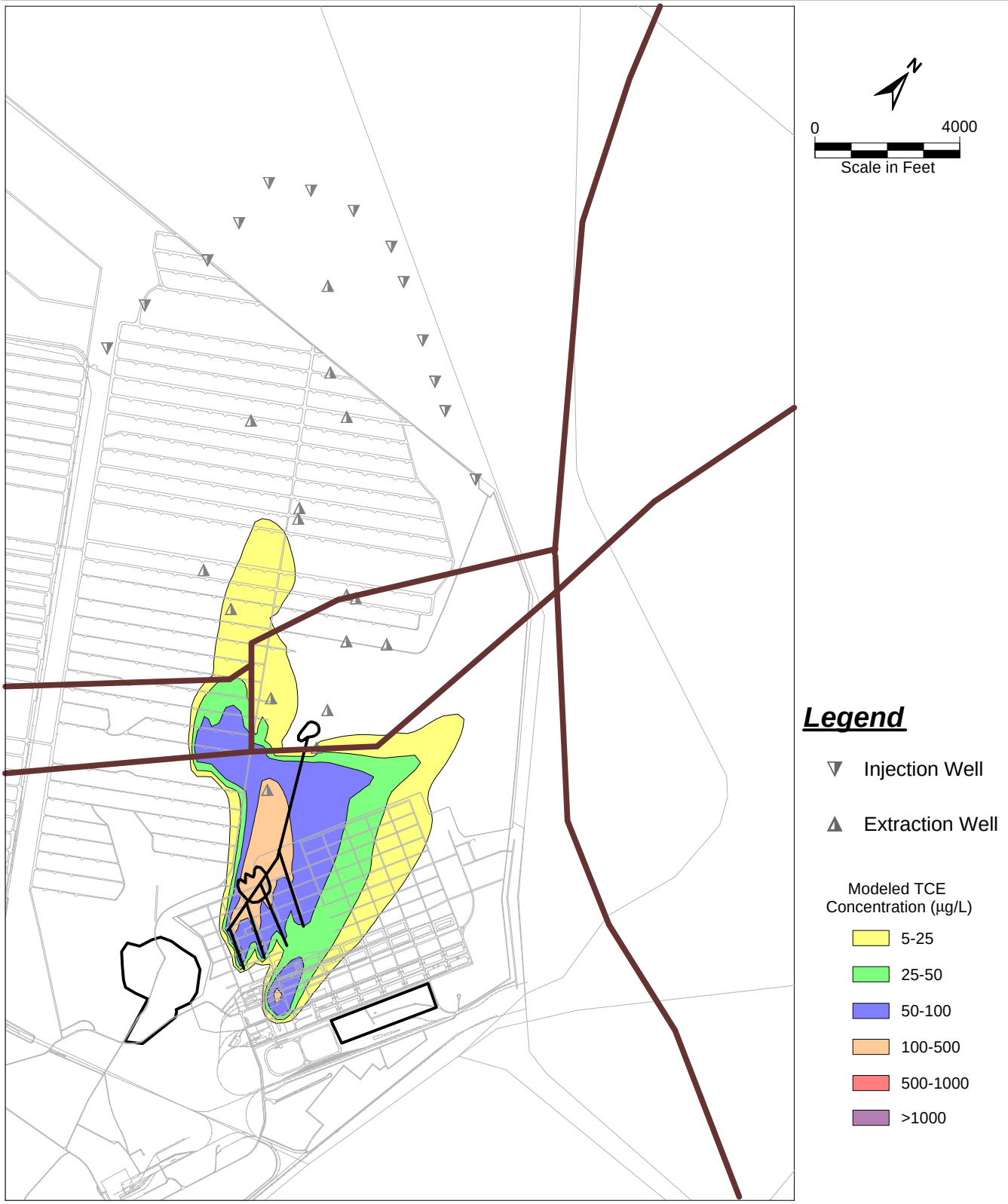

Figure 25. Modeled TCE Plume in 1965

P:\Tooele Modeling\Figures\Conc1965.srf

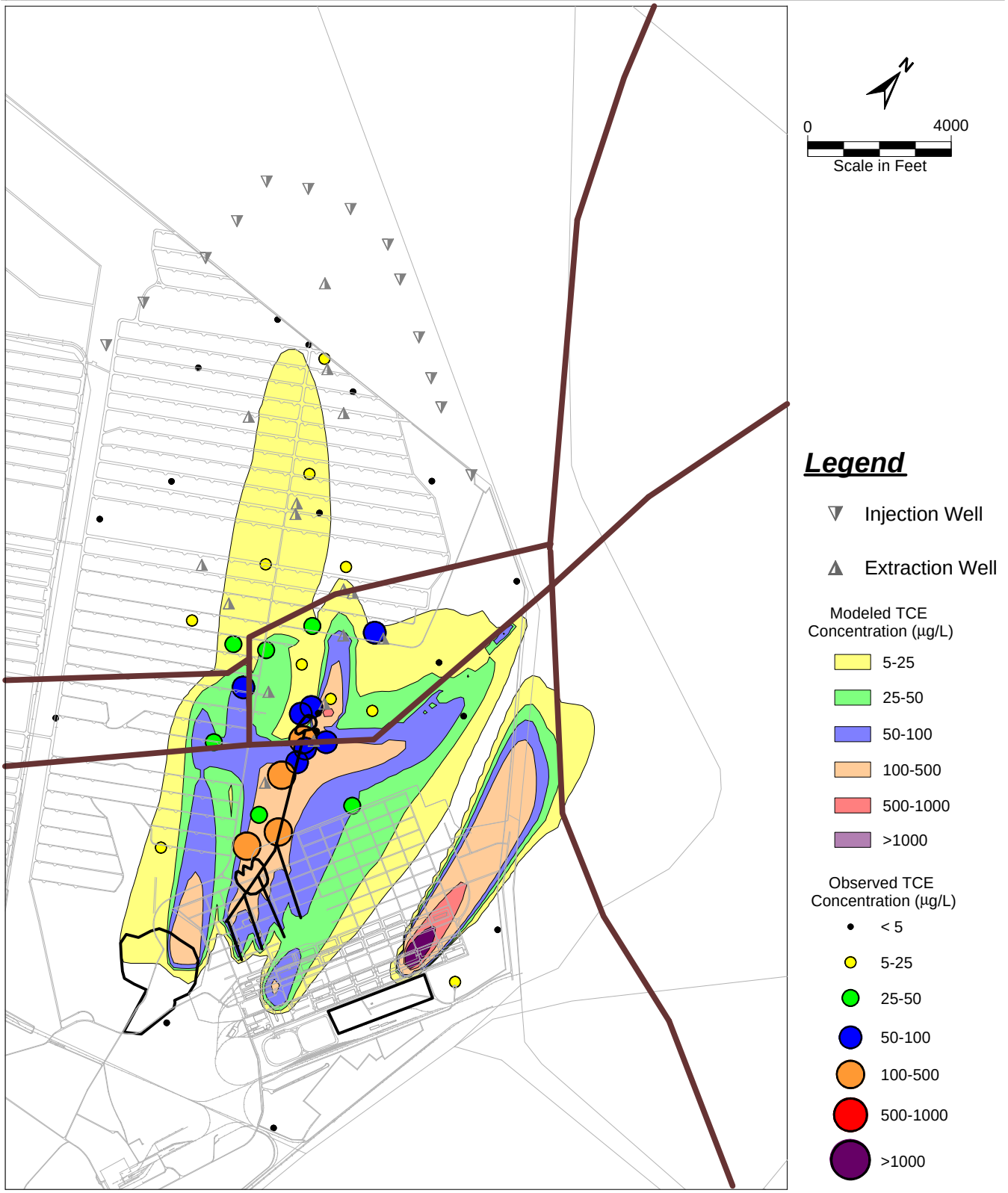

Figure 26. Modeled TCE Plume in 1986 with Observed TCE Concentrations

P:\Tooele Modeling\Figures\Conc1986.srf

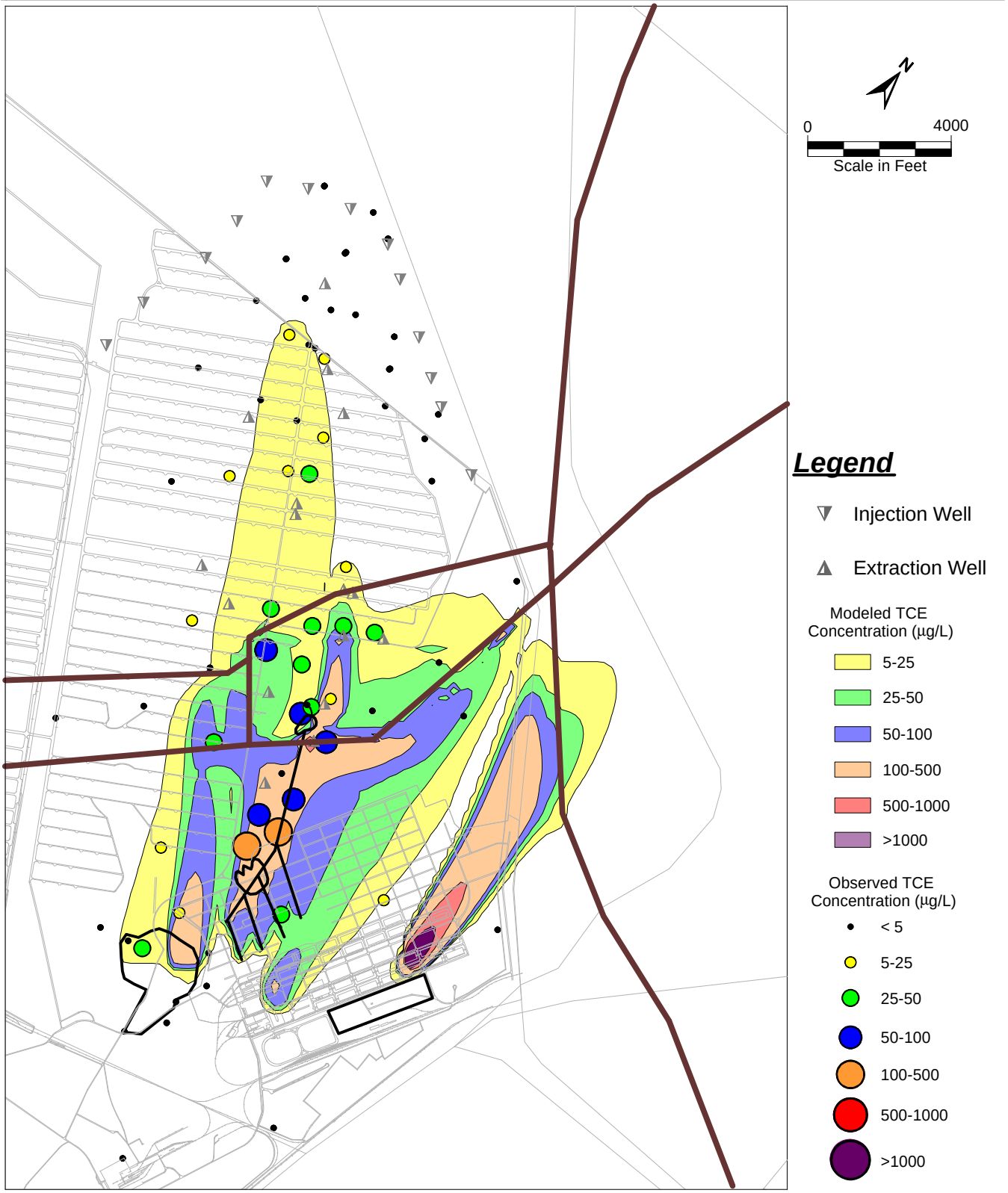

Figure 27. Modeled TCE Plume in 1989 with Observed TCE Concentrations

P:\Tooele Modeling\Figures\Conc1989.srf

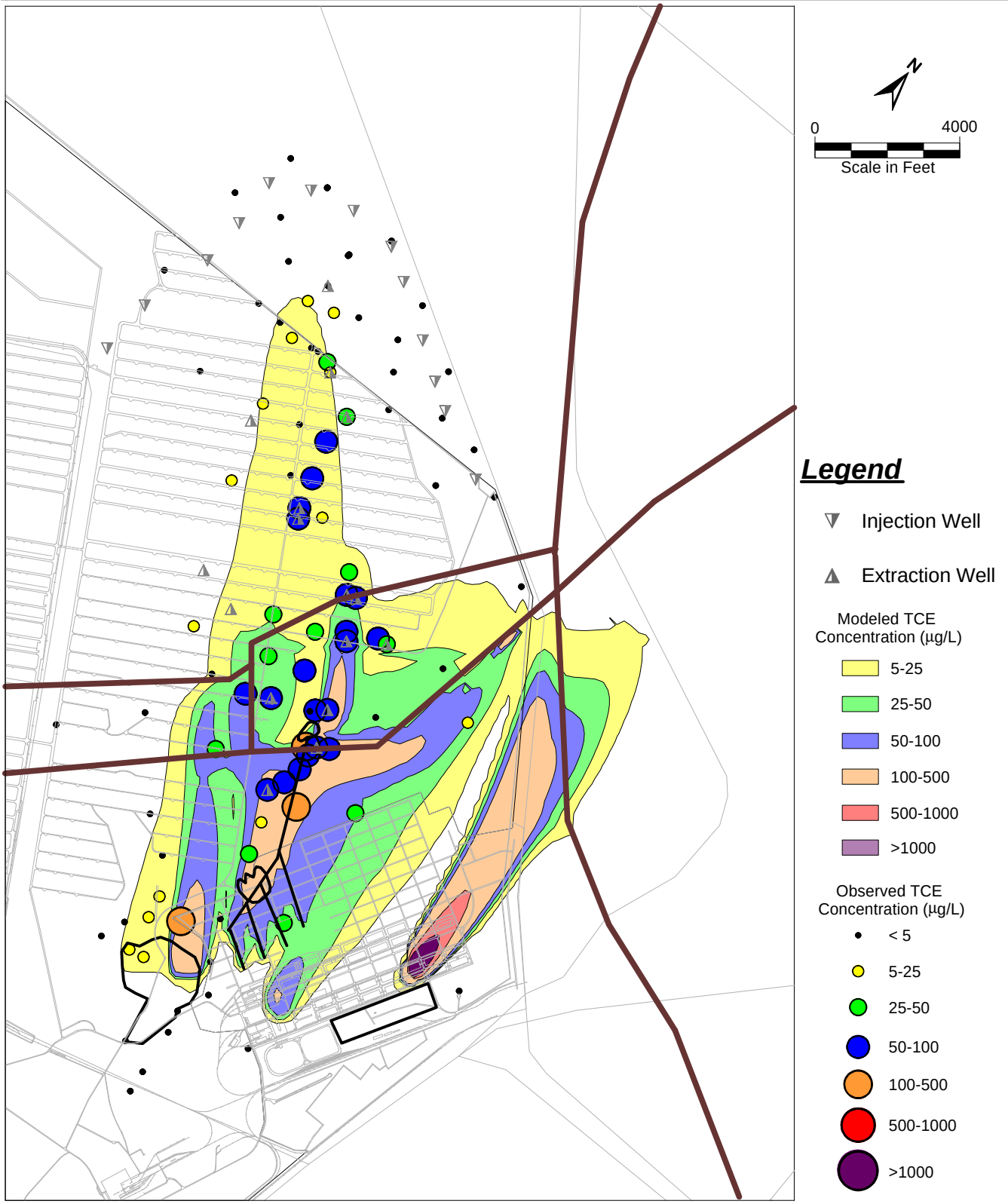

Figure 28. Modeled TCE Plume in 1992 with Observed TCE Concentrations

P:\Tooele Modeling\Figures\Conc1992.srf

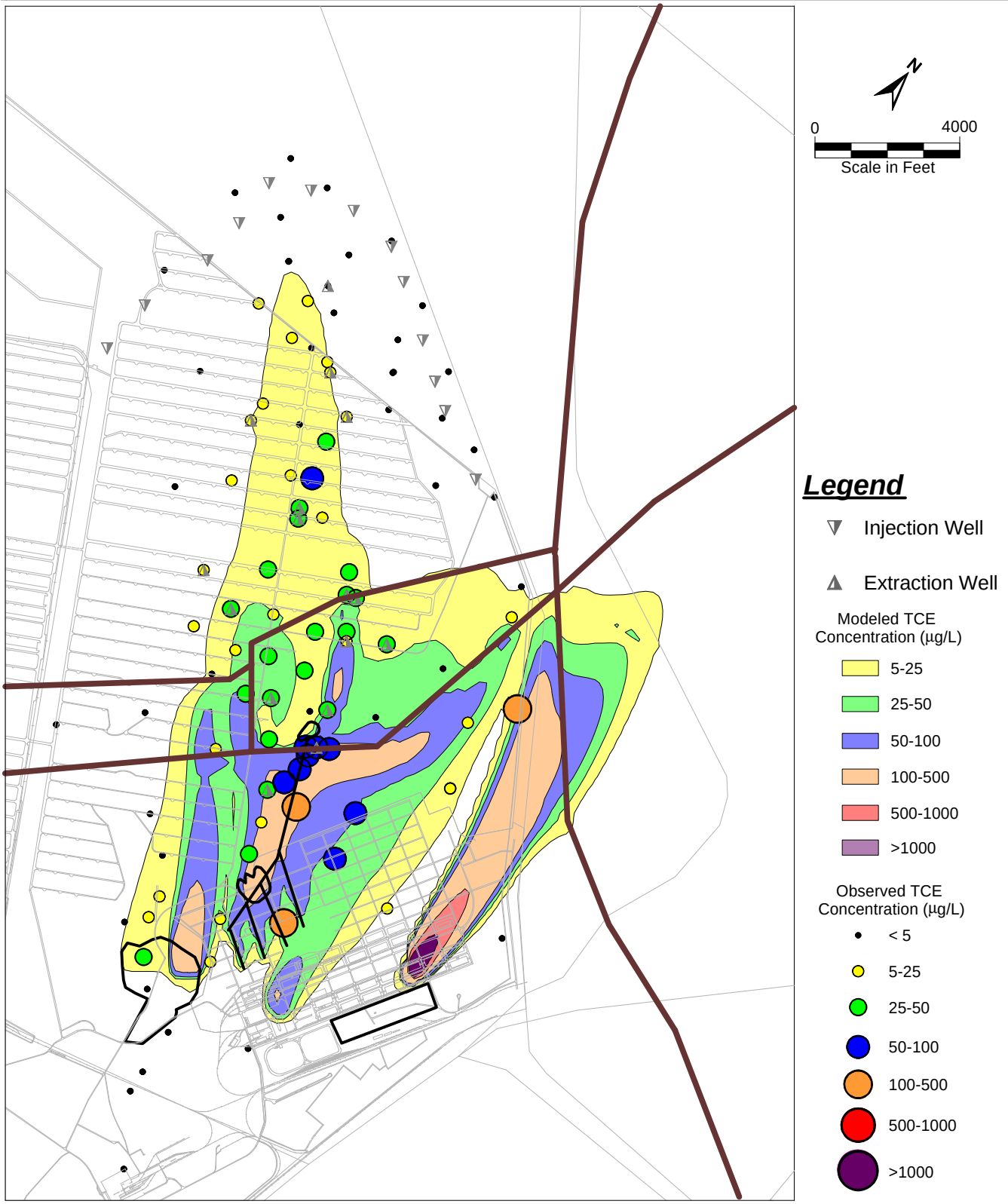

Figure 29. Modeled TCE Plume in 1995 with Observed TCE Concentrations

P:\Tooele Modeling\Figures\Conc1995.srf

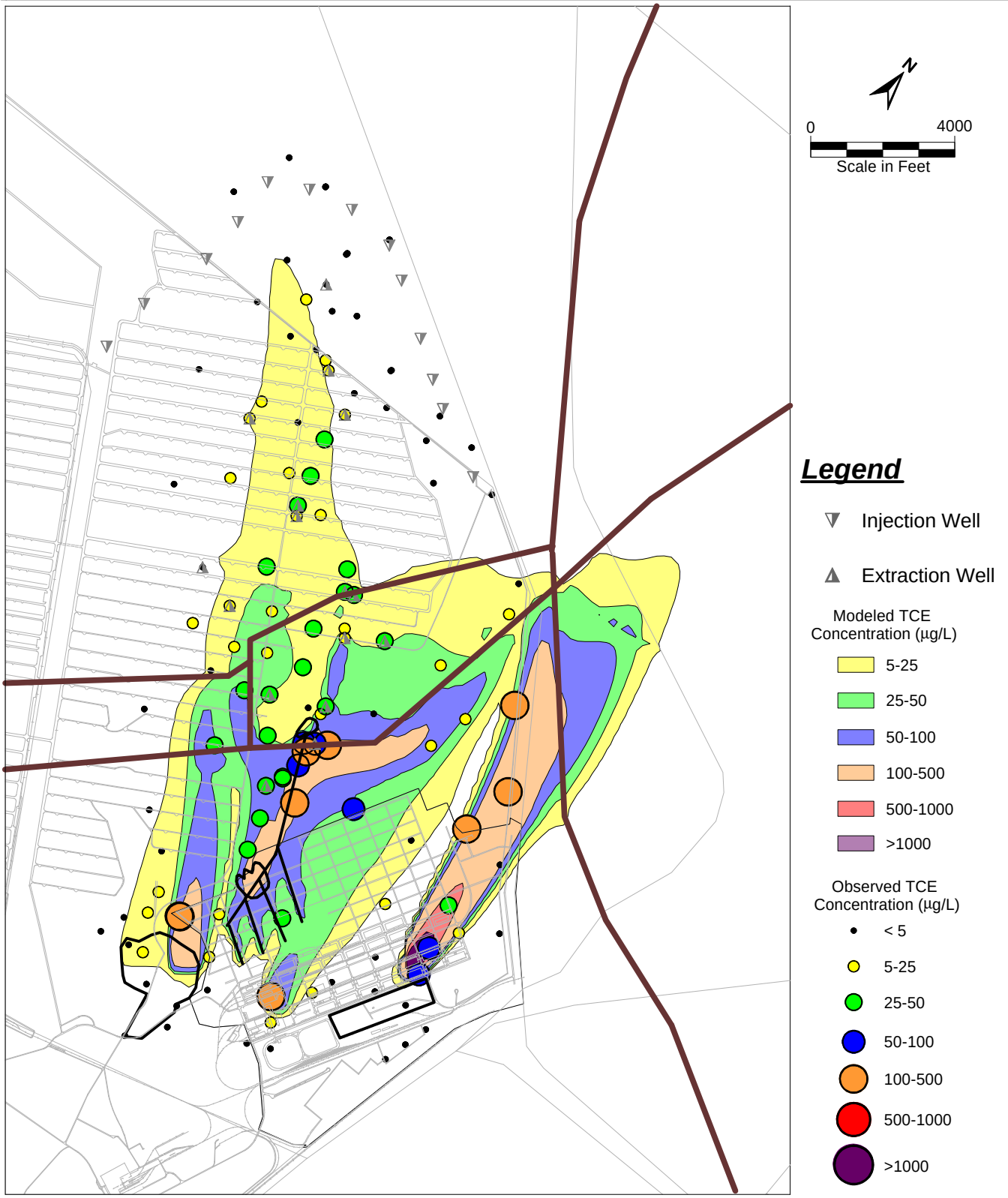

Figure 30. Modeled TCE Plume in 1998 with Observed TCE Concentrations

P:\Tooele Modeling\Figures\Conc1998.srf

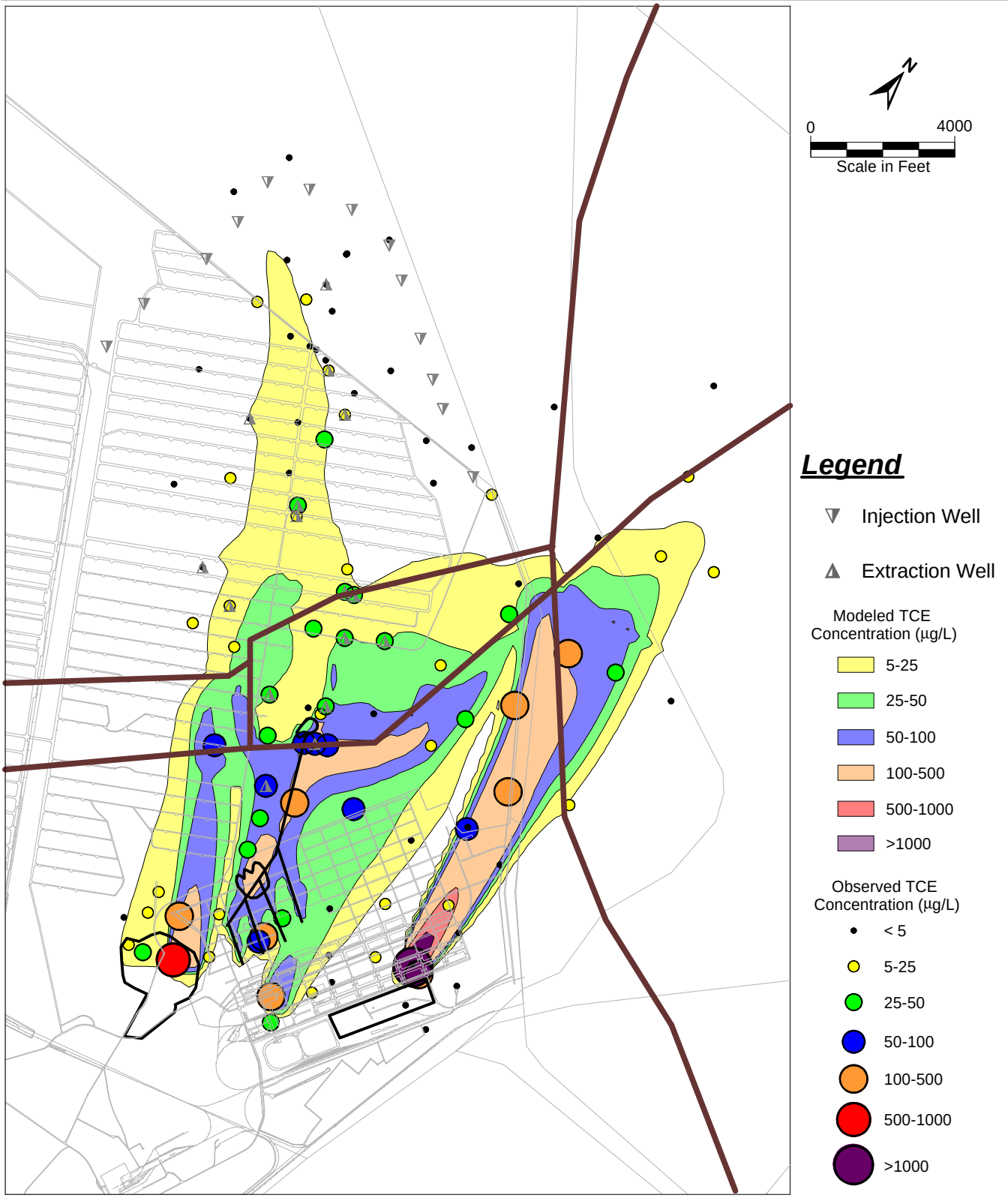

Figure 31. Modeled TCE Plume in 2001 with Observed TCE Concentrations

P:\Tooele Modeling\Figures\Conc2001.srf

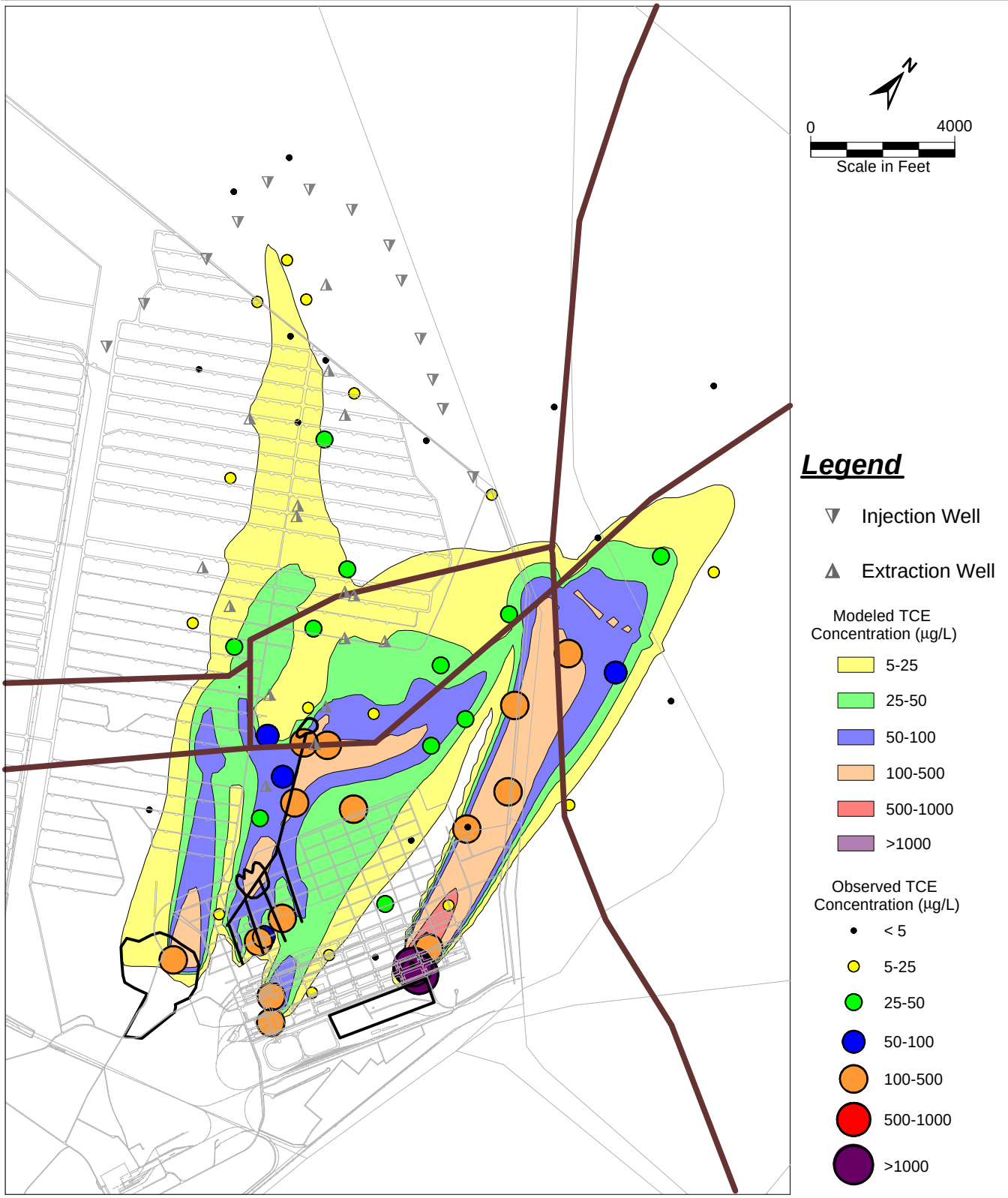

Figure 32. Modeled TCE Plume in 2003 with Observed TCE Concentrations

P:\Tooele Modeling\Figures\Conc2003.srf

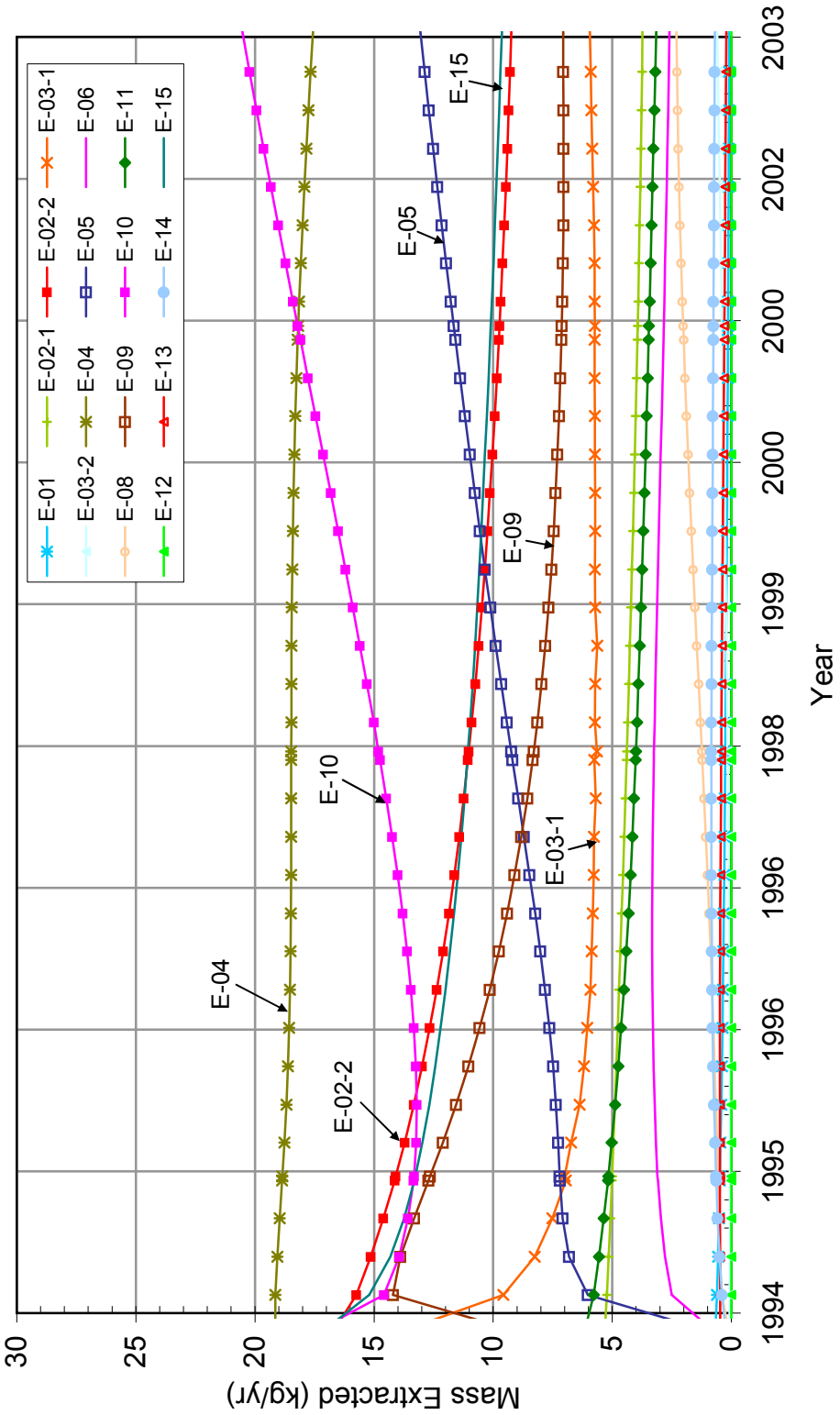

Figure 33. Modeled Mass Removed at Individual Extraction Wells

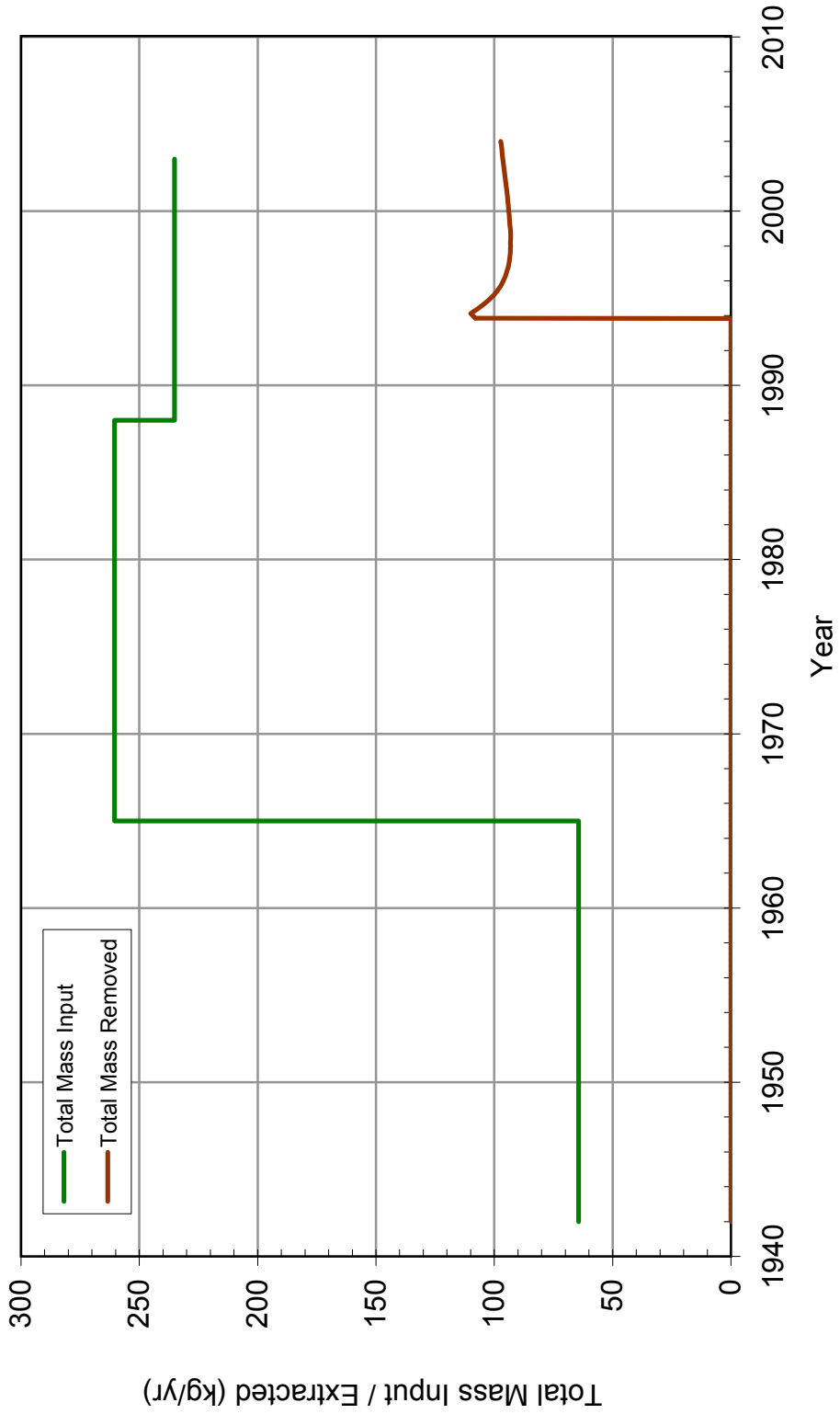

Figure 34. Comparison of Total Mass Input with Total Mass Removed

Figure 35. Modeled Mass in the Aquifer

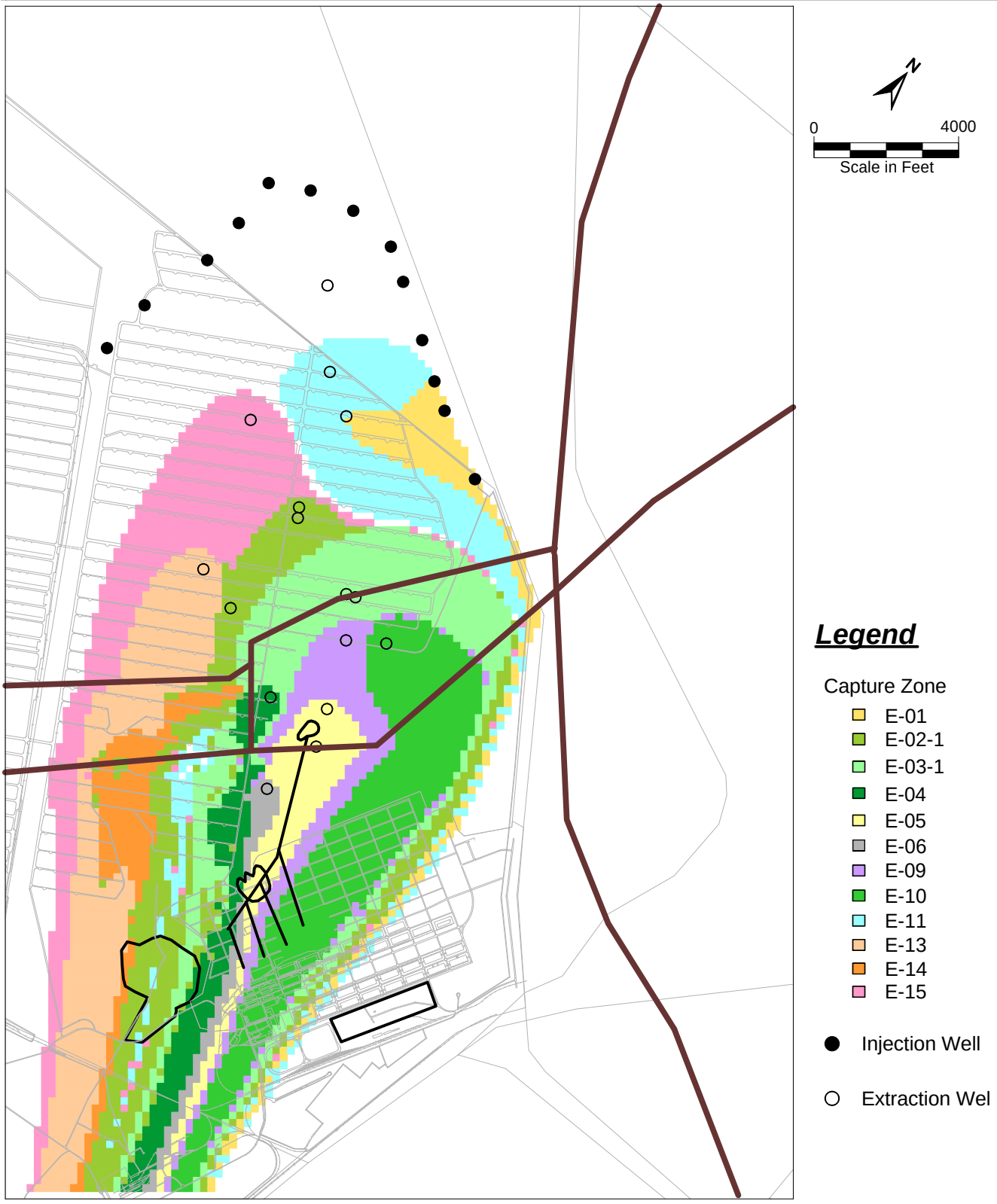

Figure 36. Modeled Capture Zone for the Extraction System

P:\Tooele Modeling\Figures\PTLay5.srf

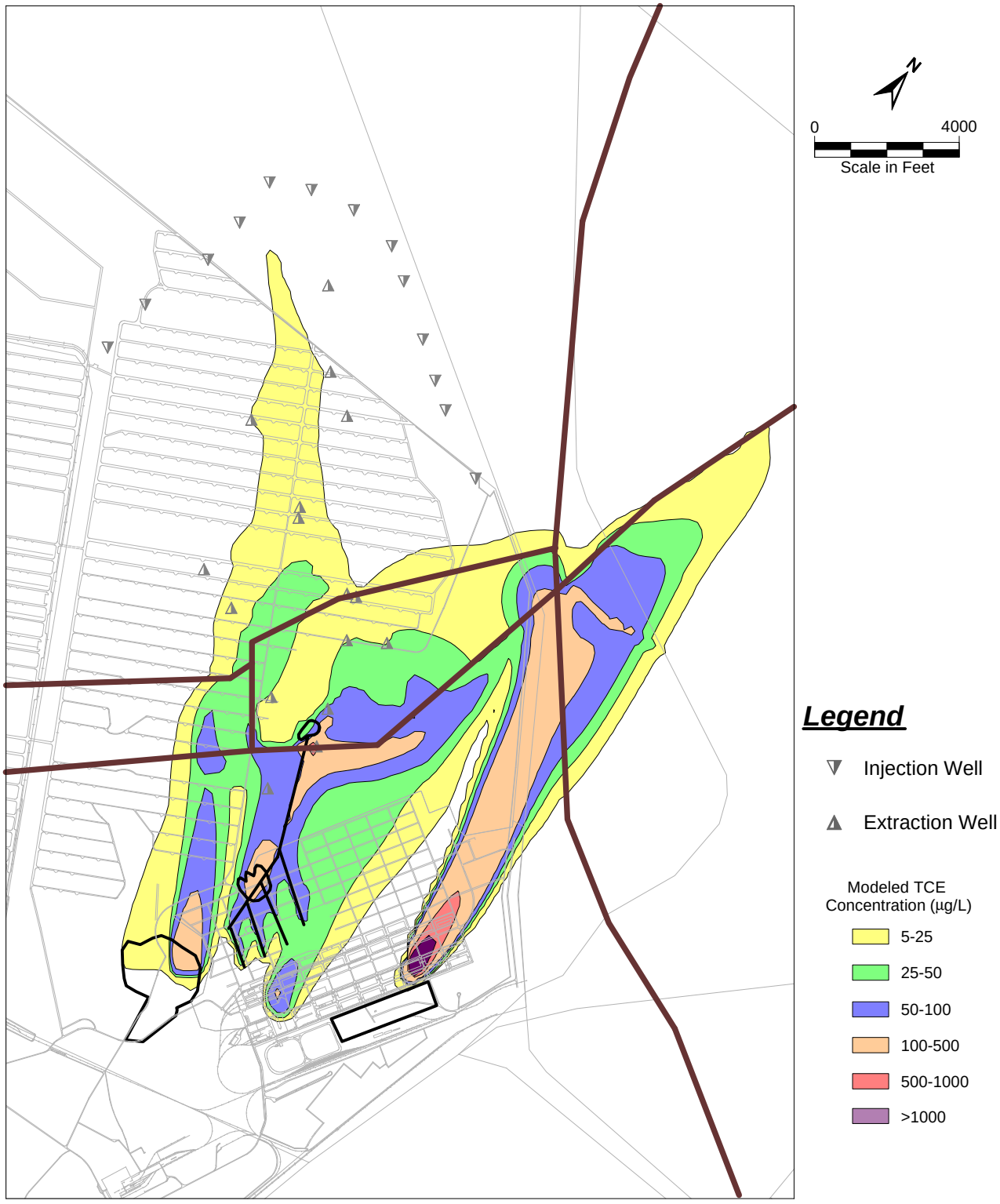

Figure 37. Modeled Plume in 2006 with Continued Pump-and-Treat Operation

C:\Tooele\Model\Pred1\Pred1Conc2006.srf

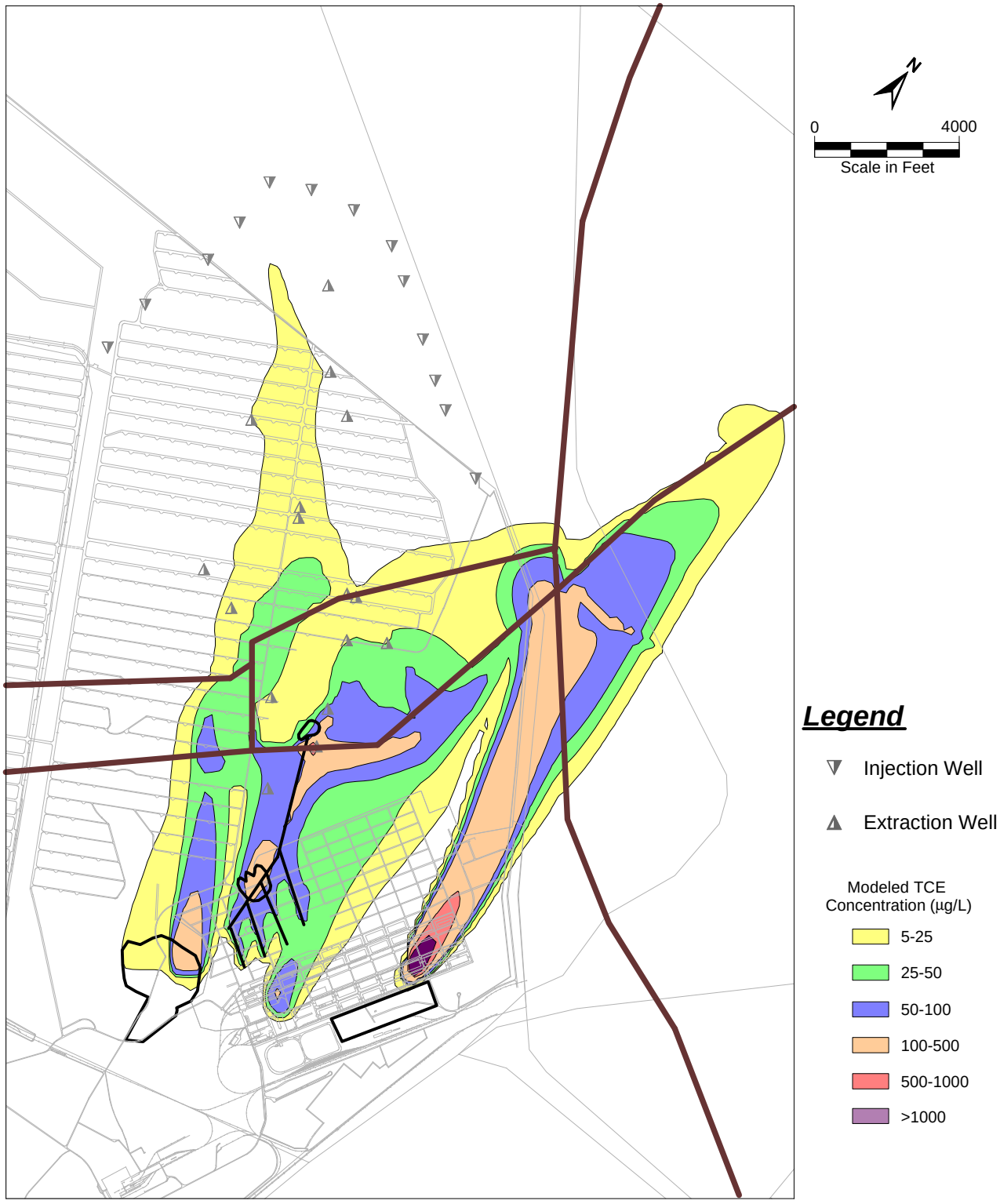

Figure 38. Modeled Plume in 2008 with Continued Pump-and-Treat Operation

C:\Tooele\Model\Pred1\Pred1Conc2008.srf

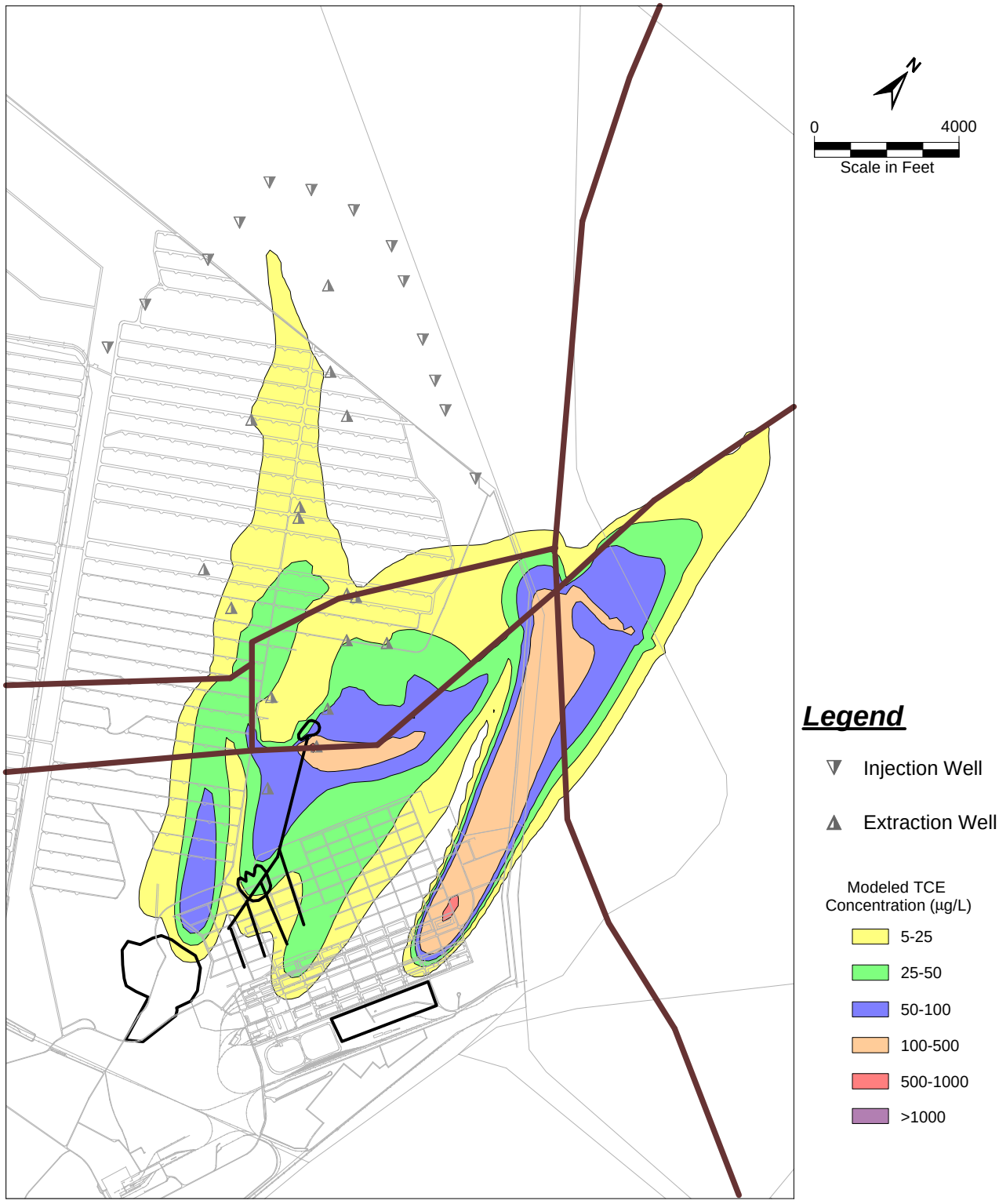

Figure 39. Modeled Plume in 2006 with Continued Pump-and-Treat Operation and No Source

C:\Tooele\Model\Pred3\Pred3Conc2006.srf

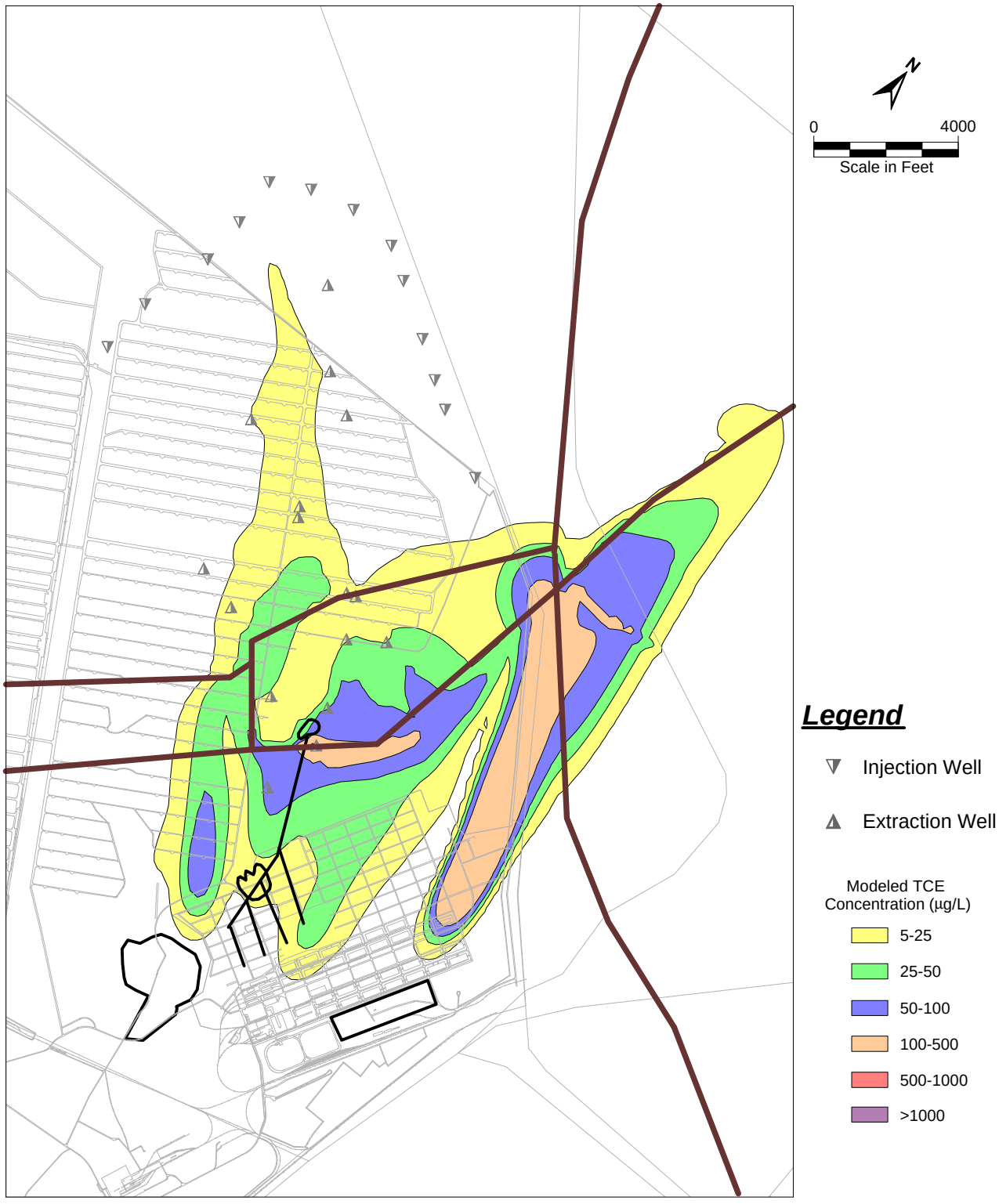

Figure 40. Modeled Plume in 2008 with Continued Pump-and-Treat Operation and No Source

C:\Tooele\Model\Pred3\Pred3Conc2008.srf

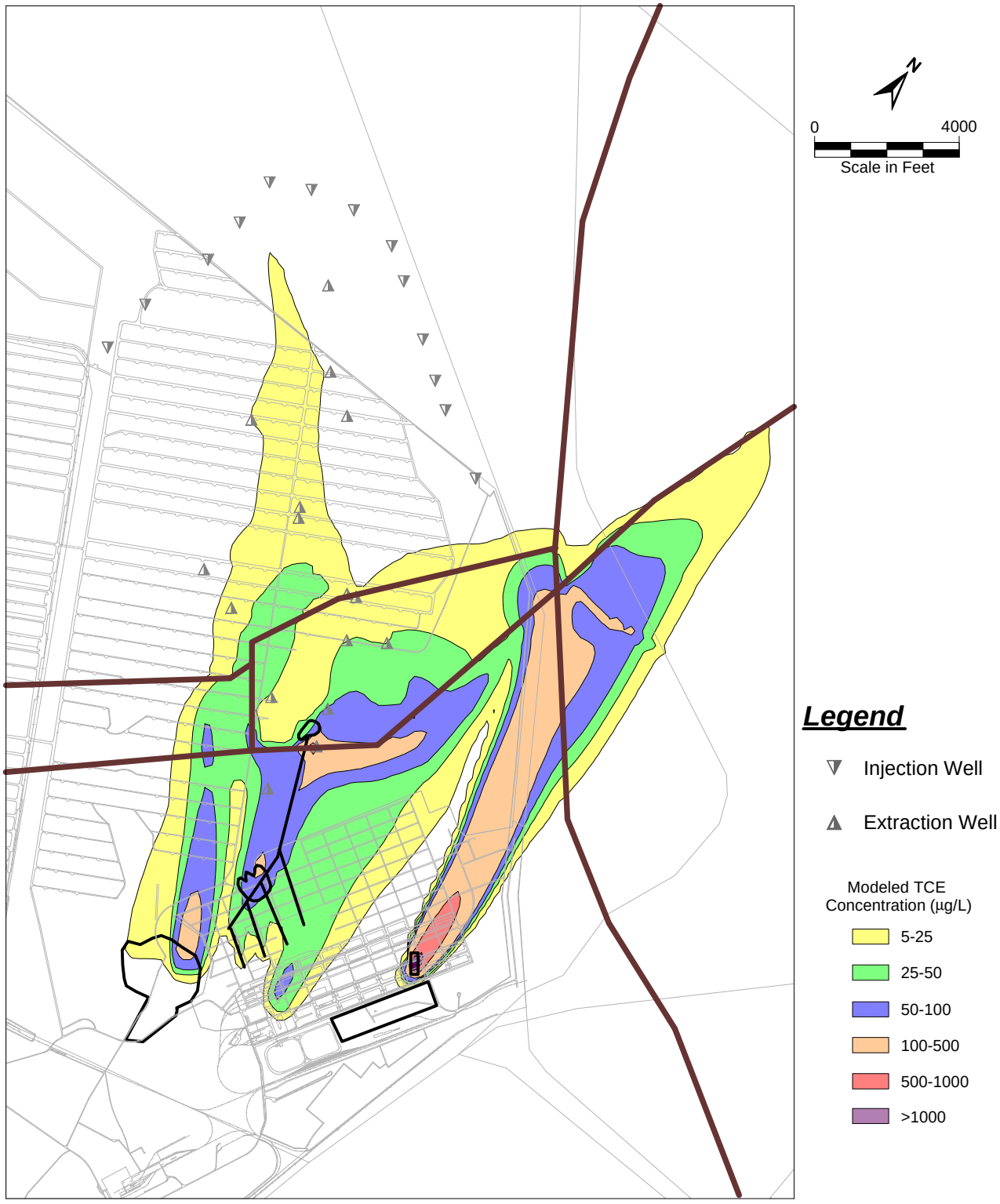

Figure 41. Modeled Plume in 2006 with Continued Pump-and-Treat Operation - Linearly Declining Source

C:\Tooele\Model\Pred6\Pred6Conc2006.srf

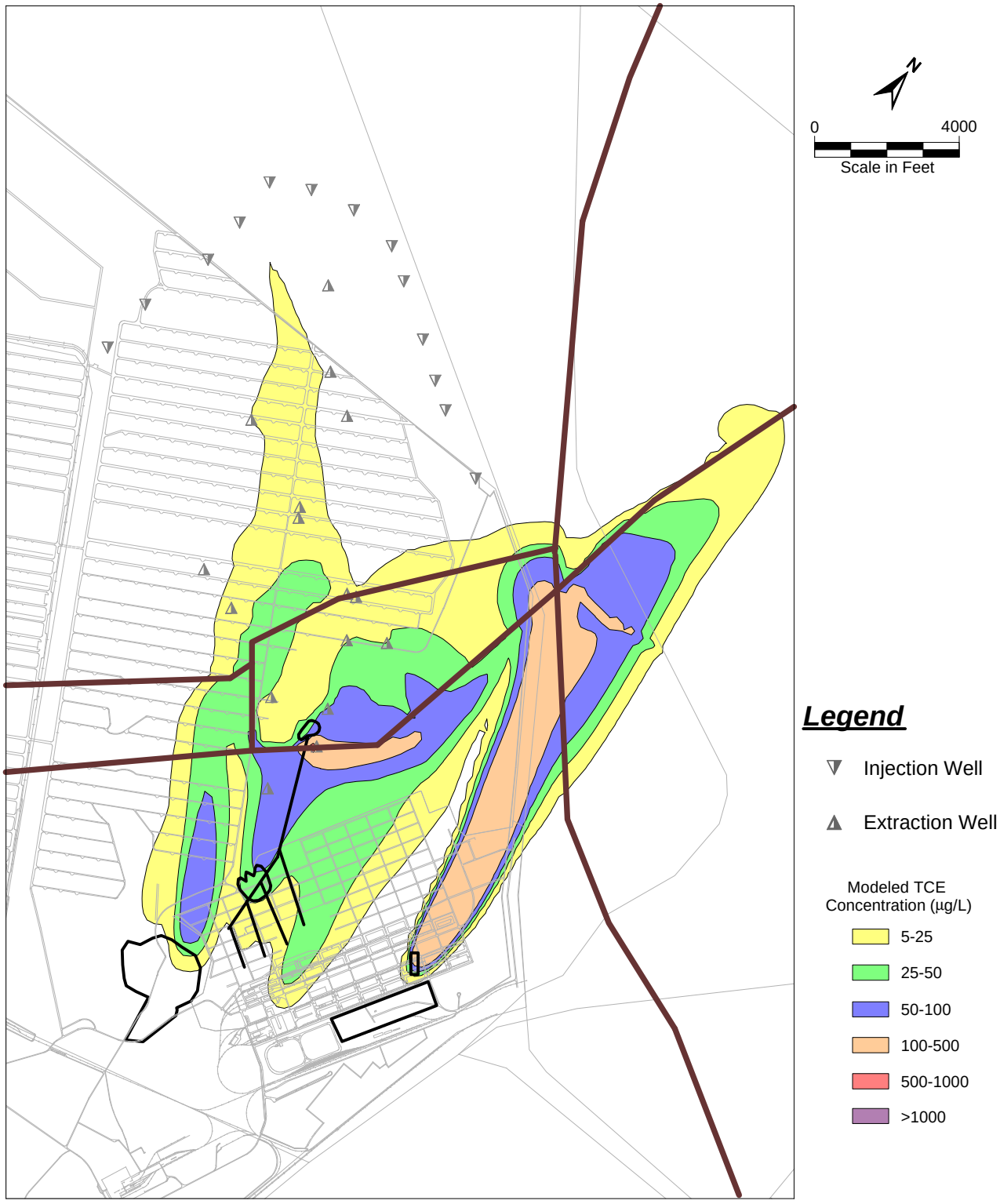

Figure 42. Modeled Plume in 2008 with Continued Pump-and-Treat Operation - Linearly Declining Source

C:\Tooele\Model\Pred6\Pred6Conc2008.srf

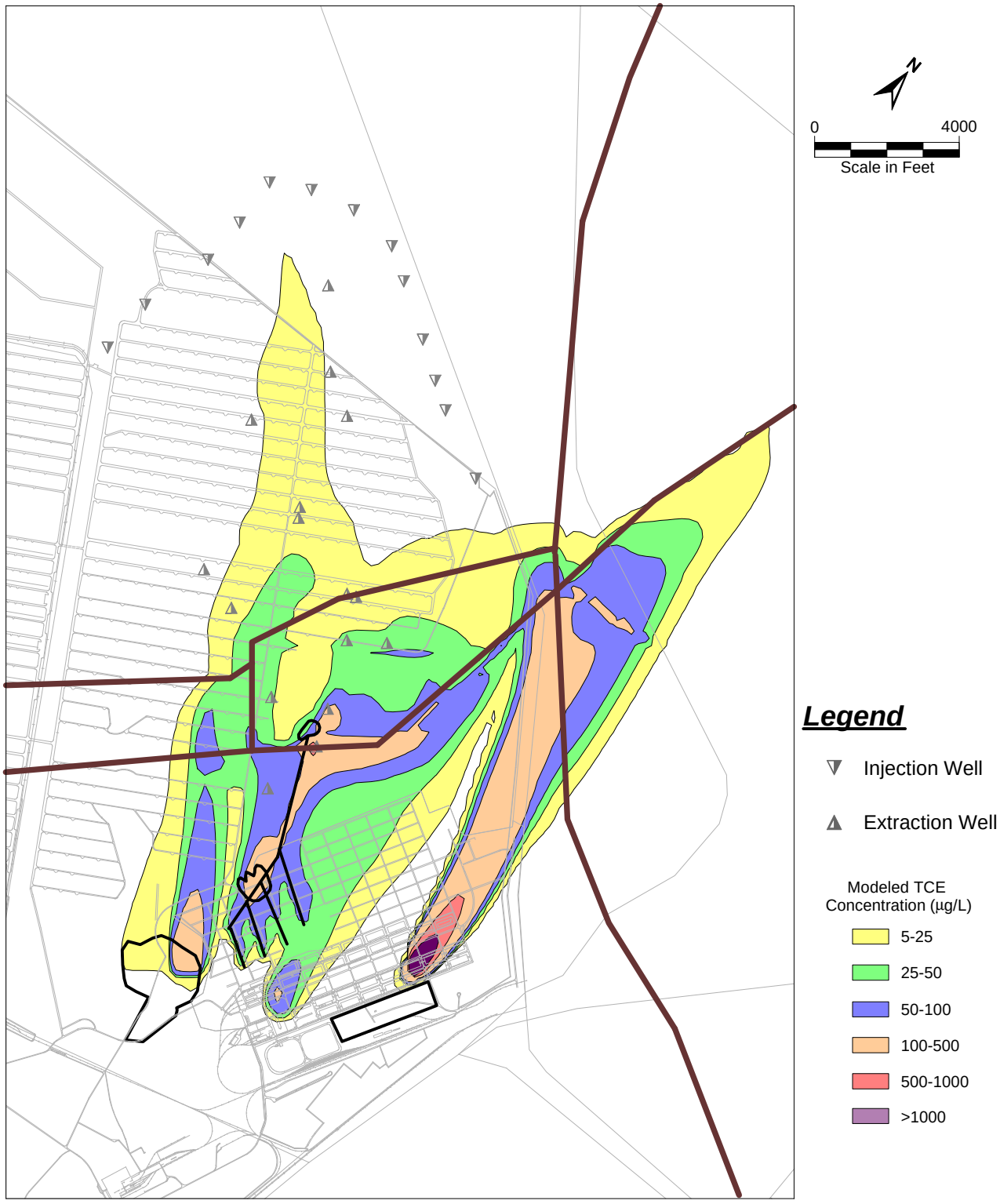

Figure 43. Modeled Plume in 2006 with No Further Action - Current Source

C:\Tooele\Model\Pred2\Pred2Conc2006.srf

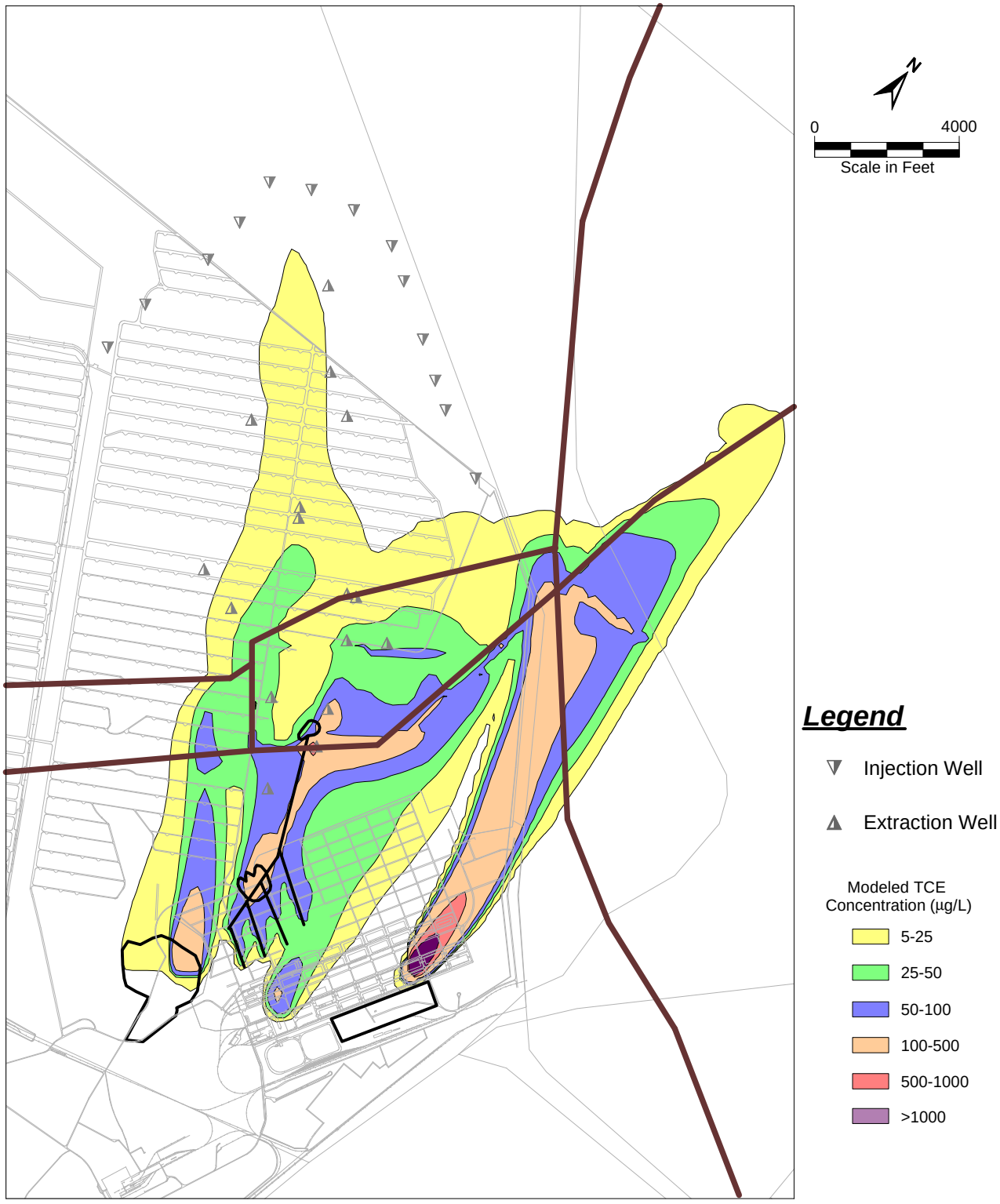

Figure 44. Modeled Plume in 2008 with No Further Action- Current Source

C:\Tooele\Model\Pred2\Pred2Conc2008.srf

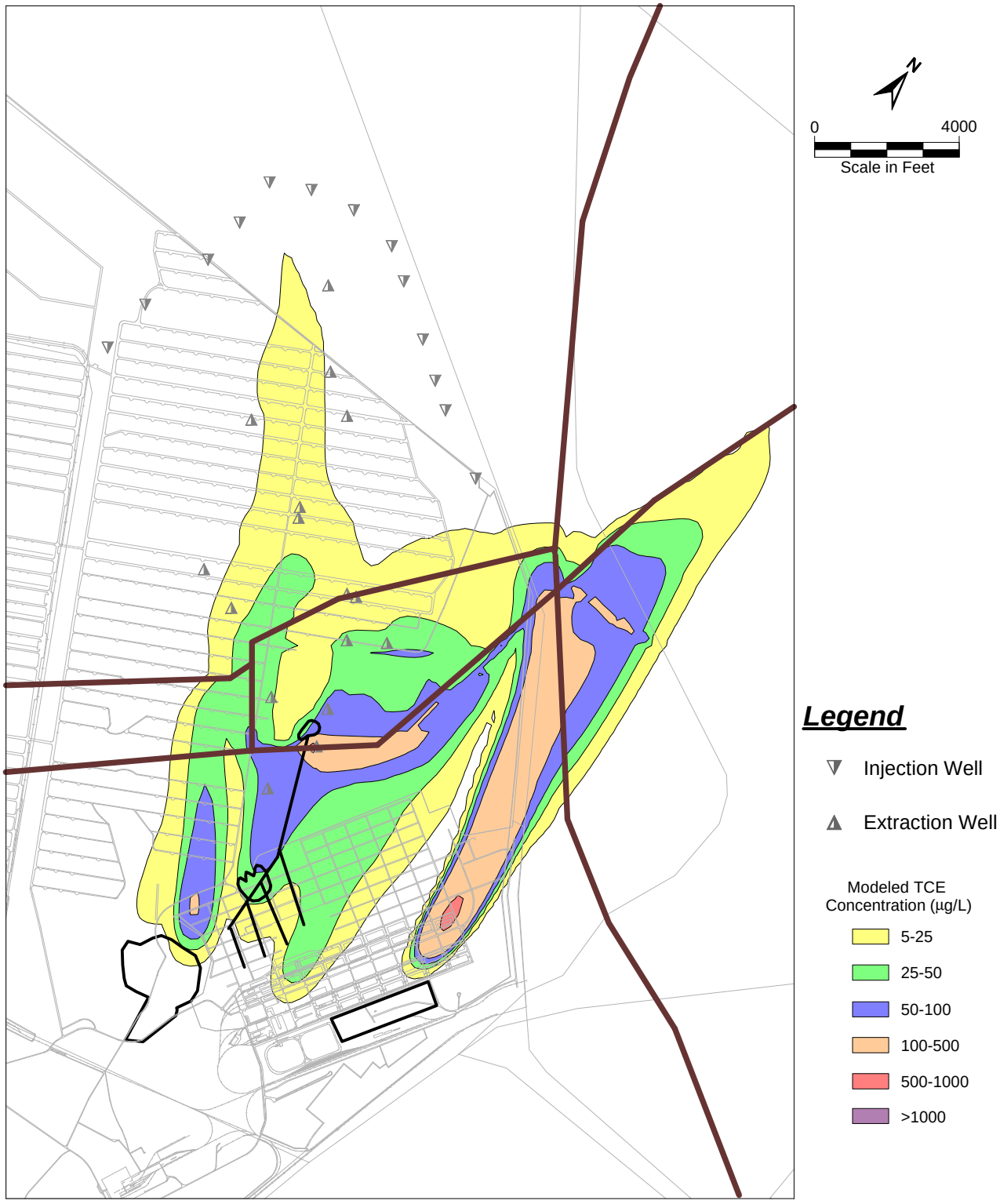

Figure 45. Modeled Plume in 2006 witd No Further Action - No Source

C:\Tooele\Model\Pred4\Pred4Conc2006.srf

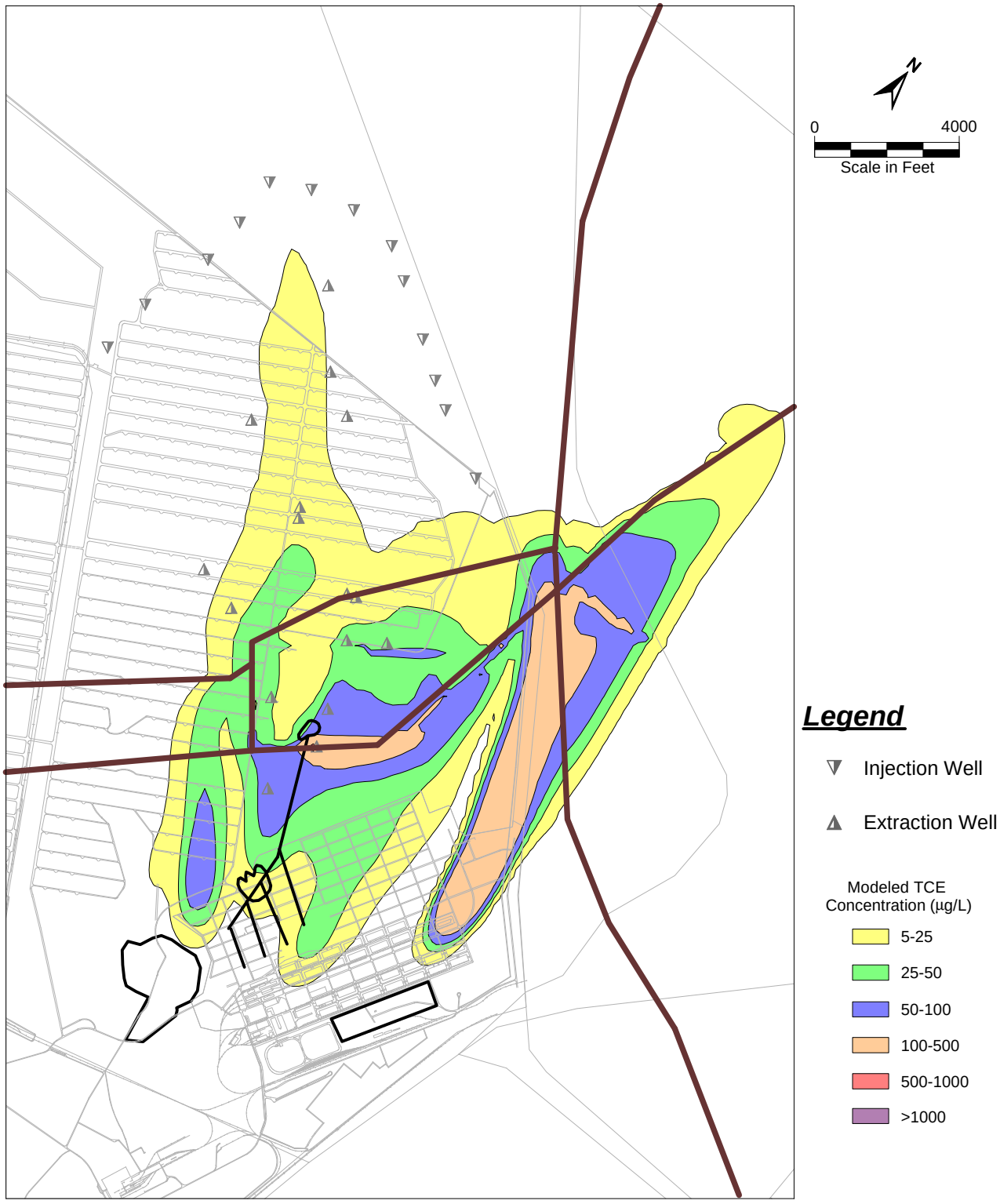

Figure 46. Modeled Plume in 2008 with No Further Action - No Source

C:\Tooele\Model\Pred4\Pred4Conc2008.srf

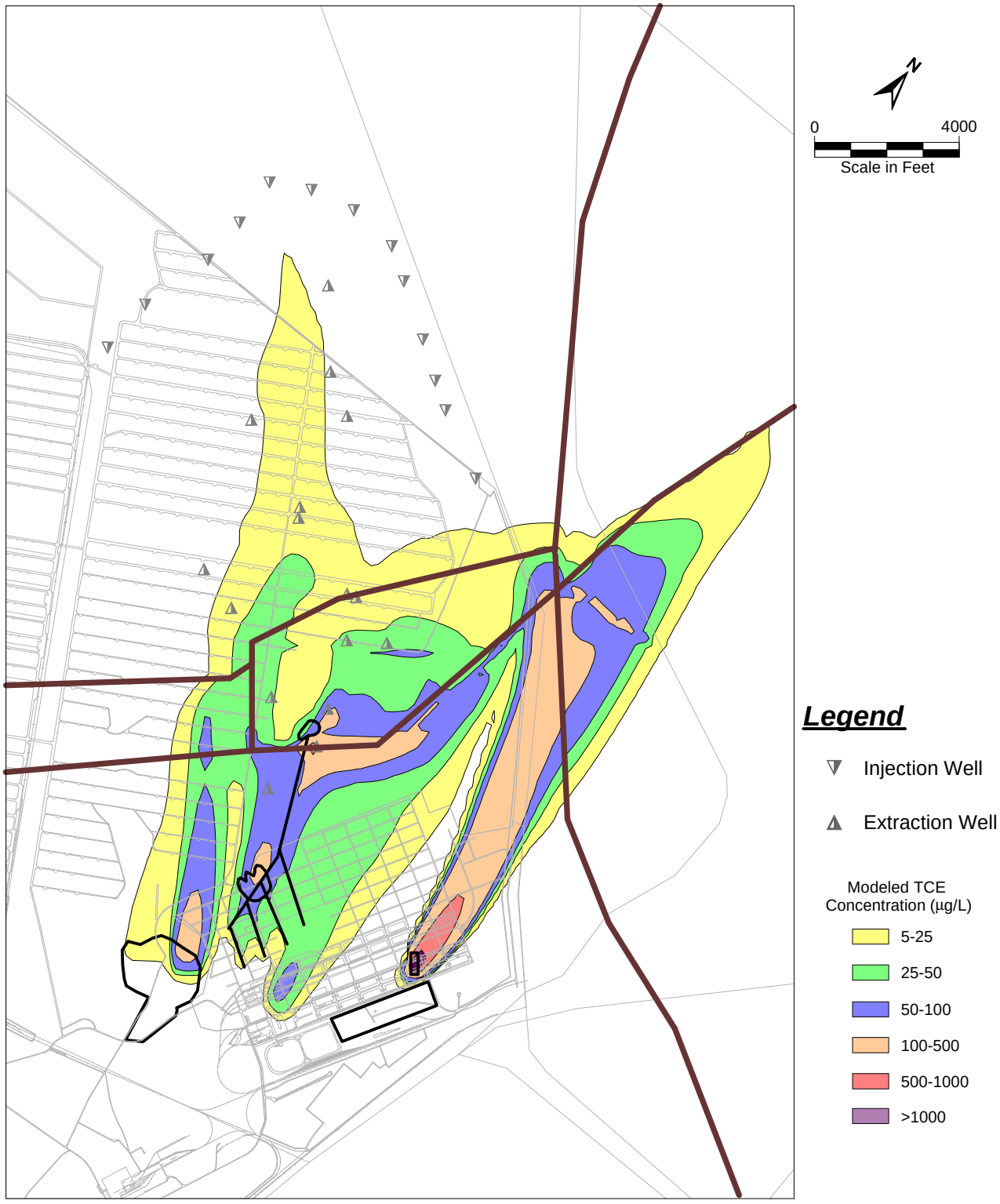

Figure 47. Modeled Plume in 2006 with No Further Action - Linearly Declining Source

C:\Tooele\Model\Pred7\Pred7Conc2006.srf

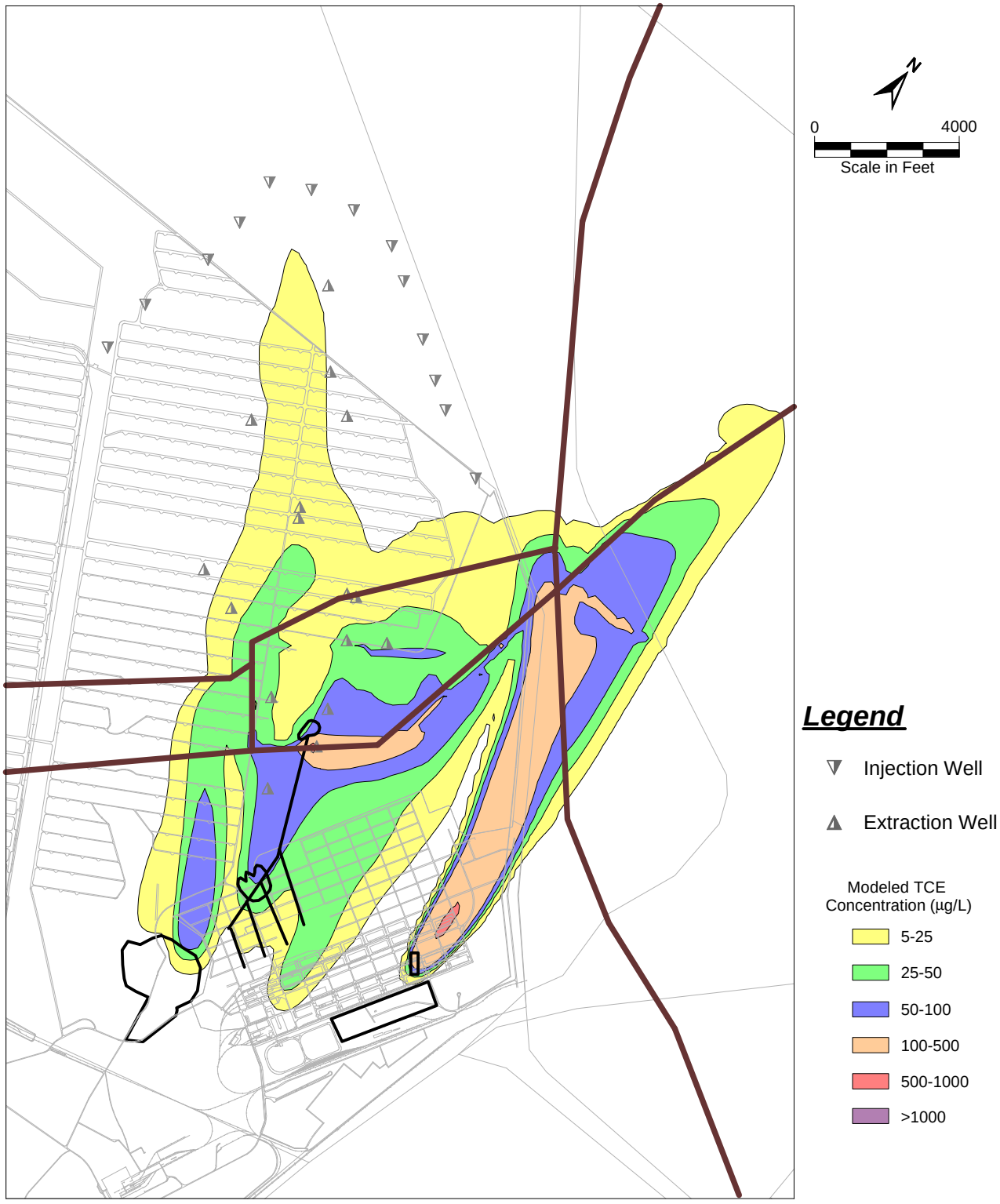

Figure 48. Modeled Plume in 2008 with No Further Action - Linearly Declining Source

C:\Tooele\Model\Pred7\Pred7Conc2008.srf

Appendix A

Prior HEC Groundwater Modeling Studies

1994 Modeling Study

The initial Tooele Army Depot groundwater flow model was developed in 1994 (HEC, 1994). The U.S. Geological Survey three-dimensional finite-difference groundwater flow model MODFLOW (McDonald and Harbaugh, 1988) was selected for application to the Tooele site. The model encompassed a 15,600 ft by 24,000 ft area, which was overlain by a 52 by 80 grid of 300-ft square cells. Three model layers were used. The model was calibrated in steady-state mode to 50 water levels measured in June 1992. Particle tracking was used to determine optimum pumping rates and pumping locations for the containment of the TCE plume. Results of this model were used to locate 3 extraction wells in addition to those originally proposed. The pump-and-treat system began operation in January 1994.

1995 Modeling Study

In 1995, a transient model was developed (HEC, 1995). Ninety-six transient water elevation measurements were selected as calibration targets. Results from the 1995 study indicated that water levels would approach steady-state conditions over a large portion of the site after two to three years of continuous pumping. This provided validation for a steady-state calibration to measured post-pumping water levels in subsequent applications

1996 Modeling Study

In 1996, the transient groundwater flow model was further developed (HEC, 1996). The model area was extended 4,200 ft to the northeast. Well extraction/injection data for the period of January 1995 through June 1996 were averaged over 4-week stress periods and input into the model, increasing the total number of stress periods from 18 to 33. Data from eight water-level measurement events in 1994 and 1995, at 69 well locations, were used as calibration targets. A calibration tool was designed, which allowed for the comparison of simulated and measured water levels using a variety of algorithms.

1997 Modeling Study

In 1997, the model was again expanded and recalibrated in steady-state mode. The model grid was extended 6,000 ft southeast, and new data were incorporated. The new data included additional water-level measurements, additional wells used as calibration targets, new boring logs, and new pumping data. Two separate calibration steps were performed – a calibration to average pre-pumping water levels (pre-pumping model) and a calibration to March 1997 water levels following over 3 years of pumping. Data from four water-level measurement events in 1992 and 1993 were used to calculate average

water levels for the pre-pumping analysis. This averaged seasonal variations and provided better steady-state calibration targets.

1998 Modeling Study

The 1998 study (HEC, 1999) included the extension of the model domain by 3,000 ft to the northwest. The 1998 model encompassed a total area of 15,000 acres (19,800 ft by 33,000 ft). Cell size was reduced to 200 ft x 200 ft (165 rows and 99 columns). The 1998 model included the recalibration of the flow model to both pre-pumping and post-pumping conditions, the application of a particle tracking model, and the development of an initial contaminant transport model. The pre-pumping calibration used water-level data from 58 observation wells averaged over four semi-annual measurements taken between June 1992 and September 1993. The post-pumping calibration used 61 water-level measurements taken in March 1997, approximately three years after the pump-and-treat operation started.

The particle-tracking processor MODPATH (Pollack, 1989) was applied to both pre-pumping and post-pumping scenarios. Results from particle tracking analysis illustrated that the faults around the bedrock block have a controlling influence on groundwater flow paths. An initial contaminant transport model was developed using the code MT3D (Zheng and Wang, 1998). Results from the transport model indicated that significant reduction in total pumping rates could be accomplished by optimizing the extraction system to focus on contaminant concentrations exceeding 50 µg/L.

1999 Modeling Study

The primary purpose of the 1999 calibration analysis (HEC, 1999) was to incorporate an additional model layer to better delineate the elevation of the bedrock beneath the southern alluvium. Previous models of the site consisted of a 150-ft thick upper layer (layer 1) with the top elevation matching the water table. Layer 2 had been specified to have a thickness of 150 ft and layer 3 had been specified to have a thickness of 300 ft. Since the construction of the original model (HEC, 1994), additional field evidence had indicated that the southern alluvium below the water table was significantly thinner than 150 ft. A new four-layer model was developed to more accurately delineate the alluvium and bedrock interface at the southern end of the site. What had been model layer 1 was divided into two layers – the upper one having a thickness of 50 ft (alluvium) and the lower one having a thickness of 100 ft (bedrock).

Additionally, this study incorporated the most recent field data available. Average extraction and injection rates were derived from the total volume of pumped water between system startup and October 1999. Water-level elevations from March 1997, April 1998, September 1998, April 1999, October 1999, and May 2000 were used in this study. Averaging the water levels over these six periods removed seasonal and annual fluctuations, allowing for a more reasonable steady-state calibration.

2000 Modeling Study

In 2000, water levels measured in March 1997, April 1998, September 1998, April 1999, October 1999, and May 2000 were incorporated into the post-pumping calibration. A geophysical survey had recently been conducted along the northeast boundary of the Tooele Army Depot that resulted in a new conceptualization of the bedrock location. The primary purpose of this calibration effort was to incorporate this new information on the location of the bedrock block.

A new transport simulation was made with the 2000 model (not formally documented). The model simulated TCE transport from source areas from 1942 to present. Constant-concentration sources were used in the top layer of the model. The concentration values for these source cells were based partly on measured concentrations at nearby groundwater wells.

2001/2002 Modeling Study

In 2001/2002, significant changes were made to the model structure (HEC, 2002). Most notably, a nine-layer model was used in place of the four-layer model developed in 1999. The reconstructed 9-layer structure of the model resulted in a more precise delineation of the hydrologic system. In the prior models, layer bottom elevations had been assigned as a function of simulated water table elevations in order to keep each layer at a constant thickness. In the 2001/2002 model, layer bottom elevations were specified as constant over the model domain. Additionally, the new layer structure included thinner layers in the upper 300 ft of the model to allow for a more accurate simulation of contaminant transport.

A revised conceptual model of the study area was integrated into the 2001/2002 model. This resulted in the adjustment of the bedrock zones and the creation of two new fault zones.

Extraction and injection pumping well data through Spring 2001 were incorporated into the model. The model was calibrated in steady-state to two sets of water level data: 157 water levels representing Spring of 2001 conditions, and the average of 7 semi-annual measurements at 54 wells between Spring 1997 and Spring 2001. Model conceptualization was initially based on the larger Spring 2001 data set. The model was then calibrated to the averaged data set. Final model adjustments were then made to achieve the best fit to both data sets. By attaining a good calibration with both data sets, the 2001/2002 modeling study provided validation for the use of the new, larger data set in future calibration studies.

2003 Modeling Study

In 2003, the model grid was extended 2,000 ft to the northeast to allow for a more accurate representation of flow at the northeast boundary. The model grid consisted of 165 rows and 109 columns, encompassing an area of 33,000 ft by 21,800 ft. Additionally, a study was performed to better represent the influence of more recent pumping rates on water levels. This study included the development of a representative model to assess the influence of pumping over time on calibration target locations. An algorithm was then developed to provide a more physically based estimation of representative steady-state pumping rates. A revised conceptualization of the bedrock, based upon recent geophysical studies, was integrated into the model.

The model was calibrated to 184 water levels measured in the spring and fall of 2002. The final model head calibration produced an absolute mean error of 1.76 ft. The absolute mean error of the prior (2001/2002) calibration study was 1.94 ft. The incorporation of a much larger calibration data set allowed for a more complex and accurate numerical representation of the site. Transport-model calibration was also included in this analysis. The model was calibrated to TCE concentrations and TCE mass removed by the extraction system. The model was additionally calibrated to regional estimates of subsurface inflow and measured drawdown in the uplifted bedrock block.

Appendix B

Determination of Calibration Targets

B.1 Selection of Representative Calibration Target Date

The average annual precipitation at Tooele from 1893 to present is 17.59 in/yr (http://www.wrc.dri.edu). The recent climate of Tooele has been characterized by a long wet period (1993-1998), followed by 3 average years (1999- 2001), and the recent 2-year dry period. An analysis of the relationship between changes in precipitation at Tooele with groundwater elevations was performed by Brad Call (written communication, January 2004). The analysis described an apparent 2 to 4 year time lag for precipitation trends to be reflected in groundwater elevation. As a result of the continuing drought in the Tooele Valley, water levels measured in 2003 were generally 2-5 ft lower than in 2002. The 2003 data set was judged to be below long-term, average water levels. The 2002 data set was judged to provide a better representation of long-term, average water levels.

The model is calibrated assuming steady-state conditions and is used as a predictive tool for the simulation of future plume migration. The data set selected for use in model calibration should provide an accurate representation of average, long-term conditions. The factors used in the selection of a representative data set include: completeness and accuracy of the data set; and the ability of the data set to represent average hydrologic conditions. The water level data sets from 2002 and 2003 were much larger and more complete than previous data sets. Analysis of long-term precipitation trends and well hydrographs indicated that 2002 water levels approximated average conditions. This, it was decided to use the average 2002 data set as the benchmark for model calibration. This data set consists of the average of measurements taken in March 2002 and September 2002. Additional calibration targets were integrated into this data set as described below.

B.2 Development of Calibration Targets

The initial water-level data set used in this study consisted of a total of 197 wells within the study area. Each measurement in the data set was analyzed for reliability and its ability to accurately represent the flow regime. Additionally, a regional map of water elevations from wells measured off-site by the U.S. Geological Survey (Lynette Brooks, written communication, January 2004) were integrated into the development of calibration targets. A total of 195 monitoring wells were used in model calibration. The following discussion details the factors used in the target analysis and development.

B.2.1 Correction of 2003 Water Levels to Representative 2002 Value

There were 10 water levels included in the data set that were measured in 2003, and were not part of the 2002 data set. These water levels were measured at well B-38, C-10, C-11, C-31, C-40, N-04, N-08B, P-11D, P-27D, P-35. Water levels at these wells were

integrated into the calibration process by adjusting them to 2002 conditions. Three proximate wells were identified for each target location. The average 2002 water levels (spring and fall) and average 2003 water levels (spring and fall) were computed for each set of three proximate wells. The average decline in water levels from 2002 to 2003 was then calculated. This value was then used as a correction factor for the 10 water levels measured solely in 2003. Table B-1 describes the data used in this calculation. The value in the right column was integrated into the calibration data set. Head elevations are relative to a 4,000 ft MSL datum.

Table B-1 Adjustment of 2003 Water Levels to Average 2002 Conditions (ft)

2003 Well	Avg. 2003	3 Closest Wells	Avg. Decline (2002 to 2003)	Adjusted WL
B-38	306.31	B-45, B-48, B-25	3.11	309.42
C-10	458.95	B-10, C-13, C-14	2.51	461.46
C -11	344.14	P-11S, D-4, P-12S	3.83	347.97
C-31	466.73	C-33, C-15, C-26	2.43	469.16
C-04	472.39	N-144, N-116, N-120	2.59	474.98
N-04	464.04	N-134, P-4S, B-4	1.42	465.46
N-08B	305.95	B-40, B-18, P-19S	2.80	308.75
P-11D	343.13	B-16, C-7, P-9D	3.09	346.22
P-27D	340.02	B-57, B-56, B-58	1.20	341.22
P-35	300.70	P-34, C-4, C-3	2.09	302.79

B.2.2 Unrealistic Discrepancies Between Spring and Fall Measurement Values

Some variations in groundwater levels are expected due to seasonal fluctuations in subsurface inflows to the site. Changes in water levels between spring and fall 2002 averaged approximately 2.5 ft across the site. During data analysis, differences in measured water-level elevations greater than 10 ft between the spring and fall measurement events were found at 2 wells. At well A-5, the measured difference was 19.5 ft. At well B-7, the measured difference was 30.9 ft. These two wells were removed from the calibration process.

B.2.3 Equipment Malfunction During Well Measurements

Two wells were removed from the calibration process due to equipment malfunction: P-5S, P-5D (Carl Cole, personal communication, January 2003).

B.2.4 Removal of Anomalous Data

The nature of groundwater flow modeling requires the averaging of parameters over space. For example, parameters are assumed homogeneous across a grid cell. Measured water levels may be influenced by small-scale heterogeneities that should not be simulated by the model. To include data outliers in the calibration process would require the delineation of a much finer grid and the creation of a more complex model. This is

not recommended for a heterogeneous site; i.e., the complexity of the model should be commensurate with the ability of the data to represent the system.

Seven wells were determined to be data outliers, and removed from the calibration process. Six water-level measurements: B-5, B-55, P-10 D, P-12S, C-36, and T-6 were identified as clear outliers from the general hydrogeologic trend the model seeks to simulate. These wells were also removed as calibration targets in the 2003 study. The following table locates these wells along with proximate wells with significantly different head values. Head elevations are relative to a 4,000 ft MSL datum.

Table B-2 Anomalous Data Removed from Calibration

Well	Row	Column	Layer	Head (ft)	Proximate Wells	Head (ft)
B-5	109	44	6	329	B-21, A-5	444, 465
B-55	113	39	7	412	P-3D, P-7D, P-4D	451,461,469
P-10D	105	64	4	352	B-10, P-10S	462, 462
P-12S	93	52	4	360	P-12D	342
C-36	132	46	1	510	B-26, C-34, C-35	471, 473, 472
T-6	95	32	4	349	P-26S, B-6, P-13S	311, 313, 315

Additionally well T-2 was removed from the calibration process. Well T-2 is located about 300 ft "upgradient" of well B-21, yet has a measured elevation which varies from 0.1 to 0.2 ft lower. The elevation of T-2 and B-21 are about 443 ft. This elevation is about 20 ft below the water levels in the southern alluvium, which range from 473 ft to 465 ft, and over 100 ft above the water level elevation in the bedrock. The elevation measured at T-2 and B-21 represents a transition from southern alluvium water levels to bedrock water levels. This transition occurs in the area of the bedrock encasing zone. This encasing zone cannot be located adjacent to both wells. In past models, the encasing zone was located between the two wells, thus "splitting the difference" in the model residual between the two wells. However, analysis of boring logs indicated significant cementation in well T-2. The measurement at well B-21 was deemed more reliable, and the location of the encasing zone was adjusted to be adjacent to well B-21.

Other data outliers, such as wells B-21, P-3D, and T-4, were not removed from the calibration process since they were not judged to be screened in a local geologic anomaly. The high calibrated residual from these wells was a function of location in or near hydrogeologic zones of low hydraulic conductivity and corresponding steep flow gradients (such as faults). The goal of data analysis was to remove inaccurate an unrepresentative data. The effect of removing data outliers on model calibration statistics is detailed below. The reason for removing these outliers was not to improve model statistics, but to provide a more accurate representation of the larger-scale hydrologic system.

Table B-3 The Effect of Data Outliers on Calibration Statistics (ft)

	Without Anomalous Data	With Anomalous Data
Mean Residual	0.08	-1.12
Mean Absolute Residual	1.36	3.31
Residual Sum of Squares	838	37,600

Table B-4 presents the simulated residual, using the calibrated model, for each of the removed data targets. The location of residuals is also listed in table B-4.

Table B-4 Simulated Residuals and Location of Data Outliers (ft)

Well	Residual (measured – simulated)	Location
B-5	-136.5	upgradient of encasing zone
B-55	-55.2	upgradient of encasing zone
P-10D	-110.3	upgradient of encasing zone
P-12S	19.3	within encased bedrock block
C-36	39.2	industrial area
T-2	-21.8	upgradient of encasing zone
T-6	23.7	downgradient of encasing zone

With the exception of well T-2, all the wells listed in Table B-4 were not used in the 2003 model calibration. The addition of well T-2 in the current calibration statistics resulted in an increase in the Mean Absolute Residual (MAR) from 1.36 to 1.46 ft. This is well below the MAR of 1.76 ft of the 2003 model.

B.2.5 Addition of Regional Wells Measured in Spring 2003

The U.S Geological Survey is currently completing a regional study of the hydrology of the Tooele Valley. As part of this study, depth to water was measured at wells throughout the Tooele Valley. Most of these wells were not surveyed and the measured water elevations are approximations. However, these measurements provided valuable new data on the regional flow regime. Nine wells were selected as calibration targets. These data points are named USGS 1-9 and are presented in Figure 2. The wells are located near the boundary of the model grid and provided a more physically based representation of the regional flow domain. Constant head boundary conditions at the southeastern, northeastern, and northwestern model boundaries were specified based on these measured values. The addition of this data is especially valuable in increasing the accuracy of predictive simulations of contaminant plume migration.

Appendix C. Water-Level Residuals in the Current Conditions Model

(Depth: S = Shallow (<= 100 ft below water table), M = Medium, D = Deep (> 300 ft below water table))

Well ID	East	North	Layer	Row	Column	Depth	Mid-Point of Screen Interval Elevation (ft)	Avg. Observed Head (ft)	Computed Head (ft)	Residual
A-02A	1402244	7361634	1	133	30	S	4470.18	4472.95	4471.83	-1.12
B-01	1399898	7361970	3	124	22	S	4387.06	4471.58	4470.29	-1.29
B-03	1403268	7366267	1	118	49	S	4456.12	4469.86	4467.24	-2.62
B-04	1399165	7365179	1	109	30	S	4470.58	4467.43	4466.49	-0.94
B-06	1396534	7367409	5	92	27	S	4297.63	4312.54	4312.79	0.25
B-09	1402598	7370884	5	98	61	S	4279.76	4345.40	4345.43	0.03
B-10	1404073	7370170	3	105	64	S	4392.42	4462.56	4462.95	0.39
B-11	1402827	7374016	5	87	72	S	4310.29	4350.63	4345.14	-5.49
B-12	1398896	7371293	5	85	48	S	4308.29	4308.33	4308.68	0.35
B-13	1397125	7369926	7	84	37	S	4117.6	4309.63	4309.95	0.32
B-14	1393678	7370055	5	73	24	S	4322.9	4308.98	4309.76	0.78
B-15	1396460	7372644	6	72	43	S	4243.81	4310.56	4308.74	-1.82
B-16	1399225	7374664	6	73	60	S	4244.86	4309.40	4309.73	0.33
B-17	1395940	7375186	8	60	49	S	4049.43	4309.34	4309.43	0.09
B-18	1392185	7372958	5	57	27	S	4289.13	4307.23	4307.94	0.71
B-19	1394740	7375390	6	56	45	S	4223.5	4308.46	4306.59	-1.87
B-20	1399678	7368408	6	98	42	S	4243.63	4342.29	4343.10	0.81
B-21	1401039	7366810	4	109	42	S	4350.12	4444.07	4450.04	5.97
B-22	1401427	7364415	4	119	36	S	4335.68	4469.42	4469.09	-0.33
B-23	1395334	7362898	4	106	8	S	4349.32	4466.31	4465.27	-1.04
B-24	1402021	7368663	5	105	52	S	4298.5	4343.35	4345.19	1.84
B-25	1394153	7375411	8	54	43	D	3923.75	4308.96	4309.21	0.25
B-26	1403671	7362667	1	133	39	S	4460.12	4471.45	4471.50	0.05
B-27	1401903	7365360	2	117	41	S	4445.08	4470.55	4468.15	-2.40
B-28	1397759	7366710	6	99	29	S	4222.34	4319.10	4315.13	-3.97
B-29	1397369	7371984	8	77	44	S	4069.16	4308.13	4310.00	1.87
B-30	1394782	7371181	5	72	32	S	4305.64	4311.64	4309.07	-2.57
B-31	1398319	7375444	8	67	59	S	4087.17	4309.43	4309.78	0.35
B-32	1396888	7375447	6	62	53	S	4272.46	4307.91	4309.03	1.12
B-33	1394355	7375452	8	54	44	S	4098.35	4308.83	4309.23	0.40
B-34	1393561	7375285	6	52	40	S	4248.79	4309.01	4307.43	-1.58
B-35	1392248	7375433	6	48	35	S	4252.53	4305.06	4307.04	1.98
B-36	1397012	7364714	3	104	20	S	4389.85	4465.33	4465.45	0.12
B-37	1392148	7376854	6	42	40	S	4248.09	4304.50	4306.50	2.00
B-38	1392150	7376865	8	42	40	D	3960.08	4309.42	4309.34	-0.08
B-39	1394631	7376894	7	50	49	M	4155.17	4309.40	4307.92	-1.48

Appendix C. Water-Level Residuals in the Current Conditions Model

(Depth: S = Shallow (<= 100 ft below water table), M = Medium, D = Deep (> 300 ft below water table))

Well ID	East	North	Layer	Row	Column	Depth	Mid-Point of Screen Interval Elevation (ft)	Avg. Observed Head (ft)	Computed Head (ft)	Residual
B-40	1393251	7376349	5	47	42	S	4282.72	4306.87	4307.10	0.23
B-41	1396330	7376342	5	57	54	S	4297.35	4309.45	4309.32	-0.13
B-42	1393981	7379103	6	39	54	S	4228.31	4307.08	4306.42	-0.66
B-43	1393981	7379093	8	39	54	D	3934.75	4309.03	4309.49	0.46
B-44	1393319	7378052	6	41	48	S	4266.92	4304.33	4306.77	2.44
B-45	1393321	7378063	8	41	48	D	3942.1	4309.08	4309.41	0.33
B-46	1393197	7379407	6	35	52	M	4204.8	4304.93	4305.11	0.18
B-47	1391678	7379101	6	32	45	S	4211.52	4304.09	4304.74	0.65
B-48	1391678	7379111	8	32	45	D	3937.24	4308.94	4309.68	0.74
B-49	1393317	7378027	7	41	48	M	4170.17	4310.68	4306.08	-4.60
B-50	1394019	7376556	6	49	46	S	4218.79	4309.71	4307.53	-2.18
B-51	1395858	7377105	7	53	55	S	4197.71	4310.39	4308.60	-1.79
B-52	1396325	7376317	6	57	54	S	4213.95	4309.25	4309.13	-0.12
B-53	1398178	7376211	6	63	61	S	4236.85	4309.54	4309.67	0.13
B-54	1405621	7364793	2	131	53	S	4431.43	4470.18	4469.38	-0.80
B-56	1400506	7367633	8	104	43	D	4005.3	4341.27	4344.51	3.24
B-57	1399890	7369976	8	93	48	M	4089.55	4342.14	4340.63	-1.51
B-58	1398026	7369062	7	91	38	M	4159.47	4342.48	4337.91	-4.57
B-59	1395955	7372332	9	71	40	S	3838.53	4310.29	4310.39	0.10
B-60	1394099	7373378	6	61	36	S	4236.8	4310.66	4307.59	-3.07
B-61	1395246	7373569	8	64	41	M	4065.37	4310.29	4309.53	-0.76
B-62	1396116	7373675	6	67	45	S	4246.91	4309.03	4308.49	-0.54
C-01	1389650	7374485	7	43	22	M	4186.32	4304.60	4305.68	1.08
C-02	1391199	7377659	7	36	39	S	4178.27	4303.87	4304.54	0.67
C-03	1389798	7377380	7	32	32	S	4165.23	4303.13	4303.14	0.01
C-04	1390381	7379087	7	28	40	M	4173.34	4302.35	4301.31	-1.04
C-05	1395780	7378266	7	48	58	M	4195.47	4310.16	4307.81	-2.35
C-06	1397494	7377319	7	57	62	M	4195.86	4309.88	4309.10	-0.78
C-07	1399416	7376098	6	68	65	S	4204.9	4309.61	4309.74	0.13
C-08	1400677	7375445	7	74	68	S	4192.21	4310.51	4310.08	-0.43
C-09	1400130	7366319	5	108	37	S	4300.2	4342.88	4347.62	4.74
C-10	1404892	7371338	3	104	71	S	4408.94	4461.46	4462.07	0.61
C-11	1403163	7373189	4	91	70	S	4328.29	4347.97	4346.10	-1.87
C-12	1406046	7367841	2	121	65	S	4433.93	4466.19	4465.74	-0.45
C-13	1406279	7369366	3	116	70	S	4419.94	4463.61	4464.30	0.69
C-14	1403812	7368994	2	109	60	S	4425.16	4459.58	4464.20	4.62

Appendix C. Water-Level Residuals in the Current Conditions Model

(Depth: S = Shallow (<= 100 ft below water table), M = Medium, D = Deep (> 300 ft below water table))

Well ID	East	North	Layer	Row	Column	Depth	Mid-Point of Screen Interval Elevation (ft)	Avg. Observed Head (ft)	Computed Head (ft)	Residual
C-15	1407008	7365882	1	131	62	S	4453.6	4467.48	4468.27	0.79
C-16	1405859	7362168	1	142	46	S	4469.75	4468.09	4472.33	4.24
C-17	1405624	7361595	1	143	43	S	4468.64	4466.83	4472.85	6.02
C-18	1407389	7367660	2	126	69	S	4434.41	4467.91	4466.31	-1.60
C-19	1404812	7360793	1	144	37	S	4456.08	4472.81	4473.45	0.64
C-20	1406354	7363481	2	139	52	S	4441.29	4470.51	4471.02	0.51
C-21	1405264	7360227	1	148	37	S	4460.48	4469.88	4474.05	4.17
C-22	1406950	7362734	2	143	52	S	4449.31	4468.94	4471.82	2.88
C-23	1405722	7359666	1	151	37	S	4455.23	4474.10	4474.66	0.56
C-24	1407339	7364618	2	137	59	S	4447.76	4470.17	4469.81	-0.36
C-25	1400883	7367720	5	105	44	S	4321.47	4341.51	4344.04	2.53
C-26	1407590	7363873	1	141	58	S	4456.8	4470.44	4470.67	0.23
C-27	1408714	7362818	1	149	59	S	4453.94	4466.87	4471.86	4.99
C-28	1408540	7362132	2	151	56	S	4443.85	4471.53	4472.49	0.96
C-29	1408370	7361467	1	153	53	S	4459.16	4471.86	4473.12	1.26
C-30	1405052	7366613	1	122	57	S	4463.37	4467.64	4466.94	-0.70
C-31	1407718	7365472	1	135	64	S	4454.02	4469.16	4468.89	-0.27
C-32	1407849	7362986	1	145	56	S	4463.73	4471.47	4471.62	0.15
C-33	1407329	7363927	1	140	57	S	4459.63	4470.22	4470.59	0.37
C-34	1405325	7362707	1	138	45	S	4453.49	4472.89	4471.80	-1.09
C-35	1403599	7361944	1	136	36	S	4464.64	4472.39	4472.13	-0.26
C-37	1403574	7361746	4	136	36	M	4350.19	4472.78	4472.44	-0.34
C-38	1406032	7367898	6	120	65	M	4239.61	4463.98	4465.04	1.06
C-39	1407265	7363976	4	140	57	M	4369.98	4470.47	4470.57	0.10
C-40	1402064	7359850	1	139	24	S	4466.61	4474.98	4473.34	-1.64
D-01	1406471	7373822	4	99	85	S	4361.86	4379.01	4378.90	-0.11
D-02	1407818	7370165	4	117	79	S	4361.34	4381.62	4384.11	2.49
D-03	1403714	7376399	5	80	83	S	4324.08	4356.45	4355.55	-0.90
D-04	1405128	7373393	4	96	79	S	4350.35	4379.36	4379.33	-0.03
D-05	1405389	7377114	4	83	92	S	4351.67	4374.48	4375.06	0.58
D-06	1408165	7374189	4	103	93	S	4358.47	4378.90	4378.98	0.08
D-07	1406808	7377708	4	85	99	S	4351.54	4376.79	4374.51	-2.28
D-08	1404575	7379304	5	72	95	S	4322.06	4358.08	4358.88	0.80
D-09	1403517	7381697	5	59	99	S	4311.62	4337.10	4331.83	-5.27
D-10	1400463	7378426	5	62	77	S	4281.52	4308.36	4309.22	0.86
N-4	1399679	7362839	1	120	24	NA	4460.65	4465.46	4469.25	3.79

Appendix C. Water-Level Residuals in the Current Conditions Model

(Depth: S = Shallow (<= 100 ft below water table), M = Medium, D = Deep (> 300 ft below water table))

Well ID	East	North	Layer	Row	Column	Depth	Mid-Point of Screen Interval Elevation (ft)	Avg. Observed Head (ft)	Computed Head (ft)	Residual
N-08B	1393036	7375407	5	50	38	NA	4280.3	4308.75	4307.23	-1.52
N-111	1402368	7357369	1	149	17	S	4478.04	4475.88	4475.75	-0.13
N-112	1402954	7358919	1	145	24	S	4481.24	4474.39	4474.56	0.17
N-114	1403332	7359801	1	143	29	S	4473.54	4474.58	4473.90	-0.68
N-115	1400842	7359384	1	137	18	S	4466.61	4474.56	4473.15	-1.41
N-116	1401282	7359477	1	138	20	S	4481.22	4474.79	4473.29	-1.50
N-117	1400688	7360414	1	132	20	S	4477.09	4474.79	4472.15	-2.64
N-118	1400008	7359179	1	135	14	S	4463.46	4474.84	4472.87	-1.97
N-120	1402790	7360551	1	139	29	S	4469.29	4473.93	4473.02	-0.91
N-134	1398903	7362641	1	118	20	S	4464.21	4468.50	4468.91	0.41
N-135	1400555	7361047	1	129	22	S	4470.41	4472.76	4471.50	-1.26
N-136	1400257	7359886	1	133	17	S	4471.7	4471.90	4472.39	0.49
N-142	1403355	7356382	1	156	18	S	4464.36	4476.83	4477.19	0.36
N-143	1403277	7357012	1	154	19	S	4463.22	4475.64	4476.52	0.88
N-144	1401923	7358852	1	142	20	S	4471.7	4475.03	4474.17	-0.86
N-150	1401425	7360892	1	133	25	S	4469.48	4471.92	4472.10	0.18
P-01D	1399928	7362040	7	124	23	M	4189.83	4471.52	4471.59	0.07
P-03D	1399143	7365214	7	109	30	M	4196.05	4451.38	4457.71	6.33
P-03S	1399143	7365214	1	109	30	S	4450.05	4467.58	4466.44	-1.14
P-04D	1401452	7365075	4	117	38	M	4332.06	4469.42	4468.25	-1.17
P-04S	1401452	7365073	1	117	38	S	4468.12	4468.87	4468.28	-0.59
P-06D	1408547	7366256	4	135	69	M	4369.12	4469.83	4467.98	-1.85
P-06S	1408529	7366232	2	135	69	S	4449.96	4469.60	4468.16	-1.44
P-07D	1404856	7368459	5	115	62	M	4301.91	4461.11	4464.35	3.24
P-07S	1404856	7368458	2	115	62	S	4425.84	4464.96	4464.74	-0.22
P-08D	1401213	7367472	5	107	45	S	4324.44	4346.72	4344.92	-1.80
P-09D	1401460	7368814	6	102	50	S	4260.44	4344.80	4344.17	-0.63
P-10S	1404016	7370258	1	105	64	S	4454.2	4462.40	4463.06	0.66
P-11D	1402803	7374061	6	86	72	M	4224.76	4346.22	4345.08	-1.14
P-11S	1402803	7374060	4	86	72	S	4348.71	4352.74	4345.09	-7.65
P-12D	1400649	7370474	5	93	52	S	4313.99	4342.82	4340.83	-1.99
P-13D	1396538	7365958	8	98	22	D	4013.86	4313.93	4313.37	-0.56
P-13S	1396538	7365958	5	98	22	S	4313.85	4314.70	4314.92	0.22
P-14D	1399628	7368436	5	98	42	S	4291.18	4343.12	4343.04	-0.08
P-15D	1398710	7373054	8	77	53	M	4036.61	4310.56	4310.04	-0.52
P-16D	1397038	7370409	8	82	38	D	3927.59	4308.88	4310.50	1.62

Appendix C. Water-Level Residuals in the Current Conditions Model

(Depth: S = Shallow (<= 100 ft below water table), M = Medium, D = Deep (> 300 ft below water table))

Well ID	East	North	Layer	Row	Column	Depth	Mid-Point of Screen Interval Elevation (ft)	Avg. Observed Head (ft)	Computed Head (ft)	Residual
P-16S	1397053	7370418	5	82	38	S	4289.59	4309.56	4309.60	0.04
P-17D	1393601	7370100	8	72	24	D	3976.9	4311.18	4310.43	-0.75
P-17S	1393601	7370100	5	72	24	S	4315.03	4311.41	4309.73	-1.68
P-18D	1400651	7367525	5	105	43	S	4291.53	4342.93	4344.58	1.65
P-19D	1392148	7372984	8	57	27	D	3955.85	4308.99	4309.35	0.36
P-19S	1392148	7372983	5	57	27	S	4286.59	4306.58	4307.93	1.35
P-20D	1395870	7375245	9	60	49	D	3898.2	4310.02	4309.97	-0.05
P-20S	1395870	7375245	5	60	49	S	4307.93	4308.93	4308.26	-0.67
P-21D	1393135	7368439	8	77	17	M	4087.4	4311.72	4311.12	-0.60
P-21S	1393135	7368439	5	77	17	S	4309.23	4311.57	4310.82	-0.75
P-22D	1393150	7368477	8	77	17	M	4086.91	4311.57	4311.11	-0.46
P-22S	1393150	7368475	7	77	17	M	4177.12	4310.94	4310.88	-0.06
P-23D	1393134	7368501	8	77	17	M	4087	4311.04	4311.09	0.05
P-23S	1393134	7368500	6	77	17	S	4227.16	4311.06	4310.78	-0.28
P-24D	1393108	7368554	8	77	17	M	4085.68	4311.48	4311.06	-0.42
P-25D	1397979	7363910	7	110	21	M	4175.83	4462.93	4460.17	-2.76
P-25S	1397979	7363909	3	110	21	S	4422	4467.32	4466.69	-0.63
P-26D	1398004	7369117	7	90	38	M	4123.59	4342.48	4336.84	-5.64
P-26S	1397994	7369110	5	90	38	S	4280.05	4311.25	4312.08	0.83
P-27D	1399912	7369990	8	93	48	D	3930.66	4341.22	4340.58	-0.64
P-28D	1388457	7375352	8	36	21	D	3969.46	4309.19	4309.49	0.30
P-28S	1388457	7375352	5	36	21	S	4279.28	4303.69	4302.94	-0.75
P-29	1396234	7361131	3	115	5	S	4418.61	4469.20	4468.47	-0.73
P-32	1390476	7376132	7	39	31	M	4186.12	4304.09	4305.37	1.28
P-33	1390393	7377419	7	34	35	M	4174.4	4303.36	4304.09	0.73
P-34	1391200	7377659	7	36	39	M	4181.83	4303.48	4304.54	1.06
P-35	1390757	7378431	7	31	39	M	4173.97	4302.79	4303.16	0.37
P-36	1389116	7372824	7	48	15	M	4190.25	4305.15	4306.82	1.67
P-37	1392711	7378157	7	39	46	M	4175.8	4304.82	4305.45	0.63
P-38	1393052	7377400	7	43	45	M	4171.28	4309.86	4306.35	-3.51
P-39	1395727	7377929	7	49	57	M	4184.9	4309.29	4308.09	-1.20
P-40	1395510	7364382	5	101	13	M	4319.31	4446.03	4449.81	3.78
P-41	1395480	7364369	7	101	13	D	4129.24	4460.59	4457.83	-2.76
P-42	1393736	7365698	5	90	10	S	4290.03	4315.01	4313.42	-1.59
P-43	1393765	7365709	8	90	10	D	4020.01	4313.60	4312.73	-0.87
P-44	1403190	7373160	7	91	70	M	4129.2	4345.97	4346.10	0.13

Appendix C. Water-Level Residuals in the Current Conditions Model

(Depth: S = Shallow (<= 100 ft below water table), M = Medium, D = Deep (> 300 ft below water table))

Well ID	East	North	Layer	Row	Column	Depth	Mid-Point of Screen Interval Elevation (ft)	Avg. Observed Head (ft)	Computed Head (ft)	Residual
T-03	1401208	7365673	2	114	39	S	4429.41	4468.66	4467.78	-0.88
T-04	1398825	7366882	2	101	34	S	4439.81	4450.11	4460.15	10.04
T-05	1398657	7368084	5	96	37	S	4296.51	4344.23	4342.96	-1.27
T-07	1403129	7358303	1	148	23	S	4473.36	4475.04	4475.21	0.17
USGS1	1403850	7355334	1	162	16	NA	4460	4477.10	4478.53	1.43
USGS2	1416594	7365655	3	163	98	NA	4400	4459.60	4459.14	-0.46
USGS3	1422360	7368462	4	170	130	NA	4350	4388.90	4388.95	0.05
USGS4	1425611	7374038	4	159	160	NA	4360	4392.45	4391.93	-0.52
USGS5	1412248	7372441	4	123	103	NA	4358.44	4382.99	4382.72	-0.27
USGS6	1419011	7380803	4	112	156	NA	4350	4376.08	4377.69	1.61
USGS7	1408972	7388546	4	50	142	NA	4340	4358.65	4358.79	0.14
USGS8	1409521	7393539	5	20	128	NA	4280	4321.50	4321.51	0.01
USGS9	1402975	7391423	6	10	88	NA	4310	4291.47	4292.88	1.41
WW-07	1393164	7368450	8	77	17	M	4087.5	4311.39	4311.12	-0.27
WW-08	1399926	7369976	4	93	48	S	4366.02	4345.15	4340.42	-4.73